

NAM

Report on the v5 Fragility and Consequence Models for the Groningen Field

Helen Crowley and Rui Pinho

Date November 2017

Editors Jan van Elk & Dirk Doornhof

General Introduction

Crucially important for the assessment of seismic risk in the Groningen area are the fragility curves describing the response of the building stock and the consequence model describing the impact on life safety risk. The fragility curves describe the probability of exceedance of a given damage state for a building typology (structural system) in the Groningen field area depending on the ground motion.

These fragility curves have been developed based on an experimental and modelling. The experimental program incorporates both in-situ and laboratory tests, to determine the properties of building materials, the behavior of wall elements and wall units and on tests of full-scale buildings. These tests have been conducted at the facilities of TU Delft TU Eindhoven, Eucentre (Pavia, Italy) and LNEC (Lisbon, Portugal). In these experiments much attention was given to masonry, but also pre-fab elements and pre-fab and cast-in-place concrete structures have been tested.

The results of these experiments were used to model the seismic response of different structural systems (typologies) encountered in the Groningen building stock and further calibrate these models. Modelling was carried out by teams in ARUP, TU Delft, MOZAYK and Eucentre.

Although much attention was given to unreinforced masonry building, cast-in-place concrete and pre-fab buildings have also been tested and modeled. Timber and steel frame buildings have also been studied and modelled. The hazard and risk assessment has been updated regularly (Ref. 1 to 4). Fragility curves used in these hazard and risk assessment of November 2015 (version 2) and for Winningsplan 2016 have been documented (Ref. 5). The current report describes the hazard and risk assessment version 5, used in the hazard and risk assessment of November 2017 (Ref. 6).

References

1. Hazard and Risk Assessment for Induced Seismicity in Groningen Interim Update November 2015, Nederlandse Aardolie Maatschappij BV (Jan van Elk and Dirk Doornhof, eds), 1st November 2015.
2. Winningsplan Groningen 2016, Nederlandse Aardolie Maatschappij BV, 1st April 2016.
3. Technical Addendum to the Winningsplan Groningen 2016 - Production, Subsidence, Induced Earthquakes and Seismic Hazard and Risk Assessment in the Groningen Field, PART III - Hazard Assessment, Nederlandse Aardolie Maatschappij BV (Jan van Elk and Dirk Doornhof, eds), 1st April 2016.
4. Technical Addendum to the Winningsplan Groningen 2016 - Production, Subsidence, Induced Earthquakes and Seismic Hazard and Risk Assessment in the Groningen Field, PART IV - Risk Assessment, Nederlandse Aardolie Maatschappij BV (Jan van Elk and Dirk Doornhof, eds), 1st April 2016.
5. Development of v2 fragility and consequence functions for the Groningen Field, H. Crowley, R. Pinho, B. Polidoro, P. Stafford, October 2015.
6. Induced Seismicity in Groningen – Assessment of Hazard, Building Damage and Risk, NAM, Jan van Elk and Dirk Doornhof, NAM, November 2017



NAM

Title	Report on the v5 Fragility and Consequence Models for the Groningen Field		Date	October 2017
			Initiator	NAM
Autor(s)	Helen Crowley and Rui Pinho	Editors	Jan van Elk and Dirk Doornhof	
Organisation	Independent Academics	Organisation	NAM	
Place in the Study and Data Acquisition Plan	<p><u>Study Theme:</u> Development of Fragility Curves</p> <p><u>Comment:</u> Crucially important for the assessment of seismic risk in the Groningen area are the fragility curves describing the response of the building stock and the consequence model describing the impact on life safety risk. The fragility curves describe the probability of exceedance of a given damage state for a building typology (structural system) in the Groningen field area depending on the ground motion.</p> <p>These fragility curves have been developed based on an experimental and modelling. The experimental program incorporates both in-situ and laboratory tests, to determine the properties of building materials, the behavior of wall elements and wall units and on tests of full-scale buildings. These tests have been conducted at the facilities of TU Delft TU Eindhoven, Eucentre (Pavia, Italy) and LNEC (Lisbon, Portugal). In these experiments much attention was given to masonry, but also pre-fab elements and pre-fab and cast-in-place concrete structures have been tested.</p> <p>The results of these experiments were used to model the seismic response of different structural systems (typologies) encountered in the Groningen building stock and further calibrate these models. Modelling was carried out by teams in ARUP, TU Delft, MOZAYK and Eucentre.</p> <p>Although much attention was given to unreinforced masonry building, cast-in-place concrete and pre-fab buildings have also been tested and modeled. Timber and steel frame buildings have also been studied and modelled. The hazard and risk assessment has been updated regularly (Ref. 1 to 4). Fragility curves used in these hazard and risk assessment of November 2015 (version 2) and for Winningsplan 2016 have been documented (Ref. 5). The current report describes the hazard and risk assessment version 5, used in the hazard and risk assessment of November 2017 (Ref. 6).</p>			
Directly linked research	<ul style="list-style-type: none"> (1) Building Material properties (2) Shake table tests (3) Seismic Response of Buildings (URM and non-URM) (4) Risk Assessment 			
Used data	Full experimental and Modelling program into seismic response URM & non-URM buildings.			
Associated organisation	NAM			
Assurance	Independent Assurance Panel			

GRONINGEN FIELD SEISMIC HAZARD AND RISK ASSESSMENT

**Report on the v5 Fragility and Consequence
Models for the Groningen Field**

Authors:

Helen CROWLEY and Rui PINHO

October, 2017

Contents

Acknowledgements	iii
1 Introduction	1
1.1 Overview	1
1.2 Outline of Methodology	2
1.3 Risk Metrics	5
2 Seismic Performance of Buildings from the Groningen Field	7
2.1 Structural Systems in the v5 Exposure Model	7
2.1.1 V5 exposure model	7
2.1.2 Index buildings	12
2.2 Nonlinear Dynamic and Static Analysis of Index Buildings	15
3 Single Degree of Freedom (SDOF) Models	22
3.1 SDOF Backbone Curves and Hysteretic Models	22
3.1.1 Transformation to SDOF	22
3.1.2 Backbone curves	23
3.1.3 Comparisons with experimental test backbone curves	27
3.1.4 OpenSees hysteresis models	27
3.1.5 Final SDOF models	29
3.2 Foundation Flexibility and Radiation Damping	32
3.3 Nonlinear Dynamic ‘Cloud’ Analysis	35
3.3.1 Selection of records	35
3.3.2 Multivariate linear regression	36
3.3.3 Influence of building-to-building variability	39
3.3.4 Model Uncertainty	39
4 Damage and Collapse Fragility Functions	42
4.1 Introduction	42
4.2 Damage Limit States	43
4.2.1 Unreinforced Masonry (URM) Buildings	43
4.2.2 Reinforced Concrete (RC) Buildings	44
4.2.3 Timber and Steel Buildings	45
4.2.4 Summary of damage limit states	47
4.3 Collapse Limit States	47

4.3.1	Collapse states from dynamic analysis of URM buildings	47
4.3.2	Collapse states for non-URM buildings	47
4.3.3	Global Collapse Capacity	49
4.3.4	Summary of collapse limit states	49
4.4	Fragility Functions	49
4.4.1	Structural Fragility Functions	49
4.4.2	Chimney Fragility Functions	49
5	Fatality Consequence Model	56
5.1	Methodology	56
5.2	Probability of dying, given collapse	57
5.2.1	Inside the building	57
5.2.2	Outside the building	59
5.2.3	Final model	59
6	Conclusions and Future Plans	67
7	References	68
A	Explanation of Structural System and Layout Attributes	73
B	Representativeness of Index Buildings	74
C	Cloud Plots for all Models	84
D	Collapse Mechanisms of URM Index Buildings	90
D.1	De Haver	91
D.2	Solwerderstraat 55	93
D.3	Julianalaan 52	94
D.4	Zijlvest 25	95
D.5	Koeriersterweg 20-21	97
D.6	Nieuwstraat 8	99
D.7	Kwelder 1	101
D.8	Schuitenzandflat 2-56	103
D.9	Badweg 12	105
E	Structural Fragility Functions	107

Acknowledgements

The authors would like to express their gratitude to Jan van Elk who, with the assistance of Dirk Doornhof, has provided the support, guidance and conditions that have allowed this study to be carried out and completed within the necessary timeframe. Additional support from Jeroen Uilenreef is also gratefully acknowledged, in particular for what concerns the management of the numerical modelling and experimental testing campaign.

The work presented herein has benefitted greatly from discussions and feedback from Julian Bommer, who is responsible for the development of the ground-motion prediction equations for the region. The important interface between ground shaking and building damage has been ensured through this strong collaboration with Julian. Other members of NAM's Hazard and Risk Assessment Team, namely Stephen Bourne, Steve Oates, Pourya Omidi and Tomas Storck, have also provided useful feedback and checks, in particular whilst implementing the fragility and consequence models in the risk calculation engines, and to Assaf Mar-Or for generating hazard and risk results that have provided useful insights into the performance of the models.

There is a large team working on modelling and testing of components and structures for calibration of the numerical models used herein, with the main contributions coming from collaborators at Arup, Eucentre, and Mosayk. Not all of those involved can be mentioned and acknowledged here, but particular thanks for the identification and numerical modelling of index buildings is given to Michele Palmieri, Candice Avanes and Damian Grant (from Arup) and Daniele Malomo (from Mosayk), whilst Francesco Graziotti, Umberto Tomassetti, Emanuele Brunesi, Simone Peloso and Filippo Dacarro (from Eucentre) and Antonio Correia (from LNEC) are gratefully acknowledged for all the dedication and hard work that went into ensuring the tests were completed to schedule.

The fatality model has been developed following useful input and discussions with Emily So, Robin Spence (CAR Ltd) and Tony Taig (TTAC Ltd).

A significant part of the strong-motion database used for the derivation of the v5 fragility functions was provided by Julian Bommer. The Groningen recordings were provided to Julian by Bernard Dost of KNMI. The European database was made available to Julian by Professor Sinan Akkar from Bogazici University, Istanbul.

Chapter 1

Introduction

1.1 Overview

Gas production in the Groningen field in the northern Netherlands is inducing earthquakes, the largest of which to date was the magnitude M_L 3.6 (**M** 3.4) Huizinge event of August 2012. In response to this induced seismicity, NAM has been developing a comprehensive seismic hazard and risk model for the region, which comprises the entire gas field plus a 5 km buffer zone onshore.

A key component of the risk assessment involves the definition of fragility functions (which provide the probability of exceeding a given damage or collapse state, conditional on a level of input ground motion) for each structural system that has been identified within the region, and included within the exposure model. Although many fragility functions have been developed over the years (see e.g. Calvi et al., 2006; D'Ayala et al., 2014), the vast majority are not appropriate for use in Groningen, mainly due to the unusual detailing of these structures, which is not typically seen in tectonic seismically active areas. A predominantly analytical approach, which also includes elements of expert judgment and empirical and experimental data calibration, is thus being followed for developing new Groningen-specific fragility and consequence functions.

An iterative approach to the development of these new functions has been followed, with functions being updated every 6-12 months (from v0 in October 2014 to v5 now in October 2017), to allow the lessons learned from these intermediate development phases to be fed back into the methodology. The v2 fragility and consequence models were used for the underlying risk assessment for the 2016 Winningsplan, as documented in Crowley et al. (2015), and were reviewed by an international panel of experts. Developments to the methodology during the v3 and v4 phases have been published in peer-reviewed literature (Crowley et al., 2017). This report provides a comprehensive overview of the status of the v5 fragility and consequence models, which have been used in NAM's v5 risk assessment of October 2017.

The main novelties of these models with respect to those used in the v2 version of the 2016 Winningsplan include:

- All capacity curves for URM buildings are identified through nonlinear dynamic analysis (as opposed to nonlinear static analysis) of representative buildings using a number of recordings (with triaxial components) of increased levels of intensity, ensuring that global collapse is observed in the analyses.
- The results of seven full-scale shake-table tests and a number of component tests have been used to calibrate the software packages used to run the nonlinear dynamic analyses.
- Out-of-plane failure of URM walls is no longer treated separately from the global performance, but is explicitly modelled in the aforementioned nonlinear dynamic analyses.
- Collapse of URM buildings is no longer considered through a single collapse state, but the impact of up to three collapse states are considered in the fatality model.
- The fatality consequence model has been further developed, and considers the impact of debris both inside and outside the building. For the latter, collapse fragility functions for chimneys are also now included in the risk assessment.
- Fragility functions for damage have also been produced using the results of the experimental tests to better constrain the displacement thresholds at which a range of damage states occur.
- Intensity measures in the fragility development are explicitly checked for sufficiency, leading to a number of different scalar and vector intensity measures.

1.2 Outline of Methodology

The initial focus of NAM's risk assessment has been on the safety of the population exposed to induced earthquakes. Methodologies for estimating fatalities from earthquakes range from those that directly attempt to predict the number of casualties from the magnitude of the earthquake (e.g. Samardjieva and Badal, 2002) or a level of ground shaking such as macroseismic intensity (e.g. Jaiswal et al., 2009), to those that propose ratios between the mean number of casualties (or injured persons) and the number of people exposed to a building with a given level of damage, so-called mean fatality ratios (e.g. So and Pomonis, 2012). An approach that estimates the fatality risk from the probability of collapse of the buildings has been selected for the Groningen gas field risk model, given that it has been observed in past earthquakes that the number of earthquake shaking casualties is clearly related to the number of buildings that fully or partially collapse (e.g. Coburn and Spence 2002). Furthermore, by estimating in this manner the fatality risk for different typologies of buildings, additional knowledge on the structural defects of the buildings is obtained, which can then be used to guide the strengthening efforts to be applied to the buildings in the region.

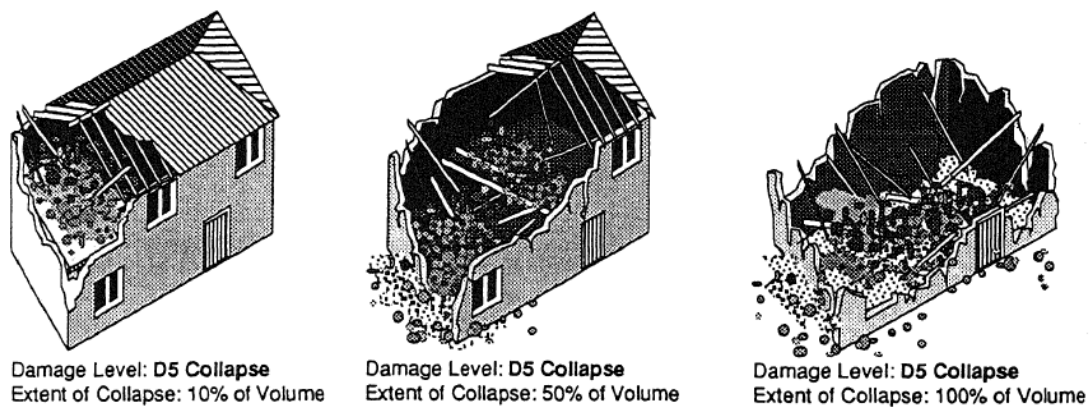


Figure 1.1 Varying volumetric reduction of a building defined as having “total destruction” or D5 damage level (from Coburn et al., 1992)

The probability of collapse of the buildings is assessed through an analytical approach, rather than an empirical approach, as during post-earthquake reconnaissance missions buildings are often defined as having the same ‘damage state’ despite having very different volumes of collapsed debris, which would imply very different fatality risks (see Figure 1.1). This feature is thus one of the drawbacks in using empirical data to derive fragility and fatality models, and this can be overcome by using analytical structural models that allow different collapse mechanisms and associated collapsed debris to be estimated.

Hence, the methodology presented herein attempts to use a predominantly analytical approach, that is augmented where possible with empirical and experimental data, to estimate both fragility and consequence models for damage estimation and local personal risk (Figure 1.2). The main causal pathways for loss of life that are currently being considered include the following: being hit by the collapse of a chimney outside of the building, or being hit by the debris caused by different structural collapse states of the building (both inside and outside) brought about by the global dynamic response of the structure to an input acceleration.

In order to model the dynamic response of a large population of buildings in a given region, it is common practice to first classify the buildings into building classes or types, which have similar structural and architectural characteristics (see e.g. FEMA, 2004). Once these typologies have been identified, at least one real representative building from the region is found for each typology (so-called index building) and the structural drawings are used to develop a multi-degree-of-freedom (MDOF) numerical model of the structural system including the predominant non-structural elements (such as partition and external façade walls). However, the computational effort associated with running nonlinear dynamic analyses of many such numerical models (around 50 different types of building have been defined for the region of Groningen), each subjected to tens of records, was judged to be too high to allow fragility functions to be directly developed from these analyses. Therefore, a simplified single-degree-of-freedom (SDOF) equivalent system

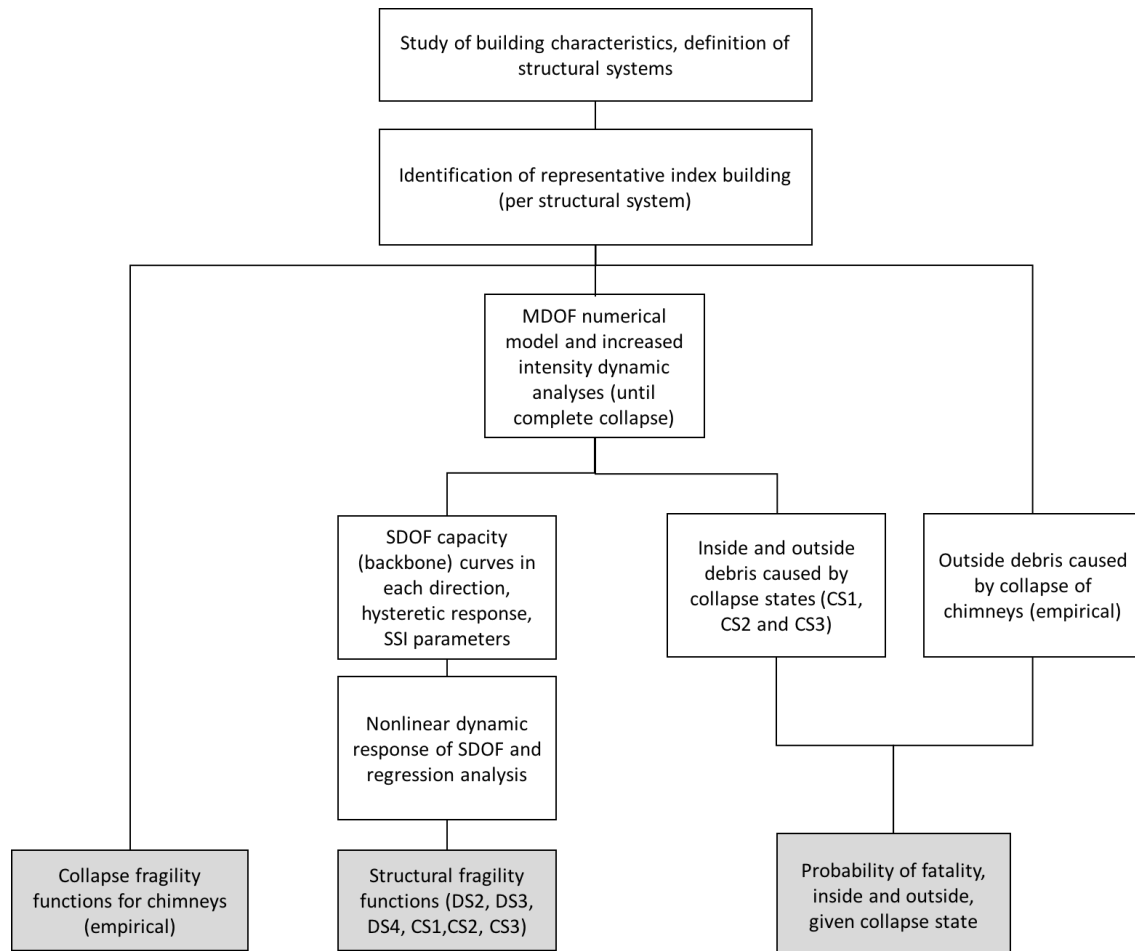


Figure 1.2 Flowchart of the main steps of the methodology used to develop the fragility and consequence models described herein. The grey boxes illustrate the three main models that are input into the risk engine, each of which is described herein.

approach has been used instead to analytically represent each typology.

Figure 1.3 shows the equivalent SDOF model that is used to represent each structural system. This model requires the definition of the effective mass (m), a hysteretic force displacement (F-D) model to describe the dynamic response of the system, and a lateral spring with stiffness K_x and a dashpot damper with viscous damping coefficient C_x that represent the foundation flexibility and damping (so-called soil-structure interaction, SSI), respectively. Chapters 2 and 3 describe the calibration of this SDOF model.

For the global response, nonlinear dynamic analysis of the MDOF numerical models using records with increasing intensity has been employed to produce the SDOF backbone capacity curves and to identify the consequences of different collapse mechanisms. A large suite of records was then utilised in the nonlinear dynamic analyses of these SDOF systems to model the record-to-record variability, and regression analysis is used to relate various ground shaking parameters to the nonlinear response in order to produce the fragility functions. Consequence models based on the extent of partial and complete collapse debris observed in the MDOF numerical analyses are then developed. A study of the collapse of chimneys of URM buildings from a number of earthquakes has been undertaken by Taig

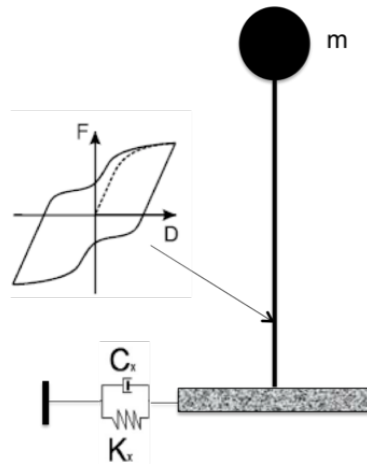


Figure 1.3 SDOF model used to develop structural fragility functions

and Pickup (2016), in order to develop empirical fragility functions and consequence models that have been used in the v5 risk model.

1.3 Risk Metrics

As discussed in Jonkman et al. (2003), there are a number of established fatality risk metrics, including Individual Risk (the probability that an average unprotected person, permanently present at a certain location, is killed due to an accident resulting from a hazardous activity). This metric is often referred to as Location Risk and has been adopted by the Dutch Ministry of Housing, Spatial Planning and Environment when setting risk standards for the Netherlands. In early 2015, an advisory committee (Commissie Meijdam) was established to advise on risk policy related to Groningen earthquakes, including the selection of risk metrics. The first advice of this committee was that an inside local personal risk (ILPR) metric, defined as the annual probability of fatality for a hypothetical person who is continuously present without protection inside a building, should be evaluated for all buildings in the Groningen gas field. ILPR differs from the aforementioned Location Risk metric in that it refers to the area inside a building rather than a single arbitrary location inside or outside buildings. Given that unreinforced masonry buildings also pose a significant threat to people that are outside buildings (due to out-of-plane failure of lightly loaded walls, chimneys and parapets), the outside local personal risk is also calculated, and is weighted by the probability that the aforementioned continuously present hypothetical person would be outside at the time of the earthquake, in order to obtain a single local personal risk (LPR) value per building.

In 2016 the Dutch Ministry of Economic Affairs (MEA) also requested the forecast of group risk for damage (so-called Maatschappelijk Risico (Schade)). To meet this request, F-N curves that present the annual frequency of exceedance against number of damaged buildings have been calculated using the fragility functions for damage states DS2 and DS3 presented herein. It is noted that this is not standard practice, and it is more common to

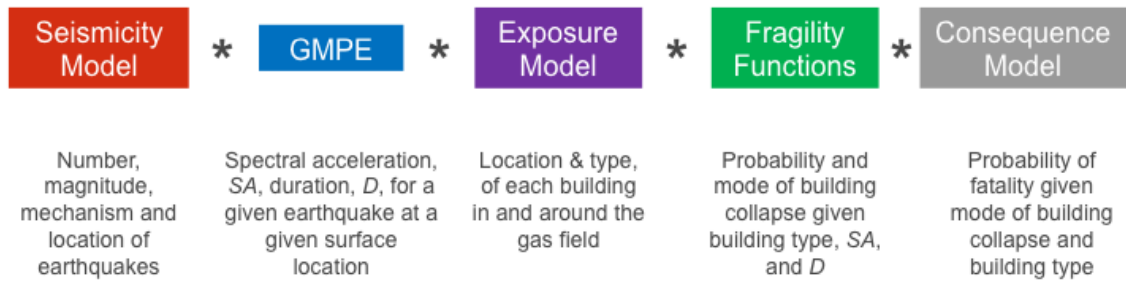


Figure 1.4 Components of the risk engine for the calculation of Local Personal Risk. For the calculation of group damage, fragility functions for damage states are required, and there is no consequence model. For group risk, the exposure model includes the number of people in and around buildings.

calculate loss exceedance curves for groups of buildings that report the annual frequency of exceedance of loss (e.g. due to the repair of damage or due to loss of life). Indeed, group risk for fatalities can also be calculated using the input models presented herein, by combining the inside and outside LPR by the average number of people present in and around the buildings during the day and night, as provided in the exposure model.

The estimation of group damage, group risk and local personal risk is undertaken within an engine (Figure 1.4) that uses Monte Carlo simulation to generate a catalogue of events from the seismicity model, and then correlated estimates of ground motion parameters at the location of the buildings in the exposure model are produced using the ground-motion prediction equation (GMPE) for the field (Bommer et al., 2016; Bommer et al., 2017). The probability of exceeding a given damage or collapse state, conditional on the aforementioned ground motion parameters, is then estimated for a building type at a given location using the fragility functions described herein. The probability of loss of life both inside and outside the building, given that collapse occurs, is calculated from the consequence model for the building type (as also presented in this report), and the results are combined considering the relative probability of being inside or outside the building type (for LPR), or the relative number of people inside or outside the building (for group risk). By repeating these calculations for a large number of simulated events, the annual probability of fatality for the hypothetical person (i.e. the local personal risk) or F-N curves can be calculated.

This report describes the development of damage and collapse fragility functions and the consequence model for fatalities to be used in the risk engine for the calculation of local personal risk (both inside and outside the buildings), group damage and group risk.

Chapter 2

Seismic Performance of Buildings from the Groningen Field

2.1 Structural Systems in the v5 Exposure Model

2.1.1 V5 exposure model

The v5 exposure database (EDB) (Arup, 2017a; Arup, 2017b) contains the location and characteristics of over 250,000 buildings inside and within 5km of the Groningen gas field. The v5 risk assessment has been undertaken for all of the populated buildings (approx. 150,000), each of which is described using structural systems that combine 6 different attributes of the building according to the GEM Building Taxonomy (Brzev et al., 2013): material and type of lateral load-resisting system in each direction of the building, presence of external walls, and floor system. The structural system of each building in the exposure database has been assigned through two main routes:

- Inspection data for 26,847 buildings: this provided some or all of the attributes of the structural system.
- Inference rules that relate characteristics of the building to the structural system. The characteristics that have been considered include structural layout, function, and age of construction. A combination of data-driven and expert judgment-based inferences have been used.

Figure 2.1 shows the inspected buildings that led to the assignment of 11,555 full structural systems and 14,603 partial structural systems. The remaining buildings were assigned to a set of pre-defined structural systems based on the building typologies and inference rules used in previous exposure models. This led to a total of 75 structural systems, though some of these had unexpected combinations of attributes and were present in very low numbers. Also, it was felt that the use of different masonry typologies (e.g. calcium silicate bricks, clay bricks) to distinguish between structural systems was too detailed for the purposes of a regional risk model. Hence, by collapsing the masonry types and remapping the unknown sparse systems to well known systems, a final list of 28 structural systems has

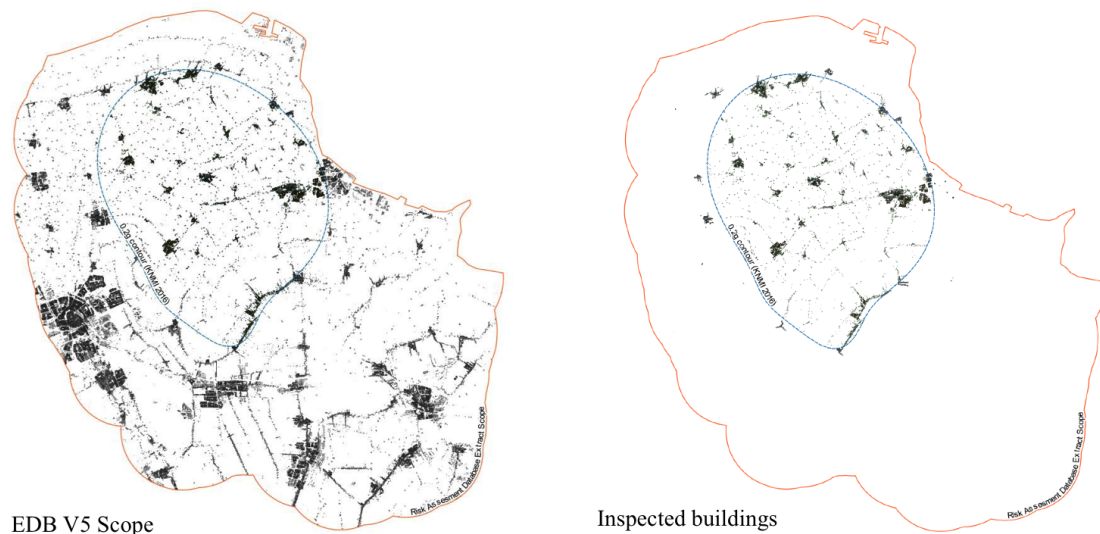


Figure 2.1 Extent of the v5 exposure model and coverage of the inspections

been obtained. Given that the height is known to influence the structural response of buildings, due to increased mass, axial load and floor amplification, two height category attributes were also considered to define the structural systems: 1-2 storeys (low-rise) and 3+ storeys (mid to high-rise). The gutter height of the buildings present in the v5 EDB was used to distinguish between low-rise (less than or equal to 7.5 m) and mid to high-rise (greater than 7.5 m) buildings, leading to the final list of 54 structural typologies, given in Table 2.2. An expansion of the GEM Building Taxonomy codes used in this table is provided in Appendix A.

The most predominant structural system in the v5 exposure model is MUR/LWAL/MUR/LN/EW/FC/HBET:1,2, i.e. unreinforced masonry (MUR) buildings with walls in one direction (LWAL) and no lateral load-resisting system in the other direction (LN), cavity walls (EW), concrete floors (FC) and height between 1 and 2 storeys (HBET:1,2). There are close to 57,000 buildings that could be assigned to the above structural system, a number that is around one-third of the total populated building stock. It was thus considered opportune to explore the possibility of further distinguishing this typology, for which reason data on the maximum opening ratio on the ground floor¹ from inspected buildings was investigated (see Figure 2.2).

¹The maximum ratio of the area of openings (due to windows and doors) to the total area of the wall, considering all ground floor façades of the building

Table 2.1 Structural systems in v5 exposure model

GEM Taxonomy String	Approx. number	Short Description
CR+PC/LPB/CR+PC/LPB/EWN/FN/HBET:1,2	108	Precast RC post and beam low-rise
CR+PC/LPB/CR+PC/LPB/EWN/FN/HBET:3,20	2	Precast RC post and beam mid to high-rise
CR+PC/LWAL/CR+PC/LN/EWN/FC/HBET:1,2	132	Precast RC wall-slab-wall low-rise without cladding
CR+PC/LWAL/CR+PC/LN/EW/FC/HBET:1,2	5583	Precast RC wall-slab-wall low-rise with cladding
CR+PC/LWAL/CR+PC/LN/EW/FC/HBET:3,20	252	Precast RC wall-slab-wall mid to high-rise with cladding
CR+PC/LWAL/CR+PC/LWAL/EWN/FC/HBET:1,2	387	Precast RC wall-wall low-rise without cladding
CR+PC/LWAL/CR+PC/LWAL/EWN/FC/HBET:3,20	226	Precast RC wall-wall mid to high-rise without cladding
CR+PC/LWAL/CR+PC/LWAL/EW/FC/HBET:1,2	2	Precast RC wall-wall low-rise with cladding
CR+CIP/LPB/CR+CIP/LPB/EWN/FN/HBET:1,2	251	Cast-in-place RC post and beam low-rise
CR+CIP/LPB/CR+CIP/LPB/EWN/FN/HBET:3,20	3	Cast-in-place RC post and beam mid to high-rise
CR+CIP/LFM/CR+CIP/LFM/EWN/FC/HBET:1,2	62	Cast-in-place RC frame low-rise
CR+CIP/LFM/CR+CIP/LFM/EWN/FC/HBET:3,20	25	Cast-in-place RC frame mid to high-rise
CR+CIP/LWAL/CR+CIP/LN/EW/FC/HBET:1,2	6492	Cast-in-place RC wall-slab-wall low-rise with cladding
CR+CIP/LWAL/CR+CIP/LN/EW/FC/HBET:3,20	232	Cast-in-place RC wall-slab-wall mid to high-rise with cladding
CR+CIP/LWAL/CR+CIP/LWAL/EWN/FC/HBET:1,2	687	Cast-in-place RC wall-wall low-rise without cladding
CR+CIP/LWAL/CR+CIP/LWAL/EWN/FC/HBET:3,20	816	Cast-in-place RC wall-wall mid to high-rise without cladding
MUR/LH/MUR/LH/EWN/FW/HBET:1,2	3130	URM house and timber post and beam low-rise
MUR/LH/MUR/LH/EWN/FW/HBET:3,20	421	URM house and timber post and beam mid to high-rise
MUR/LWAL/MUR/LN/EWN/FW/HBET:1,2	7862	URM wall-slab-wall, solid walls, timber floors low-rise
MUR/LWAL/MUR/LN/EWN/FW/HBET:3,20	4004	URM wall-slab-wall, solid walls, timber floors mid to high-rise
MUR/LWAL/MUR/LN/EW/FC/HBET:1,2	46143	URM wall-slab-wall, cavity walls, concrete floors low-rise
MUR/LWAL/MUR/LN/EW/FC/HBET:1,2/IRIR+IRVP:CHV	10679	URM wall-slab-wall, cavity walls, concrete floors low-rise and large openings on ground floor wall
MUR/LWAL/MUR/LN/EW/FC/HBET:3,20	2410	URM wall-slab-wall, cavity walls, concrete floors mid to high-rise
MUR/LWAL/MUR/LN/EW/FW/HBET:1,2	7469	URM wall-slab-wall, cavity walls, timber floors low-rise
MUR/LWAL/MUR/LN/EW/FW/HBET:3,20	1539	URM wall-slab-wall, cavity walls, timber floors mid to high-rise
MUR/LWAL/MUR/LWAL/EWN/FW/HBET:1,2	15226	URM wall-wall, solid walls, timber floors low-rise
MUR/LWAL/MUR/LWAL/EWN/FW/HBET:3,20	2993	URM wall-wall, solid walls, timber floors mid to high-rise

Table 2.2 Structural systems in v5 exposure model (cont.)

GEM Taxonomy String	Approx. number	Short Description
MUR/LWAL/MUR/LWAL/EW/FC/HBET:1,2	14633	URM wall-wall, cavity walls, concrete floors low-rise
MUR/LWAL/MUR/LWAL/EW/FC/HBET:3,20	1698	URM wall-wall, cavity walls, concrete floors mid to high-rise
MUR/LWAL/MUR/LWAL/EW/FW/HBET:1,2	7683	URM wall-wall, cavity walls, timber floors low-rise
MUR/LWAL/MUR/LWAL/EW/FW/HBET:3,20	250	URM wall-wall, cavity walls, timber floors mid to high-rise
MUR/LWAL/W/LPB/EWN/FN/HBET:1,2	243	Timber (glulam) post and beam, masonry infill walls low-rise
MUR/LWAL/W/LPB/EWN/FN/HBET:3,20	4	Timber (glulam) post and beam, masonry infill walls mid to high-rise
W/LPB/W/LPB/EW/FN/HBET:1,2	1102	Timber post and beam low-rise
W/LPB/W/LPB/EW/FN/HBET:3,20	12	Timber post and beam mid to high-rise
W/LWAL/W/LN/EWN/FW/HBET:1,2	49	Timber wall-slab-wall without cladding low-rise
W/LWAL/W/LN/EW/FW/HBET:1,2	1472	Timber wall-slab-wall with cladding low-rise
W/LWAL/W/LN/EW/FW/HBET:3,20	90	Timber wall-slab-wall with cladding mid to high-rise
W/LWAL/W/LWAL/EWN/FW/HBET:1,2	14	Timber wall-wall without cladding low-rise
W/LWAL/W/LWAL/EWN/FW/HBET:3,20	3	Timber wall-wall without cladding mid to high-rise
W/LWAL/W/LWAL/EW/FW/HBET:1,2	776	Timber wall-wall with cladding low-rise
W/LWAL/W/LWAL/EW/FW/HBET:3,20	8	Timber wall-wall with cladding mid to high-rise
S/LPB/S/LPB/EWN/FN/HBET:1,2	281	Steel post and beam, no floor low rise
S/LPB/S/LPB/EWN/FN/HBET:3,20	9	Steel post and beam, no floor mid rise
S/LFM/S/LFM/EWN/FC/HBET:1,2	195	Steel frame, concrete floor low-rise
S/LFM/S/LFM/EWN/FC/HBET:3,20	64	Steel frame, concrete floor mid to high-rise
S/LFBR/W/LPB/EWN/FN/HBET:1,2	298	Timber (glulam) post and beam, steel bracing low-rise
S/LFBR/W/LPB/EWN/FN/HBET:3,20	5	Timber (glulam) post and beam, steel bracing mid to high-rise
S/LFBR/S/LPB/EWN/FN/HBET:1,2	1219	Steel portal frame with bracing in one direction low-rise
S/LFBR/S/LPB/EWN/FN/HBET:3,20	27	Steel portal frame with bracing in one direction mid to high-rise
S/LFBR/S/LFBR/EWN/FN/HBET:1,2	995	Steel braced frame with no floor low-rise
S/LFBR/S/LFBR/EWN/FN/HBET:3,20	21	Steel braced frame, no floor mid to high-rise
S/LFBR/S/LFBR/EWN/FC/HBET:1,2	388	Steel braced frame, concrete floor low-rise
S/LFBR/S/LFBR/EWN/FC/HBET:3,20	181	Steel braced frame, concrete floor mid to high-rise

Table 2.3 Opening ratios of buildings with same structural system

Index Building	Max. ground floor opening ratio (%)
Julianalaan 52	0.71
Type C	0.60
Zijlvest 25	0.95
EUC-BUILD1	0.51
LENC-BUILD1	0.42

As will be presented in Chapter 3, a comparison of the nonlinear dynamic analyses and experimental test results of buildings with a MUR/LWAL/MUR/LN/EW/FC/HBET:1,2 structural system with different opening ratios (i.e. Julianalaan 52, Zijlvest 25, Type C, EUC-BUILD1, LNEC-BUILD1 as shown in Table 2.3) showed that a reasonable division of this structural system into two categories could be made: i) buildings with less than and equal to 80% opening ratios and ii) buildings with greater than 80% opening ratios at the ground floor. The majority of buildings with this structural system fall within the former category and so the name of the system has not been modified. Instead, to identify the buildings with maximum ground floor opening ratios greater than 80%, the primary vertical structural irregularity attribute of the GEM Building Taxonomy is given as "change in vertical structure" (i.e. IRIR+IRVP:CHV). The inspected buildings show that almost 100% of the buildings constructed with opening ratios greater than 80% were constructed between 1955 and 2000. The percentage of buildings with openings greater than 80% at the ground floor has been found to be around 30% for those constructed between 1955 and 1980, and 5% for those constructed between 1980 and 2000, and so this inference rule has been applied to the exposure database for buildings that have not yet been inspected and for which the opening ratio is not yet available, resulting in 46,143 buildings with a 'MUR/LWAL/MUR/LN/EW/FC/HBET:1,2' structural system and 10,679 buildings with a 'MUR/LWAL/MUR/LN/EW/FC/HBET:1,2/IRIR+IRVP:CHV' structural system.

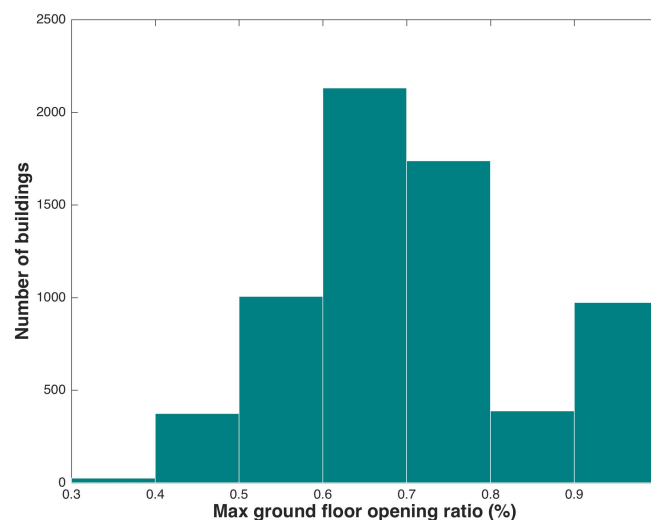
**Figure 2.2** Distribution of ground floor opening ratios of inspected buildings with the MUR/LWAL/MUR/LN/EW/FC/HBET:1,2 structural system

Table 2.4 Structural systems of the index building models

Index Building Name	GEM Taxonomy String
Precast RC post and beam*	CR+PC/LPB/CR+PC/LPB/EWN/FN/HBET:1,2
Precast RC wall-slab-wall*	CR+PC/LWAL/CR+PC/LN/EWN/FC/HBET:1,2
Cast-in-place RC post and beam*	CR+CIP/LPB/CR+CIP/LPB/EWN/FN/HBET:1,2
Cast-in-place RC wall-slab-wall*	CR+CIP/LWAL/CR+CIP/LN/EWN/FC/HBET:1,2
De Haver	MUR/LH/MUR/LH/EWN/FW/HBET:1,2
Solwerderstraat 55	MUR/LWAL/MUR/LN/EWN/FW/HBET:1,2
Julianalaan 52	MUR/LWAL/MUR/LN/EW/FC/HBET:1,2
Type C	MUR/LWAL/MUR/LN/EW/FC/HBET:1,2
Zijlvest 25	MUR/LWAL/MUR/LN/EW/FC/HBET:1,2/IRIR+IRVP:CHV
Koeriersterweg 20-21	MUR/LWAL/MUR/LN/EW/FC/HBET:3,20
Nieuwstraat 8	MUR/LWAL/MUR/LWAL/EWN/FW/HBET:1,2
Kwelder 1	MUR/LWAL/MUR/LWAL/EW/FC/HBET:1,2
Schuitenzandflat 2-56	MUR/LWAL/MUR/LWAL/EW/FC/HBET:3,20
Badweg 12	MUR/LWAL/MUR/LWAL/EW/FW/HBET:1,2
Kwelder 8	W/LWAL/W/LWAL/EW/FW/HBET:1,2
Steenweg 19	S/LFM/S/LFM/EWN/FC/HBET:1,2
Glulam portal frame*	S/LFBR/W/LPB/EWN/FN/HBET:1,2
Beneluxweg 15	S/LFBR/S/LPB/EWN/FN/HBET:1,2

* Generic model

2.1.2 Index buildings

A study of the characteristics of the buildings in the Groningen region in terms of age and geometry (e.g. height, volume, façade area, footprint area, shape in plan) has allowed a representative real building (so-called index building) to be identified for each structural system. The structural drawings of these index buildings have then been used to develop numerical models with average material properties based on the data collected during an in-situ testing campaign (Eucentre et al., 2015). Table 2.4 presents the index buildings that have been modelled and analysed for the v5 fragility and consequence models, and each model is presented in Figures 2.3 to 2.6. Further details on these models and the modelling assumptions are provided in Arup (2017c) and Mosayk (2015a; 2017). It is noted that in some cases it has not yet been possible to model real buildings, and so generic structures with typical characteristics of the structural system have been modelled; these are identified with an asterisk in Table 2.4. Whilst this list of index buildings is notably shorter than the full list of structural systems presented previously in Table 2.2, it is worth noting that they represent 75% of all buildings (and 85% of the URM buildings) in the exposure model.

In order to check that these index buildings (which in some cases were identified 2 years ago) still adequately represent the buildings within the current v5 exposure model, distributions of year of construction, structural layout, gutter height and footprint for each structural system given in Table 2.4 have been produced using the data in the v5 EDB, and compared with the characteristics of the index buildings, as presented in Table 2.5. The full distributions of these properties are presented in Appendix B and the modal value of each distribution is presented in Table 2.6. A comparison of Tables 2.5 and 2.6 shows that the majority of the index buildings match the modal characteristics of the structural systems that they are used to represent within the v5 risk model in particular for what concerns structural layout (see Appendix A for explanation of codes) and height. Any significant differences will be used to guide the identification of index buildings for future modelling.

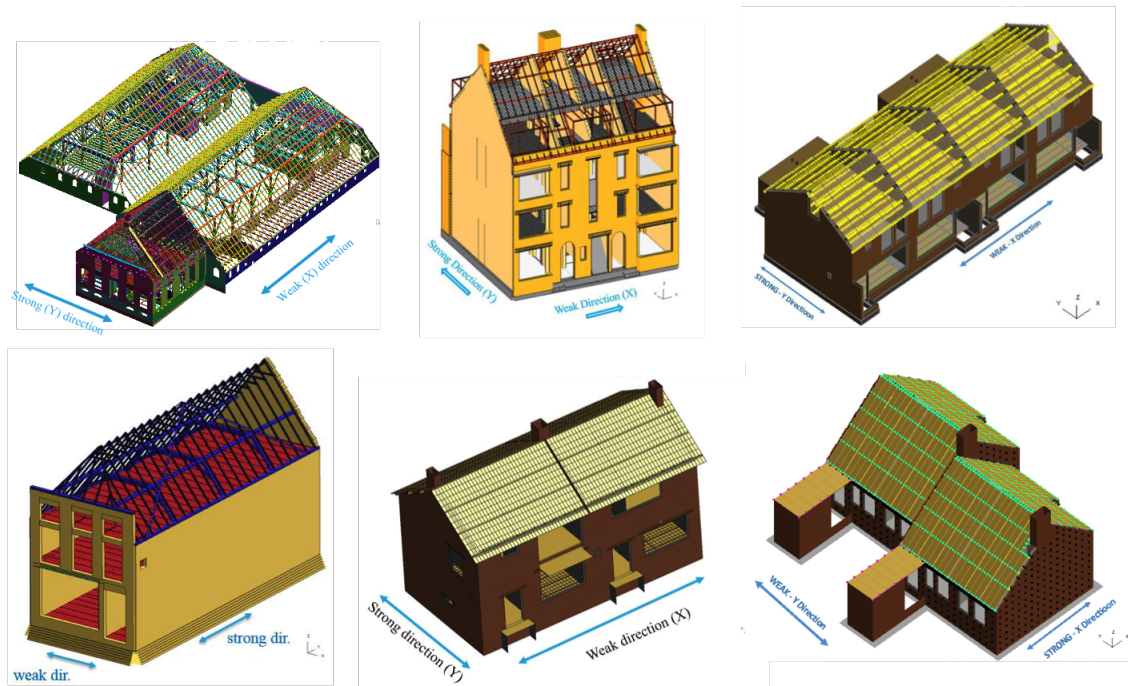


Figure 2.3 URM index building models, clockwise from top left: De Haver, Koeriersterweg 20-21, Julianalaan 52, Type C, Zijvest 25, Solwerderstraat 25



Figure 2.4 URM index building models, clockwise from top left: Nieuwstraat 8, Kwelder 1, Schuitenzandflat 2-56, Badweg 12



Figure 2.5 Non-URM index building models, left to right: Precast RC wall-slab-wall, Cast-in-place RC wall-slab-wall, Kwelder 8



Figure 2.6 Non-URM index building models, clockwise from top left: Beneluxweg 15, Glulam portal frame, RC post and beam (both precast and cast-in-place), Steenweg 19

Table 2.5 Characteristics of index building models

Index Building Name	Year of Construction	Structural Layout	Gutter Height (m)	Footprint area (m^2)
Precast RC post and beam	N/A	WBW	6.5	1880
Precast RC wall-slab-wall	N/A	UBH	5.52	44 per unit
Cast-in-place RC post and beam	N/A	WBW	6.5	1880
Cast-in-place RC wall-slab-wall	N/A	UBH	5.56	44 per unit
De Haver	1900's	WBH	2.9 (house) 3.7 (barn)	194 (house), 1530 (barn)
Solwerderstraat 55	<1945	UBA	6.1	113
Julianalaan 52	1950's	UBH	5.4	45 per unit
Type C	1970's	UBH	2.8	70 per unit
Zijlvest 25	1976	UBH	5.5	53 per unit
Koeriersterweg 20-21	TBD	UBH	8.59	50 per unit
Nieuwstraat 8	1940s	UH	3.0	70
Kwelder 1	TBD	UH	2.75	98
Schuitenzandflat 2-56	TBD	BTN	13.8	720
Badweg 12	1940's	UH	2.8	67
Kwelder 8	TBD	UH	2.75	76
Steenweg 19	2005	WBW	6.5	432
Glulam portal frame	N/A	WBW	4.0	460
Beneluxweg 15	2001	WBW	3.8	300

Table 2.6 Modal characteristics of v5 structural systems corresponding to index buildings listed in Table 2.5

Structural System	Year of Construction	Structural Layout	Gutter Height (m)	Footprint Area (m^2)
CR+PC/LPB/CR+PC/LPB/EWN/FN/HBET:1,2	1980-1999	WBW	3.1-4	>300
CR+PC/LWAL/CR+PC/LN/EWN/FC/HBET:1,2	1980-1999	UBH	5.1-6	51-100
CR+CIP/LPB/CR+CIP/LPB/EWN/FN/HBET:1,2	1960-1979	WBW	3.1-4	>300
CR+CIP/LWAL/CR+CIP/LN/EWN/FC/HBET:1,2	1960-1979	UBH	5.1-6	51-100
MUR/LH/MUR/LH/EWN/FW/HBET:1,2	<1900	WBH	3.1-4	>300
MUR/LWAL/MUR/LN/EWN/FW/HBET:1,2	1920-1939	UBH	4.1-5	51-100
MUR/LWAL/MUR/LN/EW/FC/HBET:1,2	1960-1979	UBH	5.1-6	51-100
MUR/LWAL/MUR/LN/EW/FC/HBET:1,2	1960-1979	UBH	5.1-6	51-100
MUR/LWAL/MUR/LN/EW/FC/HBET:1,2/IRIR+IRVP:CHV	1960-1979	UBH	5.1-6	51-100
MUR/LWAL/MUR/LN/EW/FC/HBET:3,20	1960-1979	UBH	8.1-9	51-100
MUR/LWAL/MUR/LWAL/EWN/FW/HBET:1,2	1920-1939	UH	3.1-4	51-100
MUR/LWAL/MUR/LWAL/EW/FC/HBET:1,2	1980-1999	UH	4.1-5	101-150
MUR/LWAL/MUR/LWAL/EW/FC/HBET:3,20	1960-1979	BTN	>11	151-200
MUR/LWAL/MUR/LWAL/EW/FW/HBET:1,2	1920-1939	UH	3.1-4	101-150
W/LWAL/W/LWAL/EW/FW/HBET:1,2	1980-1999	UH	4.1-5	101-150
S/LFM/S/LFM/EWN/FC/HBET:1,2	1980-1999	UH	3.1-4	101-150
S/LFBR/W/LPB/EWN/FN/HBET:1,2	1980-1999	WBW	3.1-4	>300
S/LFBR/S/LPB/EWN/FN/HBET:1,2	1960-1979	WBW	3.1-4	>300

2.2 Nonlinear Dynamic and Static Analysis of Index Buildings

Nonlinear dynamic analysis (using a set of 11 triaxial ground motions) of the majority of the index buildings presented in Table 2.4 have been undertaken using LS-DYNA (LSTC, 2013), ELS (ASI, 2017) and SeismoStruct (Seismosoft, 2017), and the results are fully presented in Arup (2017c) and Mosayk (2017d). For some of the stronger non-URM buildings, nonlinear static analysis has been performed, as described in Mosayk (2015a). These software tools have been validated and/or calibrated for seismic analysis of Groningen buildings using the results of a large number of experimental tests (Graziotti et al., 2015; 2016a; 2016b; 2016c; 2017a; 2017b; 2017c; Tomassetti et al., 2017; Correia et al., 2017) as documented in Mosayk (2014; 2016; 2017a; 2017b; 2017c; 2017e) and Arup et al. (2015; 2016a; 2016b; 2017).

The following plots show either the nonlinear static pushover curves or the hysteresis loops of all nonlinear dynamic analyses together with points representing the peak base shear and corresponding attic floor (i.e. highest level in the building before the roof) displacement (after removal of a time lag, identified on a case-by-case basis) in each direction of the building, for each analysis. These curves/points have been used to produce the SDOF backbone capacity curves for each structural system, as described in Chapter 3.

Shear and displacement response time-histories of MDOF structural systems are not necessarily fully in-phase, particularly when multiple modes of vibration or failure mechanisms are activated during the response of a given structure (a phenomenon that is further accentuated when the structure is pushed into the nonlinear inelastic response range). This effectively implies the presence of a time-lag between the moment when the peak value of base-shear is observed and the instant at which the corresponding displacement is recorded; the latter typically arriving with a slight delay with respect to the former. In the definition of the SDOF backbone capacity curves, such time-lag obviously needs to be removed (since it has no physical meaning within a SDOF representation of the

response), this being the reason why the black dots in the plots below (representing the max shear-displacement points with the time-lag removed) do not necessarily always appear on top of the hysteretic curves (where the time-lag is instead present).

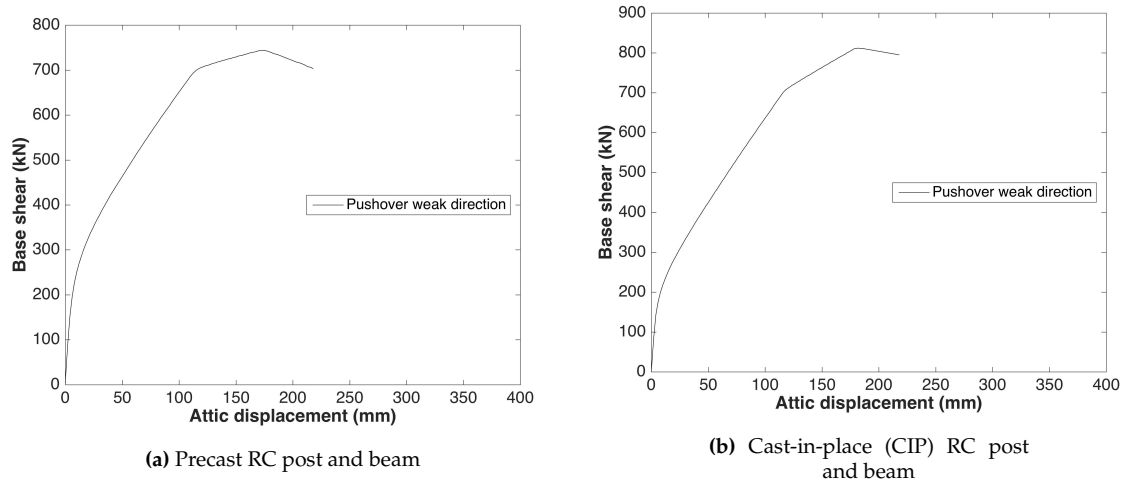


Figure 2.7 Pushover curves of the SeismoStruct precast RC and CIP RC post and beam models

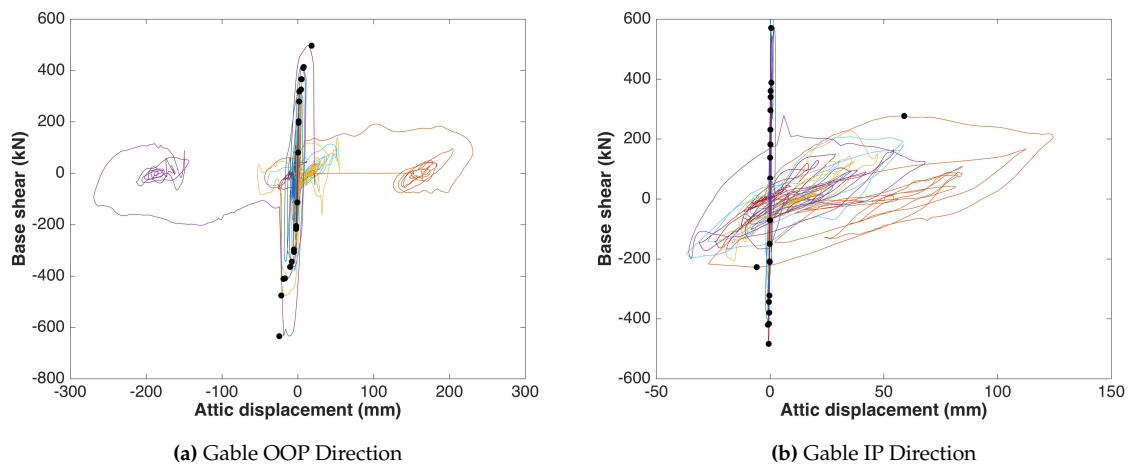


Figure 2.8 Hysteretic plots from the SeismoStruct precast RC wall-slab-wall model

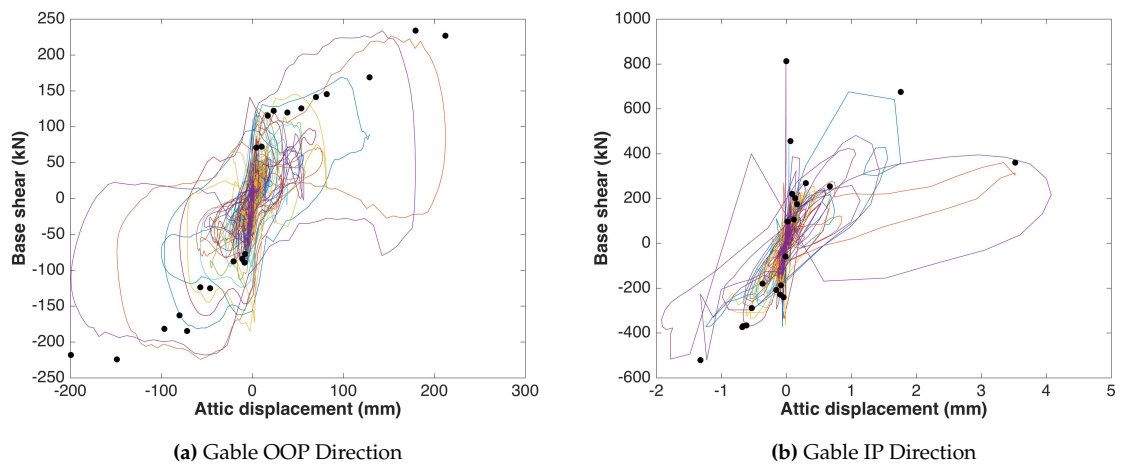


Figure 2.9 Hysteretic plots from the SeismoStruct cast-in-place RC wall-slab-wall model (note that spurious peaks have not been considered)

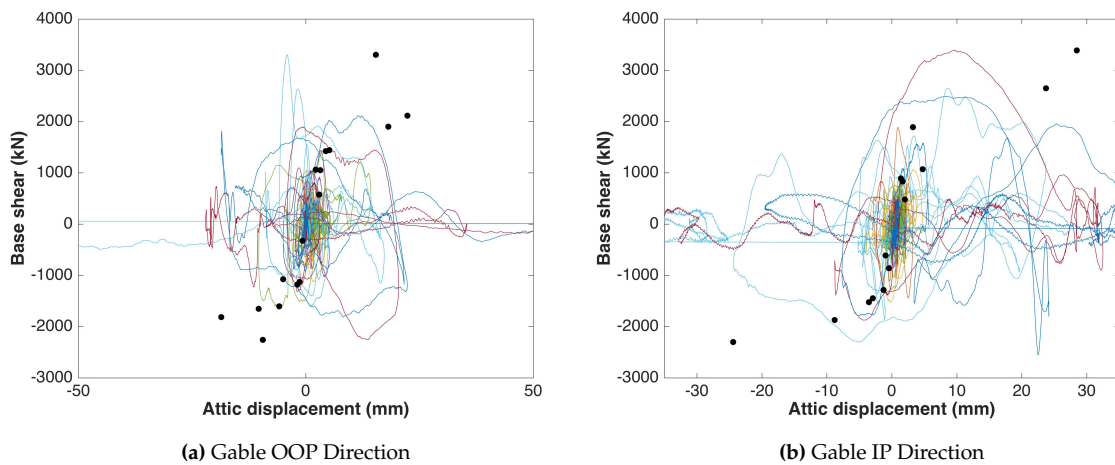


Figure 2.10 Hysteretic plots from the LS-DYNA De Haver model

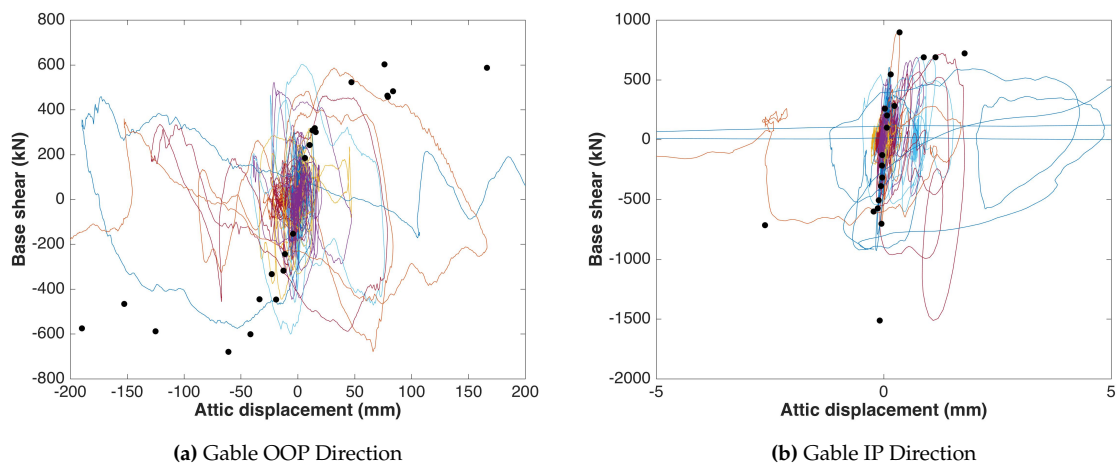


Figure 2.11 Hysteretic plots from the LS-DYNA Solwerderstraat 55 model

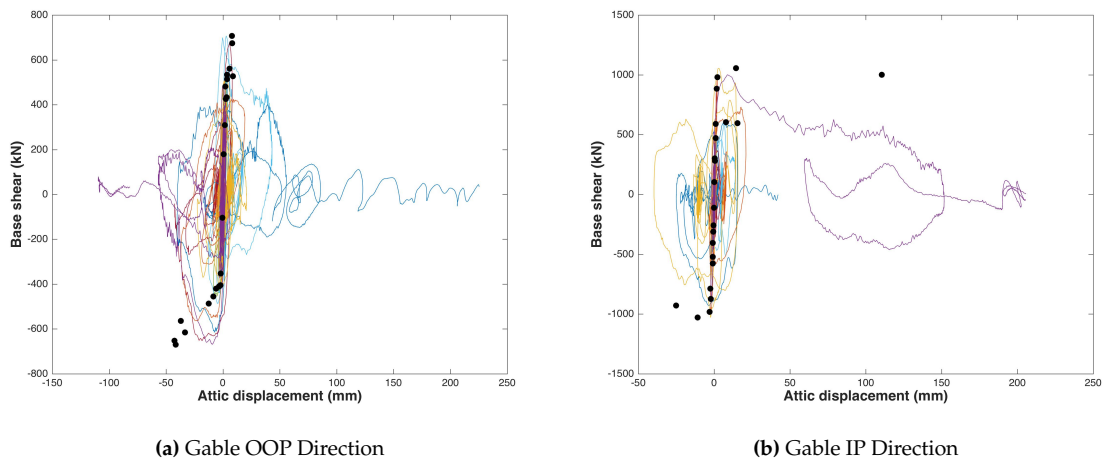


Figure 2.12 Hysteretic plots from the LS-DYNA Julianalaan 52 model

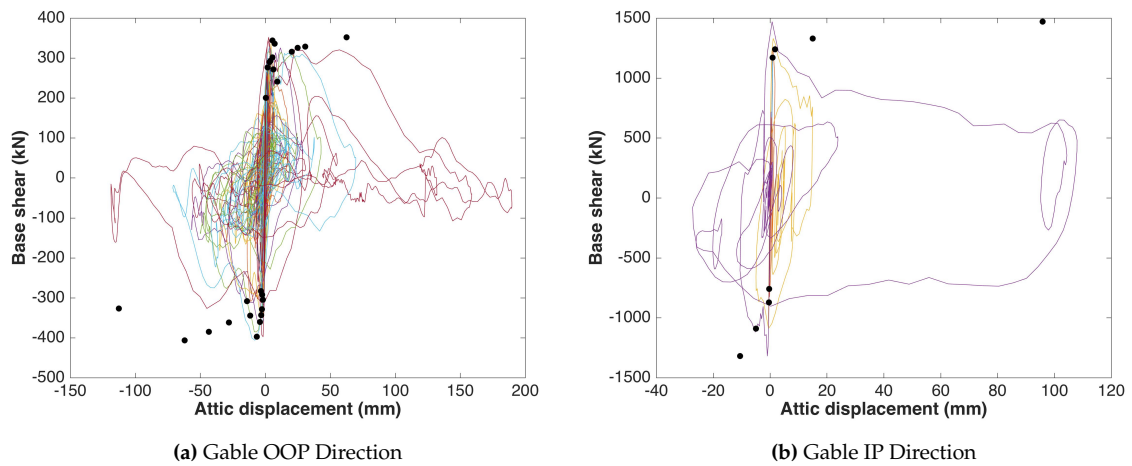


Figure 2.13 Hysteretic plots from the LS-DYNA Type C model

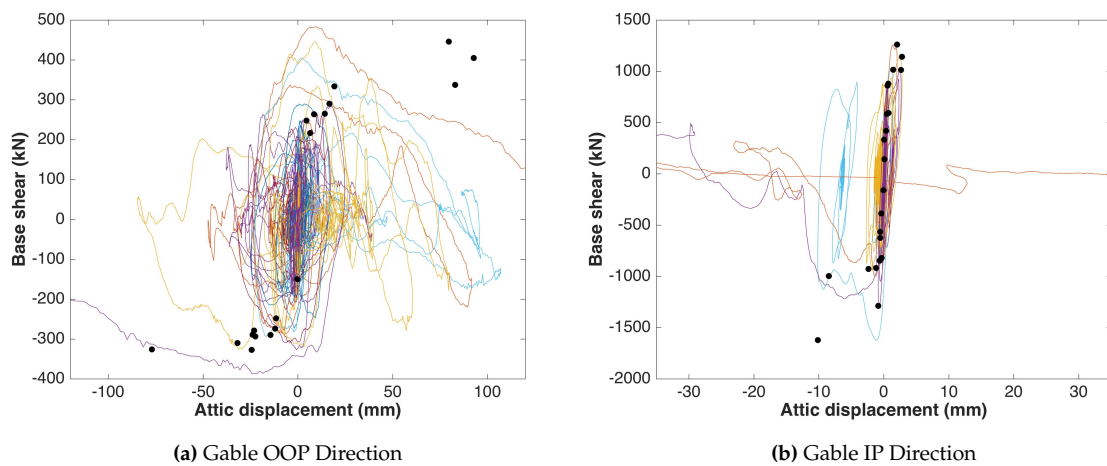


Figure 2.14 Hysteretic plots from the LS-DYNA Zijlvest 25 model

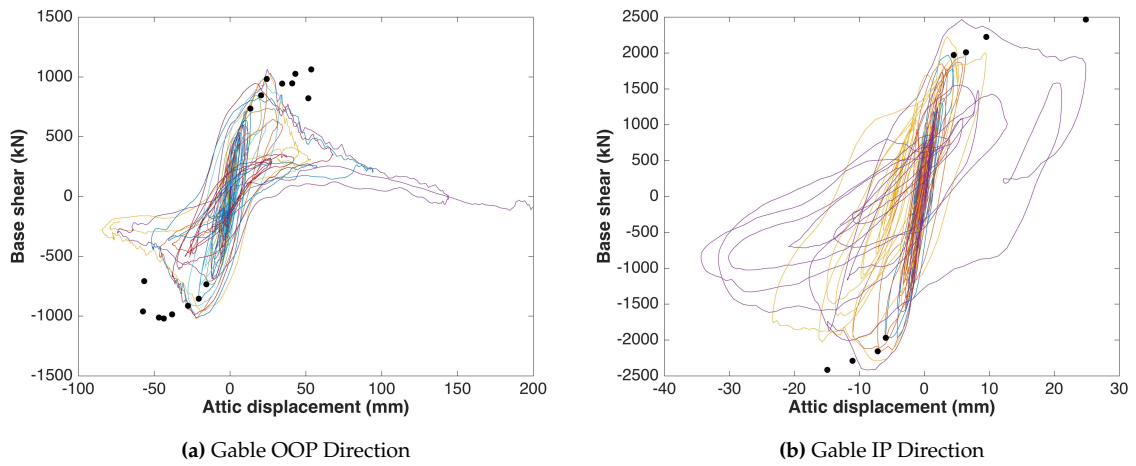


Figure 2.15 Hysteretic plots from the LS-DYNA Koeriersterweg 20-21 model

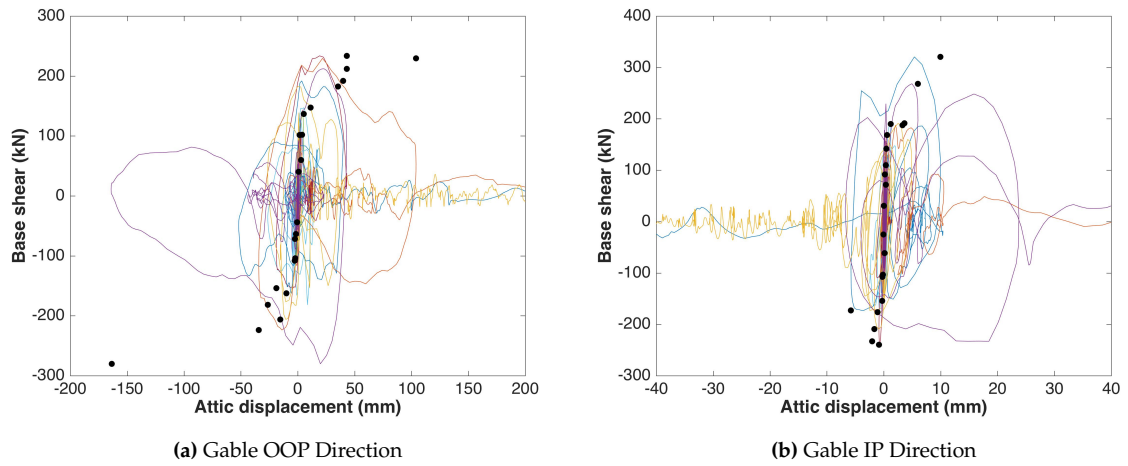


Figure 2.16 Hysteretic plots from the ELS Nieuwstraat 8 model

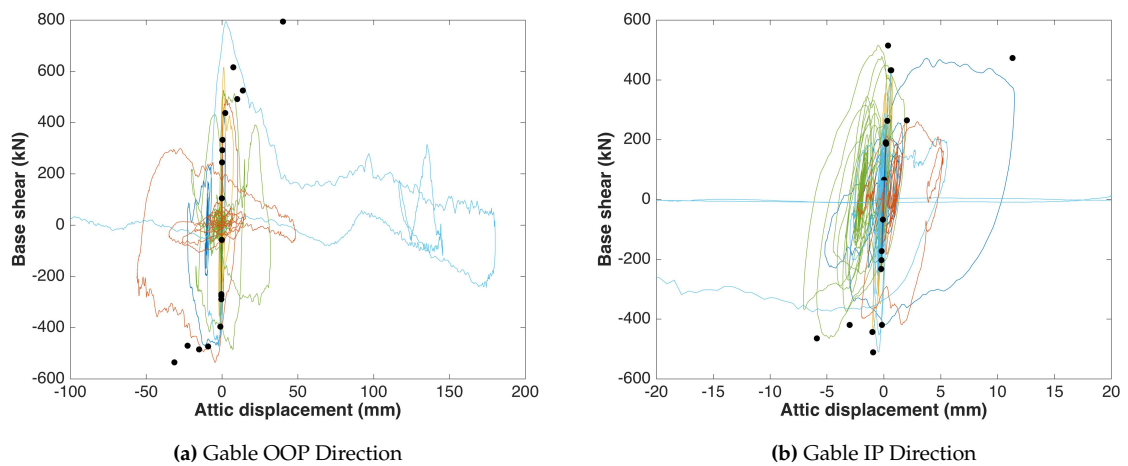


Figure 2.17 Hysteretic plots from the LS-DYNA Kwelder 1 model

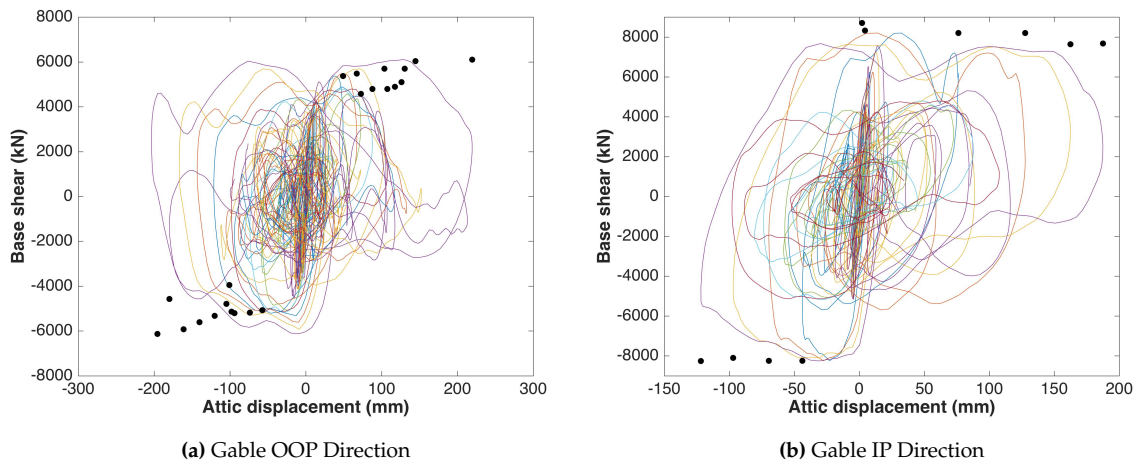


Figure 2.18 Hysteretic plots from the LS-DYNA Schuitenzandflat 2-56 model

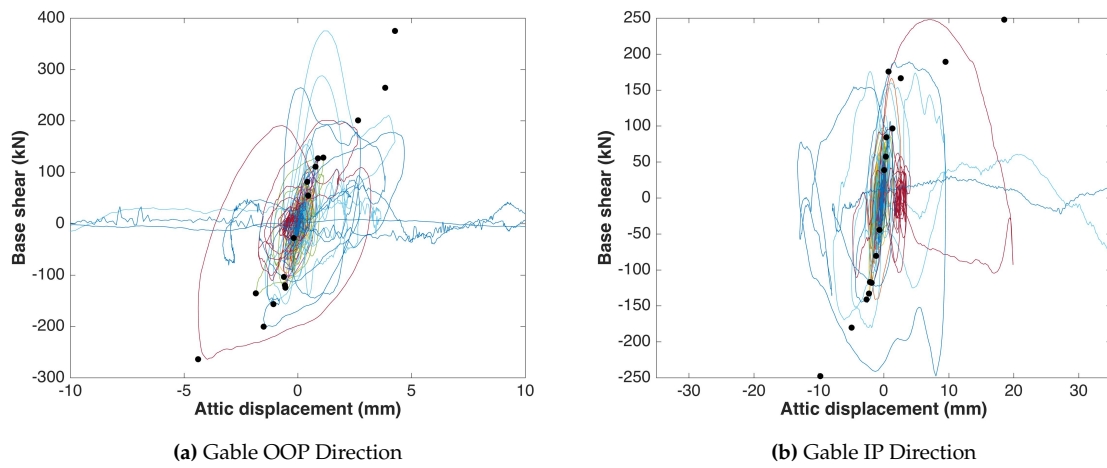


Figure 2.19 Hysteretic plots from the LS-DYNA Badweg 12 model

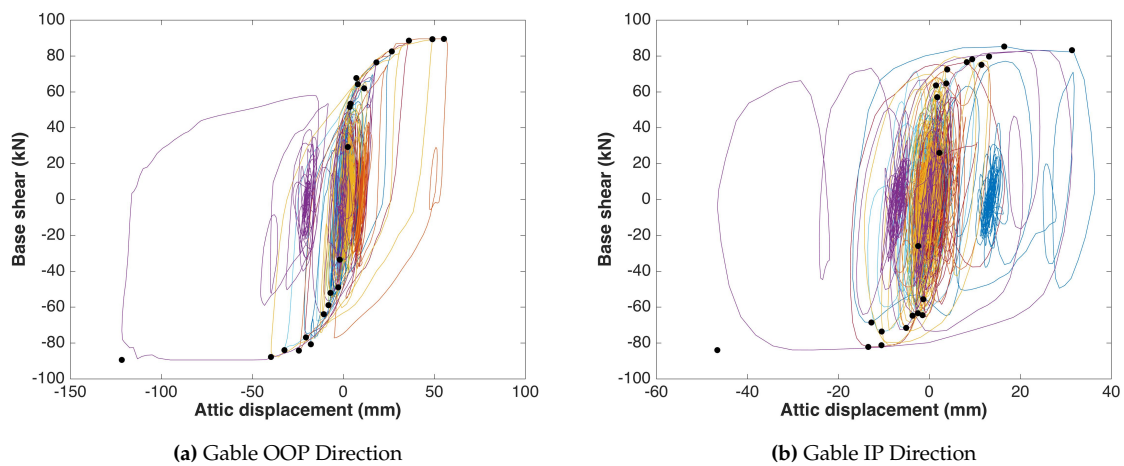


Figure 2.20 Hysteretic plots from the SeismoStruct Kwelder 8 model

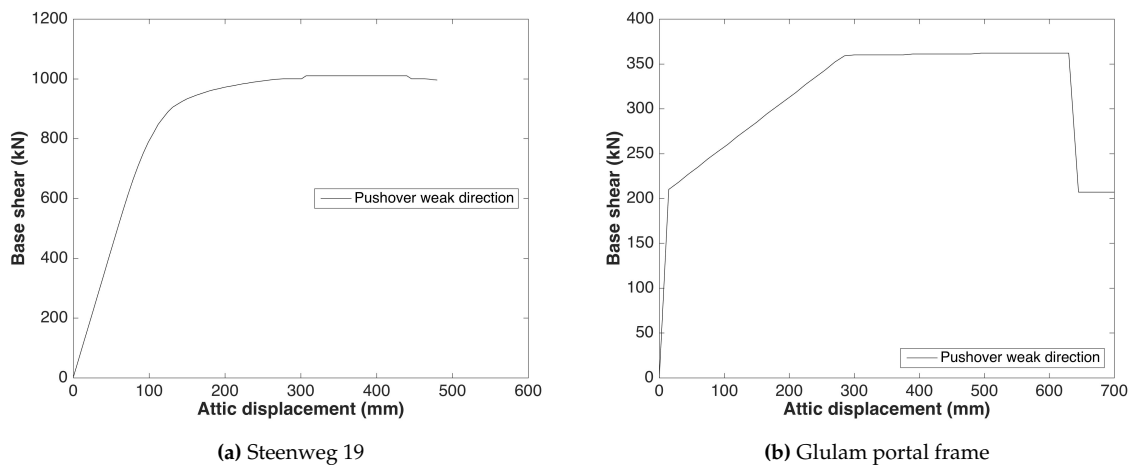


Figure 2.21 Pushover curves of the SeismoStruct Steenweg 19 and Glulam portal frame models

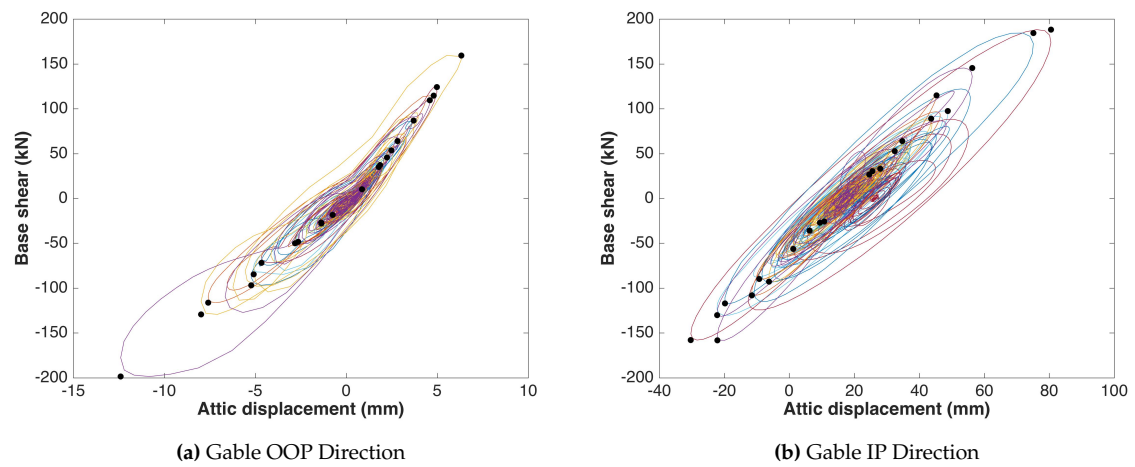


Figure 2.22 Hysteretic plots from the SeismoStruct Beneluxweg 15 model

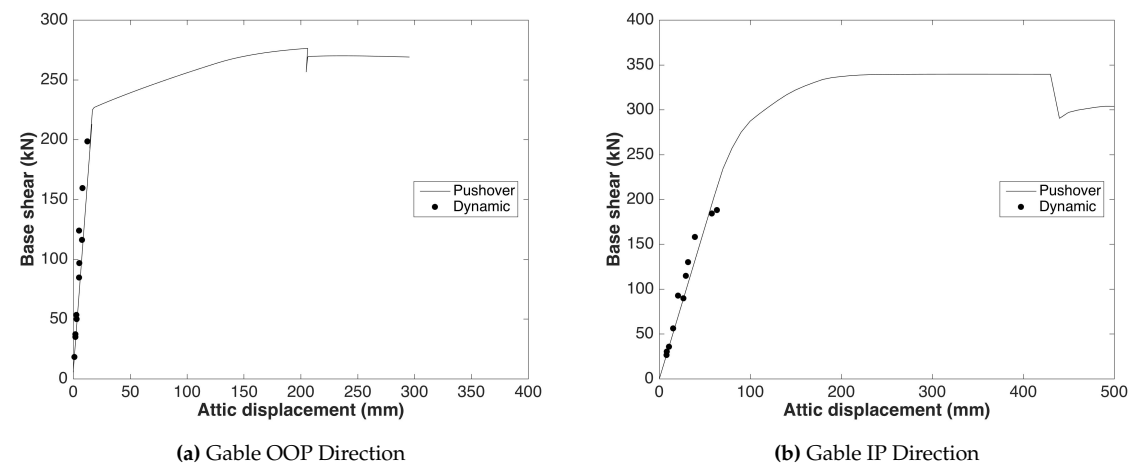


Figure 2.23 Pushover curves of the SeismoStruct Beneluxweg 15 model

Chapter 3

Single Degree of Freedom (SDOF) Models

This chapter describes the calibration of the SDOF model (see Figure 1.3) for each index building model presented previously in Chapter 3, as well as some additional models for non-URM buildings based on HAZUS (FEMA, 2004). Dynamic analyses of these SDOF models is undertaken herein for the development of fragility functions, that is described further in Chapter 4.

3.1 SDOF Backbone Curves and Hysteretic Models

The points of peak base shear and corresponding attic displacement from each nonlinear dynamic/static analysis presented in Chapter 2 have been transformed to equivalent SDOF properties, using the methodology described in the next section. This data has then been used to produce backbone curves for each index building. These backbone curves, together with a hysteresis model, and springs to represent the stiffness and damping due to foundation flexibility and radiation damping, comprise the SDOF models.

3.1.1 Transformation to SDOF

Transformation to an equivalent SDOF system has been undertaken using the transformation methodology presented in Casarotti and Pinho (2007). The transformation factor, Γ_t , has been calculated using the results of the analysis that led to the maximum attic displacement (Δ_{max}) without global collapse. At the time step, t , of maximum displacement, the transformation factor Γ_t has been calculated as follows:

$$\Gamma_t = \frac{\sum m_i \phi_{it}}{\sum m_i \phi_{it}^2} \quad (3.1)$$

where m_i is the mass of each floor of the model (noting that the roof mass is added to the attic/top floor), and ϕ_{it} are the displacements of all floors normalized by Δ_{max} . The spectral displacement (S_d) is calculated by dividing the attic/top floor displacement by Γ_t :

$$S_d = \frac{\Delta_{max}}{\Gamma_t} \quad (3.2)$$

and the base shear coefficient is estimated by dividing the base shear by the effective mass, m_{eff} , given by Equation 3.3:

$$m_{eff} = \sum m_i \phi_{it} \Gamma_t \quad (3.3)$$

The effective height (H_{eff}) of the SDOF can be calculated as follows:

$$H_{eff} = \frac{\sum m_i \phi_{it} h_i}{\sum m_i \phi_{it}} \quad (3.4)$$

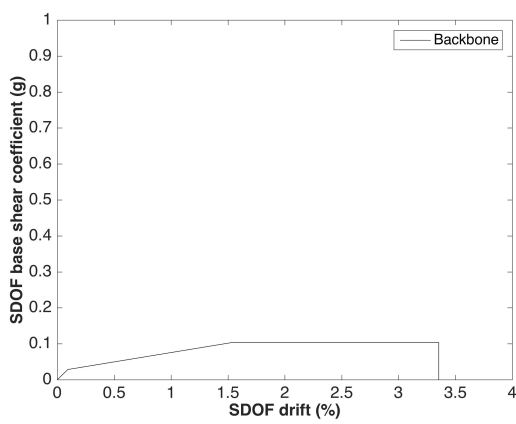
where h_i is the height to each floor and m is the total height of the structure. The SDOF drift is calculated by dividing the spectral displacement (S_d) by the effective height (H_{eff}).

3.1.2 Backbone curves

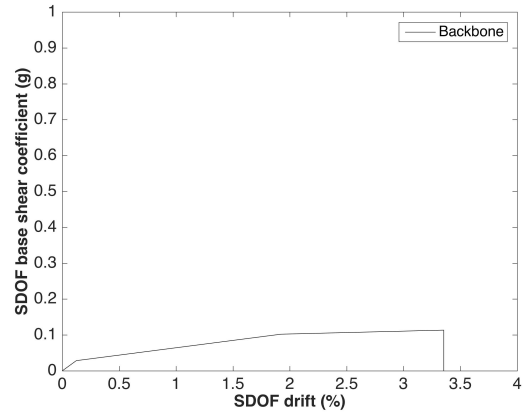
The backbone curve of the SDOF model up until peak base shear has been obtained using the hysteretic points presented in Figures 2.7 to 2.23. The reduction of base shear after peak base shear has been defined considering the post-peak hysteretic behaviour of the buildings, whilst the base shear is assumed to be zero when the global collapse capacity is reached.

For a given model, the global collapse capacity has been taken as the average of the lowest attic displacement when collapse occurs in those records that lead to global collapse, and the highest attic displacement attained in the analyses that do not lead to global collapse. Further discussion on the identification of the displacement capacity at collapse for each model is provided in Chapter 4.

The backbone curves are plotted in Figures 3.1 to 3.9 in terms of base shear coefficient and SDOF drift, using the transformation procedure described in the previous section. Only the weaker direction (with lower base shear coefficient) has been plotted, as all consequences observed in the 3D models of the buildings have been associated with the SDOF displacement in the weaker direction of the building.

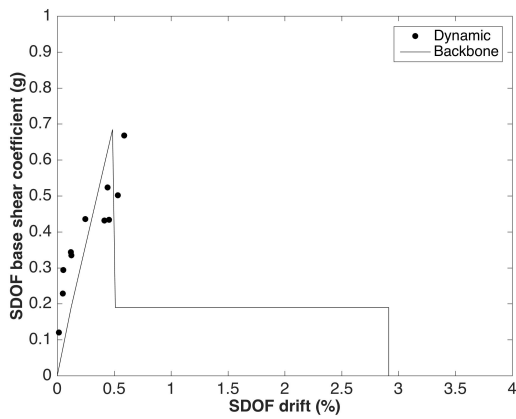


(a) Precast RC post and beam

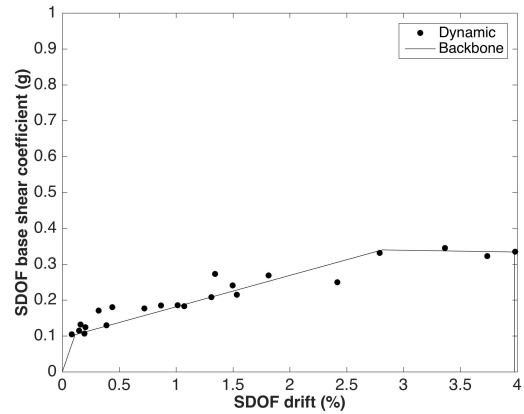


(b) Cast-in-place RC post and beam

Figure 3.1 SDOF backbone curve for the precast and cast-in-place RC post and beam models (it is recalled that, as discussed at the start of Section 2.2, for these structural systems dynamic analyses have not been carried out)

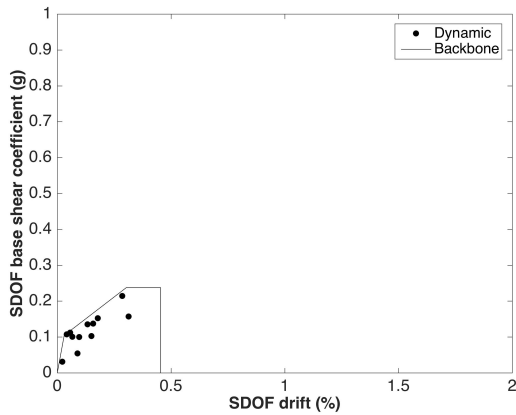


(a) Precast RC wall-slab-wall

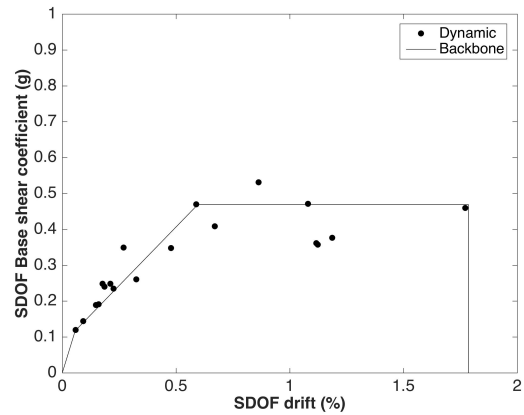


(b) Cast-in-place RC wall-slab-wall

Figure 3.2 SDOF backbone curve for the precast and cast-in-place RC wall-slab-wall models

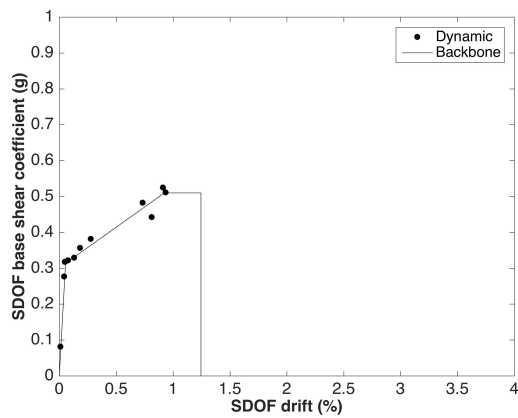


(a) De Haver

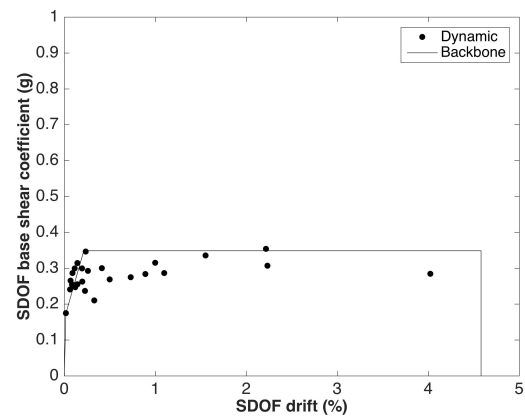


(b) Solwerderstraat 55

Figure 3.3 SDOF backbone curve for the De Haver and Solwerderstraat 55 models

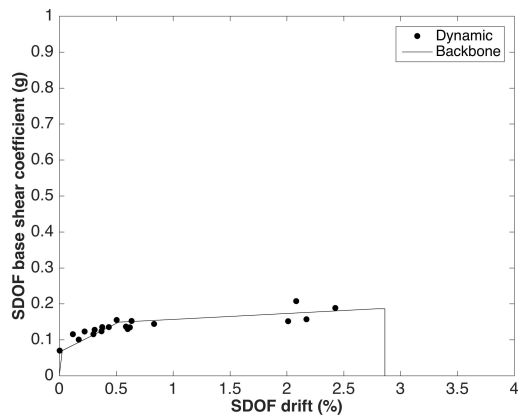


(a) Julianalaan 52

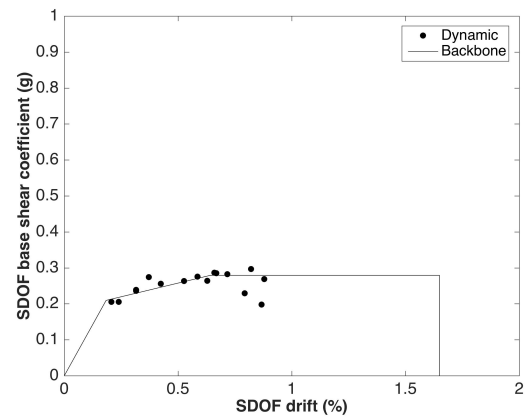


(b) Type C

Figure 3.4 SDOF backbone curve for the Julianalaan 52 and Type C models

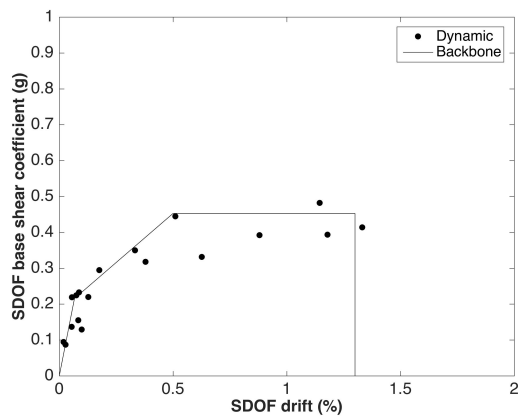


(a) Zijlvest 25

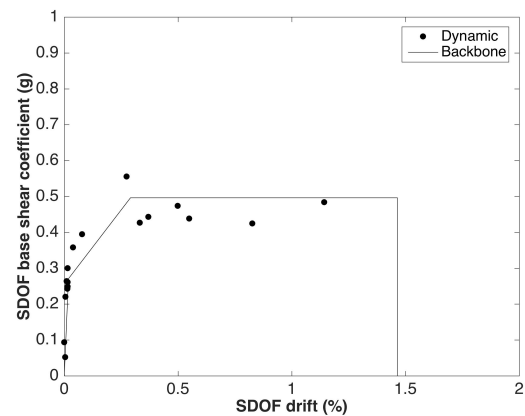


(b) Koeriersterweg 20-21

Figure 3.5 SDOF backbone curve for the Zijlvest 25 and Koeriersterweg 20-21 models



(a) Nieuwstraat 8



(b) Kwelder 1

Figure 3.6 SDOF backbone curve for the Nieuwstraat 8 and Kwelder 1 models

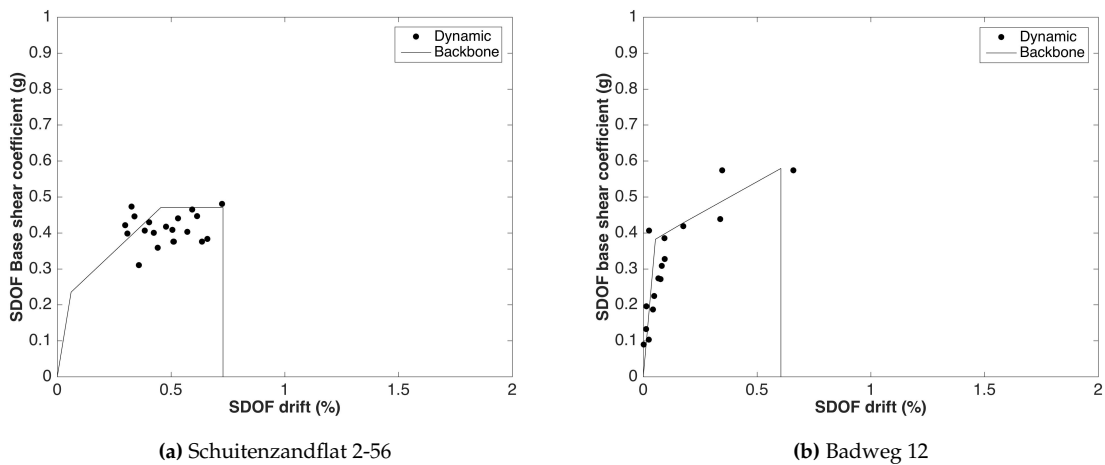


Figure 3.7 SDOF backbone curve for the Schuitenzandflat 2-56 and Badweg 12 models

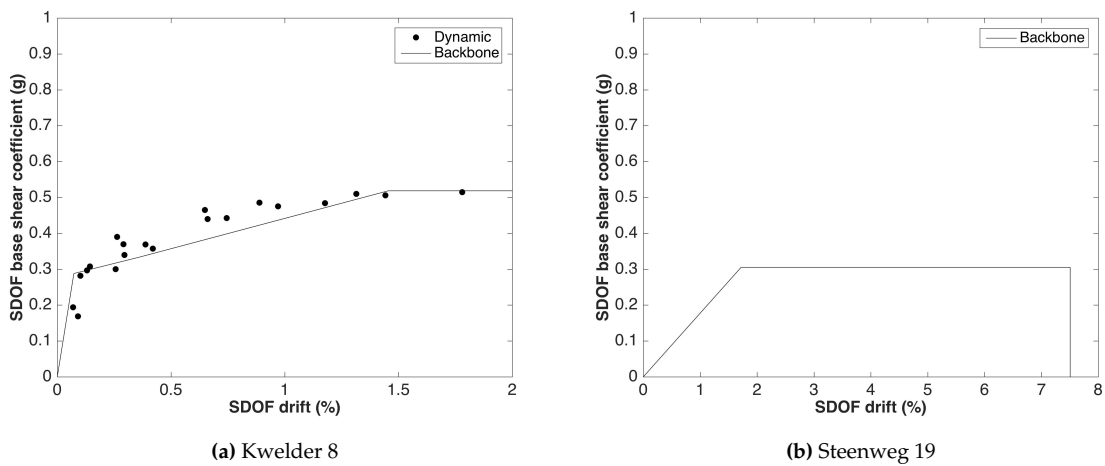


Figure 3.8 SDOF backbone curve for the Kwelder 8 and Steenweg 19 models (it is recalled that, as discussed at the start of Section 2.2, for the latter structural system dynamic analyses have not been carried out)

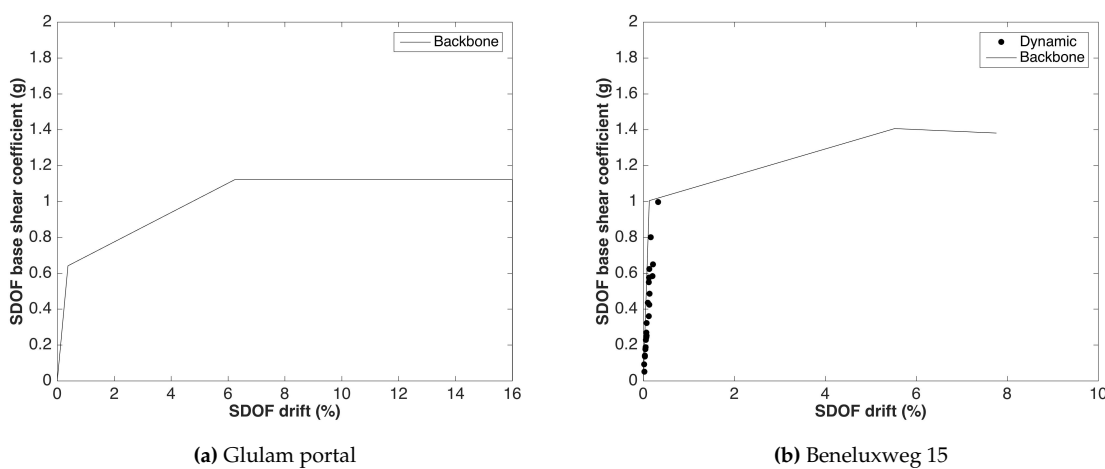


Figure 3.9 SDOF backbone curve for the Glulam portal and Beneluxweg 15 models (it is recalled that, as discussed at the start of Section 2.2, for the former structural system dynamic analyses have not been carried out)

3.1.3 Comparisons with experimental test backbone curves

In order to sanity check the backbone curves for the more predominant URM structural systems, comparisons of the numerical backbone curves with those from the experimental tests of full URM buildings (i.e. EUC-BUILD1, EUC-BUILD2 and LNEC-BUILD1) have been undertaken. More details on these experimental tests are provided in Graziotti et al. (2015; 2016a; 2016b; 2017a; 2017c) and Tomasetti et al. (2017).

The backbone curves for these experimental tests have been obtained by applying the same procedure described above for the numerical analyses, and the results for EUC-BUILD1 and LNEC-BUILD1 are shown in Figure 3.10. The structural system of EUC-BUILD1 and LNEC-BUILD1 (URM wall-slab-wall with cavity walls and concrete floors) is the same as Type C, Julianalaan and Zijlvest, though as discussed in Chapter 2 and presented in Table 2.3, the maximum ground floor opening ratio of Zijlvest is much larger than that of the other buildings. Hence, it is to be expected that the base shear coefficient of this index building is much lower than the other buildings, as seen in Figure 3.11. These findings support the subdivision of this structural system as a function of the maximum opening ratio at the ground floor (as discussed previously in Section 2.1.1).

The one-storey LNEC-BUILD1 specimen was taken to collapse, which occurred at an attic drift of around 4.5%, which is very similar to the ultimate attic drift at which collapse was observed in the one storey Type C numerical model. EUC-BUILD2 was a two-storey specimen that did not reach global collapse, but was observed to be near collapse at an ultimate SDOF drift of around 0.75%, which is consistent with the observation of a 1.2% global collapse capacity of the two-storey Julianalaan 52 model. The lower collapse capacity of these two-storey buildings is expected due to the higher axial load on the ground floor walls, which decreases the ultimate displacement capacity of URM walls.

The EUC-BUILD2 specimen represented an older building with solid walls and timber diaphragms, and the hysteretic plot and points of the backbone curve are shown in Figure 3.12a. The SDOF backbone curve is compared with those for Badweg 12 and Nieuwstraat 8 in Figure 3.12b. The specimen is seen to be much stiffer and stronger than these index buildings, which is expected given that the index buildings have a much larger footprint than the test specimen (the size of the shake-table obviously limited the dimensions that could be considered for EUC-BUILD2), and thus have less walls per unit area of building.

3.1.4 OpenSees hysteresis models

The hysteretic behaviour of the SDOF systems has been modelled using the Hysteretic and Multilinear (see Figure 3.13) hysteresis models in OpenSees (McKenna et al., 2000). Hysteretic is a general-purpose hysteretic material model that can model pinching, damage driven by both mobilised ductility and dissipated energy, and unloading stiffness degradation. By assigning values of 1 to the pinching factors for stress and strain during reloading, and using a high value for the parameter beta that is used to determine the

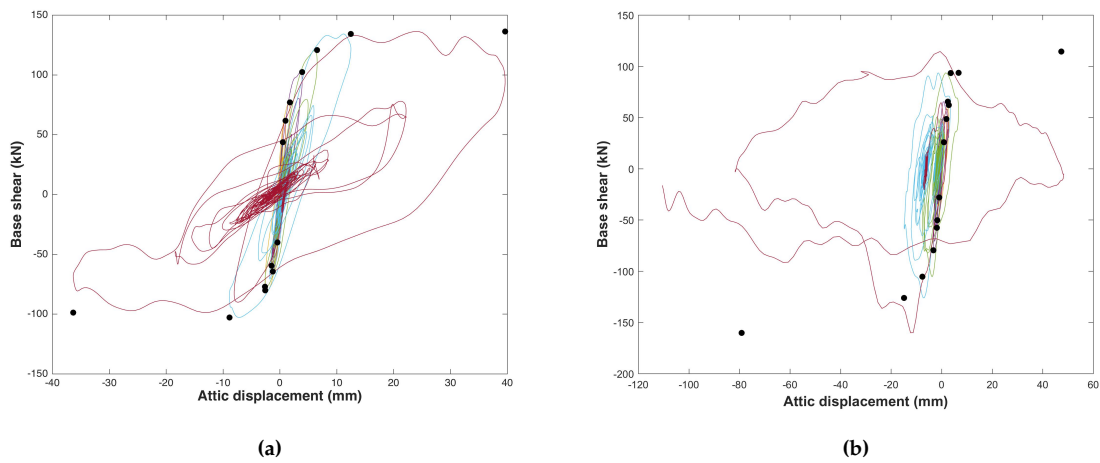


Figure 3.10 Hysteretic plots from the (a) EUC-BUILD1 and (b) LNEC-BUILD1 shake-table tests

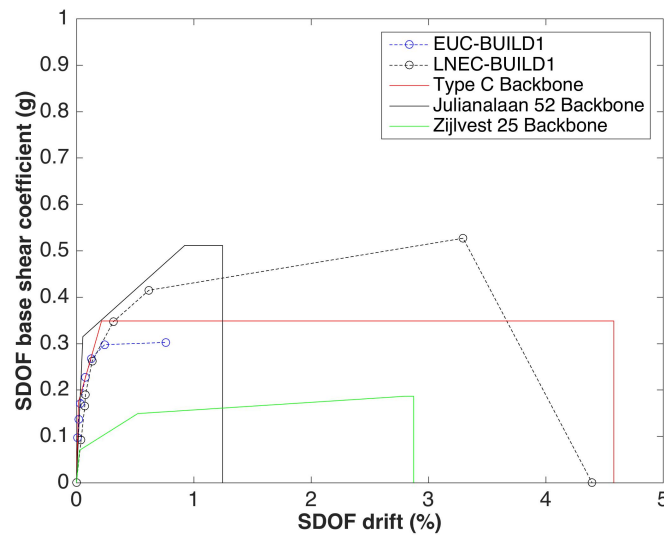


Figure 3.11 Comparison of backbone curves from experimental tests (EUC-BUILD1 and LNEC-BUILD1) with those from numerical analysis (Type C, Julianalaan, Zijlvest)

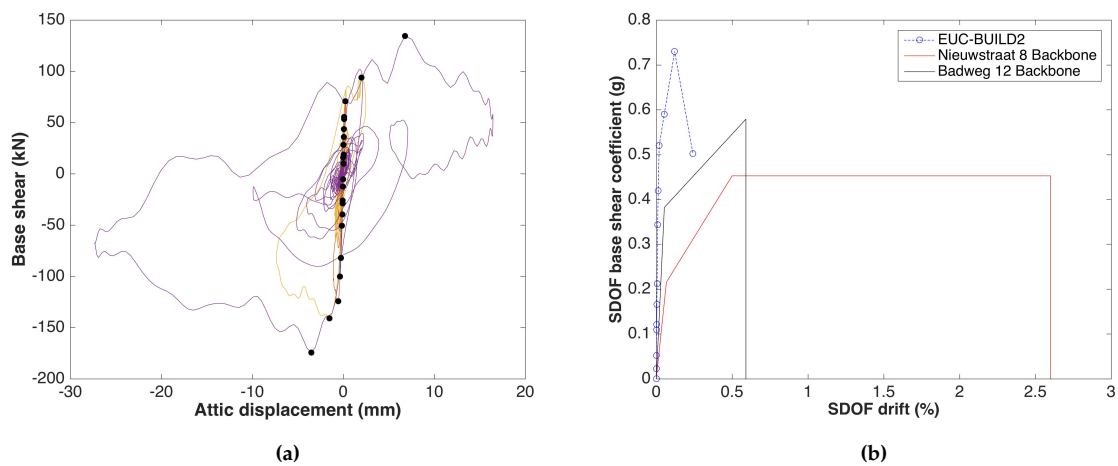


Figure 3.12 (a) Hysteretic plots from the EUC-BUILD2 shake table test and (b) SDOF comparison with the Nieuwstraat 8 and Badweg 12 backbone curves

degraded unloading stiffness based on ductility, a Takeda response (Takeda et al., 1970) can be obtained. Multilinear, on the other hand, is a uniaxial multilinear material model, which does not exhibit any stiffness or strength degradation.

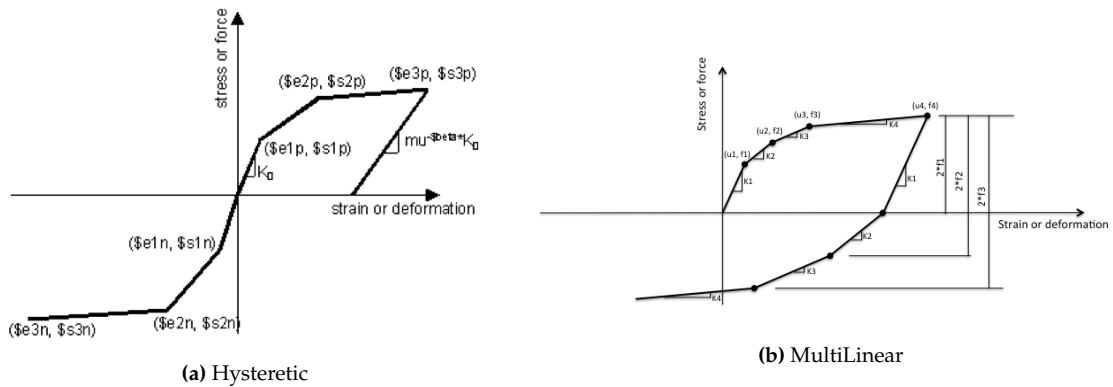


Figure 3.13 OpenSees material models

In general, the Takeda model has been used for URM buildings and the multilinear model has been used for non-URM buildings. In order to calibrate the parameters of the hysteretic models (beta and damping), the same records used to run the MDOF nonlinear dynamic analyses discussed in Chapter 2 have been applied to each SDOF model, and a comparison of the nonlinear response has been made to ensure that the records leading to collapse (of the MDOF models) were correctly identified by the SDOF model, and that the average ratio of the displacement response of the SDOF model to the original MDOF model across all records was ≥ 1 (i.e. to ensure that any bias introduced by the model was at least conservative).

3.1.5 Final SDOF models

Tables 3.1 and 3.2 present the final properties of the SDOF models from both the index buildings presented in Chapter 2 as well as some based on HAZUS (FEMA, 2004) for standard structural systems in steel and concrete (for which it was not deemed necessary to analyse specific Groningen-based index buildings, given that they do not differ from the same structural systems already studied in other parts of the World), or based on a combination of the index building results and the HAZUS capacity curves (for example, to produce higher-rise versions of the index buildings). The remaining structural systems have been assumed to be represented by a proxy system, as presented in Table 3.3.

Table 3.1 Properties of the OpenSees SDOF models (1)

Index Building	Structural System	M _{eff} (t)	H _{eff} (m)	T (s)	D1 (m)	D2 (m)	D3 (m)	BS1 (kN)	BS2 (kN)	BS3 (kN)
Precast RC post and beam	CR+PC/LPB/CR+PC/LPB/EWN/FN/HBET:1,2	710	6.5	0.92	0.006	0.1	0.218	200	730	730
Precast RC wall-slab-wall	CR+PC/LWAL/CR+PC/LN/EWN/FC/HBET:1,2	97	4.1	0.17	0.005	0.1	0.120	180	180	180*
Cast-in-place RC post and beam	CR+CIP/LPB/CR+CIP/LPB/EWN/FN/HBET:1,2	719	6.5	1.07	0.008	0.125	0.218	200	720	800
Cast-in-place RC wall-slab-wall	CR+CIP/LWAL/CR+CIP/LN/EWN/FC/HBET:1,2	69	4.5	0.44	0.005	0.127	0.18	70	230	230
De Haver	MUR/LH/MUR/LH/EWN/FW/HBET:1,2	745	3.3	0.164	0.001	0.01	0.021	1100	2500	2500
De Haver (no house)	W/LPB/W/LPB/EW/FW/HBET:1,2	576	2.9	0.25	0.002	0.01	0.026	700	1500	1500
Solwerderstraat 55	MUR/LWAL/MUR/LN/EWN/FW/HBET:1,2	106	5.396	0.298	0.003	0.033	0.138	150	600	600
Julianalaan 52	MUR/LWAL/MUR/LN/EW/FC/HBET:1,2	130	3.92	0.166	0.002	0.036	0.049	400	650	650
Zijlvest 25	MUR/LWAL/MUR/LN/EW/FC/HBET:1,2/IRIR+IRVP:CHV	219	3.75	0.238	0.001	0.02	0.107	150	320	400
Koeriersterweg 20-21	MUR/LWAL/MUR/LN/EW/FC/HBET:3,20	409	6.34	0.486	0.011	0.038	0.099	750	1000	1000
Nieuwstraat 8	MUR/LWAL/MUR/LWAL/EWN/FW/HBET:1,2	47	3	0.193	0.002	0.015	0.074	100	210	210
Kwelder 1	MUR/LWAL/MUR/LWAL/EW/FC/HBET:1,2	96	2.75	0.079	0.0005	0.008	0.119	300	550	550
Schuitenzandflat 2-56	MUR/LWAL/MUR/LWAL/EW/FC/HBET:3,20	1300	12.39	0.359	0.0075	0.056	0.118	3000	6000	6000
Badweg 12	MUR/LWAL/MUR/LWAL/EW/FW/HBET:1,2	44	2.81	0.126	0.0015	0.005	0.017	165	185	250
Kwelder 8	W/LWAL/W/LWAL/EW/FW/HBET:1,2	17.7	2.8	0.17	0.002	0.04	0.12	50	90	90
Steenweg 19	S/LFM/S/LFM/EWN/FC/HBET:1,2	334	6.3	1.20	0.11	0.225	0.48	1000	1000	1000
Glulam portal frame	S/LFBR/W/LPB/EWN/FN/HBET:1,2	32	4.0	0.31	0.015	0.25	0.64	200	350	350
Beneluxweg 15	S/LFBR/S/LPB/EWN/FN/HBET:1,2	20.3	3.8	0.14	0.005	0.21	0.295	200	280	275
HAZUS S2L	S/LFBR/S/LFBR/EWN/FC/HBET:1,2	334	5.5	0.40	0.004	0.008	0.219	328	655	655
Precast RC wall-slab-wall + HAZUS	CR+PC/LWAL/CR+PC/LN/EWN/FC/HBET:3,20	192	5.5	0.13	0.001	0.1	0.12	504	924	924
Cast-in-place RC wall-slab-wall + HAZUS	CR+CIP/LWAL/CR+CIP/LN/EWN/FC/HBET:3,20	94	6.0	0.32	0.005	0.023	0.099	168	353	353
HAZUS S2M	S/LFBR/S/LFBR/EWN/FC/HBET:3,20	438	13.7	0.85	0.015	0.031	0.366	357	718	718
Steenweg 19 + HAZUS	S/LFM/S/LFM/EWN/FC/HBET:3,20	384	11.0	0.30	0.004	0.37	0.161	635	635	635
HAZUS C1L	CR+CIP/LFM/CR+CIP/LFM/EWN/FC/HBET:1,2	138	4.6	0.44	0.003	0.008	0.183	84	253	253
HAZUS C1M	CR+CIP/LFM/CR+CIP/LFM/EWN/FC/HBET:3,20	276	11.4	0.74	0.007	0.022	0.305	141	422	422
Cast-in-place RC post and beam + HAZUS	CR+CIP/LPB/CR+CIP/LPB/EWN/FN/HBET:3,20	212	10.8	0.48	0.007	0.051	0.185	252	1008	1008
Precast RC post and beam + HAZUS	CR+PC/LPB/CR+PC/LPB/EWN/FN/HBET:3,20	35.4	5.5	0.28	0.0047	0.0624	0.161	84	151	151

* The base shear does not reach the peak given in Figure 3.2a as it is assumed that the mortar added to test specimen to fill a gap between the slab and the stability wall is not typically present in Groningen buildings (or cannot be relied on), as discussed further in Brunesi et al. (2017c)

Table 3.2 Properties of the OpenSees SDOF models (2)

Index Building	Structural System	Hysteretic model	Beta	Damping
Precast RC post and beam	CR+PC/LPB/CR+PC/LPB/EWN/FN/HBET:1,2	Multilinear	N/A	0.02
Precast RC wall-slab-wall	CR+PC/LWAL/CR+PC/LN/EWN/FC/HBET:1,2	Takeda	0.5	0.02
Cast-in-place RC post and beam	CR+CIP/LPB/CR+CIP/LPB/EWN/FN/HBET:1,2	Multilinear	N/A	0.02
Cast-in-place RC wall-slab-wall	CR+CIP/LWAL/CR+CIP/LN/EWN/FC/HBET:1,2	Takeda	0.6	0.02
De Haver	MUR/LH/MUR/LH/EW/FW/HBET:1,2	Multilinear	N/A	0.1
De Haver (no house)	W/LPB/W/LPB/EWN/FW/HBET:1,2	Multilinear	N/A	0.1
Solwerderstraat 55	MUR/LWAL/MUR/LN/EWN/FW/HBET:1,2	Takeda	0.4	0.02
Julianalaan 52	MUR/LWAL/MUR/LN/EW/FC/HBET:1,2	Takeda	0.75	0.02
Zijlvest 25	MUR/LWAL/MUR/LN/EW/FC/HBET:1,2/IRIR+IRVP:CHV	Takeda	0.75	0.02
Koeriersterweg 20-21	MUR/LWAL/MUR/LN/EW/FC/HBET:3,20	Takeda	0.4	0.02
Nieuwstraat 8	MUR/LWAL/MUR/LWAL/EWN/FW/HBET:1,2	Takeda	0	0.02
Kwelder 1	MUR/LWAL/MUR/LWAL/EW/FC/HBET:1,2	Takeda	0.75	0.02
Schuitenzandflat 2-56	MUR/LWAL/MUR/LWAL/EW/FC/HBET:3,20	Takeda	0.7	0.02
Badweg 12	MUR/LWAL/MUR/LWAL/EW/FW/HBET:1,2	Takeda	0.75	0.02
Kwelder 8	W/LWAL/W/LWAL/EW/FW/HBET:1,2	Multilinear	N/A	0
Steenweg 19	S/LFM/S/LFM/EWN/FC/HBET:1,2	Multilinear	N/A	0.01
Glulam portal frame	S/LFBR/W/LPB/EWN/FN/HBET:1,2	Multilinear	N/A	0.02
Beneluxweg 15	S/LFBR/S/LPB/EWN/FN/HBET:1,2	Multilinear	N/A	0.02
HAZUS S2L	S/LFBR/S/LFBR/EWN/FC/HBET:1,2	Multilinear	N/A	0.02
Precast RC wall-slab-wall + HAZUS	CR+PC/LWAL/CR+PC/LN/EWN/FC/HBET:3,20	Takeda	0.5	0.02
Cast-in-place RC wall-slab-wall + HAZUS	CR+CIP/LWAL/CR+CIP/LN/EWN/FC/HBET:3,20	Takeda	0.6	0.02
HAZUS S2M	S/LFBR/S/LFBR/EWN/FC/HBET:3,20	Multilinear	N/A	0.02
Steenweg 19 + HAZUS	S/LFM/S/LFM/EWN/FC/HBET:3,20	Multilinear	N/A	0.01
HAZUS C1L	CR+CIP/LFM/CR+CIP/LFM/EWN/FC/HBET:1,2	Multilinear	N/A	0.02
HAZUS C1M	CR+CIP/LFM/CR+CIP/LFM/EWN/FC/HBET:3,20	Multilinear	N/A	0.02
Cast-in-place RC post and beam + HAZUS	CR+CIP/LPB/CR+CIP/LPB/EWN/FN/HBET:3,20	Multilinear	N/A	0.02
Precast RC post and beam + HAZUS	CR+PC/LPB/CR+PC/LPB/EWN/FN/HBET:3,20	Multilinear	N/A	0.02

Table 3.3 Proxy assumptions for the remaining structural systems

Structural System	Proxy System
CR+PC/LWAL/CR+PC/LN/EW/FC/HBET:1,2	CR+PC/LWAL/CR+PC/LN/EWN/FC/HBET:1,2
CR+PC/LWAL/CR+PC/LWAL/EWN/FC/HBET:1,2	CR+PC/LWAL/CR+PC/LN/EWN/FC/HBET:1,2
CR+PC/LWAL/CR+PC/LWAL/EWN/FC/HBET:3,20	CR+PC/LWAL/CR+PC/LN/EW/FC/HBET:3,20
CR+PC/LWAL/CR+PC/LWAL/EW/FC/HBET:1,2	CR+PC/LWAL/CR+PC/LN/EWN/FC/HBET:1,2
CR+CIP/LWAL/CR+CIP/LN/EW/FC/HBET:1,2	CR+CIP/LWAL/CR+CIP/LN/EWN/FC/HBET:1,2
CR+CIP/LWAL/CR+CIP/LN/EW/FC/HBET:3,20	CR+CIP/LWAL/CR+CIP/LN/EWN/FC/HBET:3,20
CR+CIP/LWAL/CR+CIP/LWAL/EWN/FC/HBET:1,2	CR+CIP/LWAL/CR+CIP/LN/EWN/FC/HBET:1,2
CR+CIP/LWAL/CR+CIP/LWAL/EWN/FC/HBET:3,20	CR+CIP/LWAL/CR+CIP/LN/EWN/FC/HBET:3,20
MUR/LH/MUR/LH/EWN/FW/HBET:3,20	MUR/LH/MUR/LH/EWN/FW/HBET:1,2
MUR/LWAL/MUR/LN/EWN/FW/HBET:3,20	MUR/LWAL/MUR/LN/EWN/FW/HBET:1,2
MUR/LWAL/MUR/LN/EW/FW/HBET:3,20	MUR/LWAL/MUR/LN/EW/FW/HBET:1,2
MUR/LWAL/MUR/LWAL/EWN/FW/HBET:3,20	MUR/LWAL/MUR/LN/EWN/FW/HBET:1,2
MUR/LWAL/MUR/LWAL/EW/FW/HBET:1,2	MUR/LWAL/MUR/LN/EW/FW/HBET:1,2
MUR/LWAL/MUR/LWAL/EW/FW/HBET:3,20	MUR/LWAL/MUR/LN/EW/FW/HBET:1,2
MUR/LWAL/W/LPB/EWN/FN/HBET:1,2	S/LFBR/W/LPB/EWN/FN/HBET:1,2
MUR/LWAL/W/LPB/EWN/FN/HBET:3,20	S/LFBR/W/LPB/EWN/FN/HBET:1,2
W/LPB/W/LPB/EW/FN/HBET:3,20	W/LPB/W/LPB/EW/FN/HBET:1,2
W/LWAL/W/LN/EWN/FW/HBET:1,2	W/LWAL/W/LWAL/EW/FW/HBET:1,2
W/LWAL/W/LN/EW/FW/HBET:1,2	W/LWAL/W/LWAL/EW/FW/HBET:1,2
W/LWAL/W/LN/EW/FW/HBET:3,20	W/LWAL/W/LWAL/EW/FW/HBET:1,2
W/LWAL/W/LWAL/EWN/FW/HBET:1,2	W/LWAL/W/LWAL/EW/FW/HBET:1,2
W/LWAL/W/LWAL/EWN/FW/HBET:3,20	W/LWAL/W/LWAL/EW/FW/HBET:1,2
W/LWAL/W/LWAL/EW/FW/HBET:3,20	W/LWAL/W/LWAL/EW/FW/HBET:1,2
S/LPB/S/LPB/EWN/FN/HBET:1,2	CR+CIP/LPB/CR+CIP/LPB/EWN/FN/HBET:1,2
S/LPB/S/LPB/EWN/FN/HBET:3,20	CR+CIP/LPB/CR+CIP/LPB/EWN/FN/HBET:3,20
S/LFBR/W/LPB/EWN/FN/HBET:3,20	S/LFBR/W/LPB/EWN/FN/HBET:1,2
S/LFBR/S/LPB/EWN/FN/HBET:3,20	S/LFBR/S/LFBR/EWN/FC/HBET:3,20
S/LFBR/S/LFBR/EWN/FN/HBET:1,2	S/LFBR/S/LFBR/EWN/FC/HBET:1,2
S/LFBR/S/LFBR/EWN/FN/HBET:3,20	S/LFBR/S/LFBR/EWN/FC/HBET:3,20

3.2 Foundation Flexibility and Radiation Damping

Given the very soft soils found in the Groningen region (with V_{s30} values often less than 200 m/s), it was felt to be important to account for foundation flexibility and radiation damping in the derivation of the fragility functions (often referred to as soil-structure interaction or SSI). Dynamic soil-structure interaction (SSI) denotes the coupling between the structure and its supporting medium during an earthquake. SSI has been analysed for the derivation of fragility functions using a sub-structure approach, together with the principle of superposition (see Mylonakis et al., 2006). Given the small footprints of the buildings and the absence of basements, kinematic interaction has been considered negligible and so the free-field motion has been used as input to the SDOF system (see Figure 1.3). Impedance functions have been calculated using DYNA6.1 (GRC, 2015), based on typical shallow and deep foundation properties for detached, terraced and apartment buildings, as well shear wave velocity profiles that have been measured in the Groningen field (Kruiver et al., 2016). The impedance functions provide the horizontal stiffness and viscous damping of the soil-structure-foundation system as a function of frequency (in this application, corresponding to the yield period of vibration of each SDOF model); see Mosayk (2015b) for further details of the methodology and the details of all impedance functions.

It was felt that the non-URM models were currently more flexible than in reality (given that non load-bearing elements were not considered in the models, unlike in the case of URM buildings) and so additional foundation flexibility has not been considered for these buildings. They have thus been modelled as fixed base, and springs have only been added to the URM structural systems.

In order to identify the most probable foundation type for each URM structural system, inference rules were developed by Groningen engineers working for Arup. These rules assign a probability of having one of eight foundations types given the main lateral load resisting system (LWAL versus LF), structural layout, stiffness of the soil (where soft soils have $V_{s30} < 200$ m/s), and age of the building. The inference rules used for the masonry structural systems are presented in Figures 3.14 to 3.16. As only three foundation types were considered by Mosayk (2015b) - shallow masonry, shallow concrete and deep foundations - the values in the aforementioned figures have been summed to produce the probability of having one of these three foundations. Given the age and location of each building of a given structural system, the average age and V_{s30} value of each structural structural system across the field has been calculated from the v5 exposure database, and this has been used to infer the most probable foundation type for each structural system.

The final results show that the most probable foundation for masonry buildings with timber floors is shallow masonry, whereas the most probable foundation for masonry buildings with concrete floors is shallow concrete. None of the structural systems were found to have deep foundations as the most probable foundation. Although it is known that there are buildings in the field with deep foundations, given the low probabilities assigned to these foundation types for masonry building with walls, they are not found to be the most probable for any of the masonry structural systems.

The properties assumed for the springs (horizontal stiffness and horizontal damping) for each masonry structural system are presented in Table 3.4.

The figure consists of three tables, each representing a different age group of buildings. Each table has a main header for 'Foundation Type' and sub-headers for 'LWAL' and 'LF'. The 'LWAL' and 'LF' headers are further divided into 'Soft' and 'Stiff' soil conditions. The tables show the probability (in percentages) of various foundation types being used for different combinations of age and soil stiffness.

Age Group	Foundation Type		LWAL		LF																																																												
			Soft	Stiff	Soft	Stiff																																																											
	<table border="1"> <tr> <td rowspan="5">Shallow</td> <td>Masonry/Concrete Pad foundation</td> <td>5</td> <td>5</td> <td>5</td> <td>30</td> </tr> <tr> <td>Concrete raft foundation</td> <td>5</td> <td>5</td> <td>5</td> <td>5</td> </tr> <tr> <td>Concrete strip foundation</td> <td>20</td> <td>30</td> <td>20</td> <td>5</td> </tr> <tr> <td>Masonry strip foundation</td> <td>50</td> <td>60</td> <td>50</td> <td>60</td> </tr> <tr> <td>tot.</td> <td>80</td> <td>100</td> <td>80</td> <td>100</td> </tr> <tr> <td rowspan="5">Deep</td> <td>Filled foundation - concrete beams with timber piles</td> <td>-</td> <td>-</td> <td>-</td> <td>-</td> </tr> <tr> <td>Filled foundation - Masonry with timber piles</td> <td>20</td> <td>-</td> <td>20</td> <td>-</td> </tr> <tr> <td>Filled foundation, with concrete beams (in situ)</td> <td>-</td> <td>-</td> <td>-</td> <td>-</td> </tr> <tr> <td>Filled foundation, with concrete beams (prefab)</td> <td>-</td> <td>-</td> <td>-</td> <td>-</td> </tr> <tr> <td>tot.</td> <td>20</td> <td>0</td> <td>20</td> <td>0</td> </tr> <tr> <td colspan="7">tot. 100 100 100 100</td> </tr> </table>							Shallow	Masonry/Concrete Pad foundation	5	5	5	30	Concrete raft foundation	5	5	5	5	Concrete strip foundation	20	30	20	5	Masonry strip foundation	50	60	50	60	tot.	80	100	80	100	Deep	Filled foundation - concrete beams with timber piles	-	-	-	-	Filled foundation - Masonry with timber piles	20	-	20	-	Filled foundation, with concrete beams (in situ)	-	-	-	-	Filled foundation, with concrete beams (prefab)	-	-	-	-	tot.	20	0	20	0	tot. 100 100 100 100					
Shallow	Masonry/Concrete Pad foundation	5	5	5	30																																																												
	Concrete raft foundation	5	5	5	5																																																												
	Concrete strip foundation	20	30	20	5																																																												
	Masonry strip foundation	50	60	50	60																																																												
	tot.	80	100	80	100																																																												
Deep	Filled foundation - concrete beams with timber piles	-	-	-	-																																																												
	Filled foundation - Masonry with timber piles	20	-	20	-																																																												
	Filled foundation, with concrete beams (in situ)	-	-	-	-																																																												
	Filled foundation, with concrete beams (prefab)	-	-	-	-																																																												
	tot.	20	0	20	0																																																												
tot. 100 100 100 100																																																																	

Age Group	Foundation Type		LWAL		LF																																																												
			Soft	Stiff	Soft	Stiff																																																											
	<table border="1"> <tr> <td rowspan="5">Shallow</td> <td>Masonry/Concrete Pad foundation</td> <td>5</td> <td>5</td> <td>5</td> <td>10</td> </tr> <tr> <td>Concrete raft foundation</td> <td>5</td> <td>5</td> <td>5</td> <td>10</td> </tr> <tr> <td>Concrete strip foundation</td> <td>20</td> <td>30</td> <td>25</td> <td>35</td> </tr> <tr> <td>Masonry strip foundation</td> <td>30</td> <td>60</td> <td>25</td> <td>45</td> </tr> <tr> <td>tot.</td> <td>60</td> <td>100</td> <td>60</td> <td>100</td> </tr> <tr> <td rowspan="5">Deep</td> <td>Filled foundation - concrete beams with timber piles</td> <td>15</td> <td>-</td> <td>10</td> <td>-</td> </tr> <tr> <td>Filled foundation - Masonry with timber piles</td> <td>15</td> <td>-</td> <td>15</td> <td>-</td> </tr> <tr> <td>Filled foundation, with concrete beams (in situ)</td> <td>10</td> <td>-</td> <td>15</td> <td>-</td> </tr> <tr> <td>Filled foundation, with concrete beams (prefab)</td> <td>-</td> <td>-</td> <td>-</td> <td>-</td> </tr> <tr> <td>tot.</td> <td>40</td> <td>0</td> <td>40</td> <td>0</td> </tr> <tr> <td colspan="7">tot. 100 100 100 100</td> </tr> </table>							Shallow	Masonry/Concrete Pad foundation	5	5	5	10	Concrete raft foundation	5	5	5	10	Concrete strip foundation	20	30	25	35	Masonry strip foundation	30	60	25	45	tot.	60	100	60	100	Deep	Filled foundation - concrete beams with timber piles	15	-	10	-	Filled foundation - Masonry with timber piles	15	-	15	-	Filled foundation, with concrete beams (in situ)	10	-	15	-	Filled foundation, with concrete beams (prefab)	-	-	-	-	tot.	40	0	40	0	tot. 100 100 100 100					
Shallow	Masonry/Concrete Pad foundation	5	5	5	10																																																												
	Concrete raft foundation	5	5	5	10																																																												
	Concrete strip foundation	20	30	25	35																																																												
	Masonry strip foundation	30	60	25	45																																																												
	tot.	60	100	60	100																																																												
Deep	Filled foundation - concrete beams with timber piles	15	-	10	-																																																												
	Filled foundation - Masonry with timber piles	15	-	15	-																																																												
	Filled foundation, with concrete beams (in situ)	10	-	15	-																																																												
	Filled foundation, with concrete beams (prefab)	-	-	-	-																																																												
	tot.	40	0	40	0																																																												
tot. 100 100 100 100																																																																	

Age Group	Foundation Type		LWAL		LF																																																												
			Soft	Stiff	Soft	Stiff																																																											
	<table border="1"> <tr> <td rowspan="5">Shallow</td> <td>Masonry/Concrete Pad foundation</td> <td>5</td> <td>5</td> <td>5</td> <td>15</td> </tr> <tr> <td>Concrete raft foundation</td> <td>10</td> <td>20</td> <td>5</td> <td>15</td> </tr> <tr> <td>Concrete strip foundation</td> <td>40</td> <td>70</td> <td>40</td> <td>60</td> </tr> <tr> <td>Masonry strip foundation</td> <td>5</td> <td>5</td> <td>10</td> <td>10</td> </tr> <tr> <td>tot.</td> <td>60</td> <td>100</td> <td>60</td> <td>100</td> </tr> <tr> <td rowspan="5">Deep</td> <td>Filled foundation - concrete beams with timber piles</td> <td>20</td> <td>-</td> <td>20</td> <td>-</td> </tr> <tr> <td>Filled foundation - Masonry with timber piles</td> <td>-</td> <td>-</td> <td>-</td> <td>-</td> </tr> <tr> <td>Filled foundation, with concrete beams (in situ)</td> <td>20</td> <td>-</td> <td>20</td> <td>-</td> </tr> <tr> <td>Filled foundation, with concrete beams (prefab)</td> <td>-</td> <td>-</td> <td>-</td> <td>-</td> </tr> <tr> <td>tot.</td> <td>40</td> <td>0</td> <td>40</td> <td>0</td> </tr> <tr> <td colspan="7">tot. 100 100 100 100</td> </tr> </table>							Shallow	Masonry/Concrete Pad foundation	5	5	5	15	Concrete raft foundation	10	20	5	15	Concrete strip foundation	40	70	40	60	Masonry strip foundation	5	5	10	10	tot.	60	100	60	100	Deep	Filled foundation - concrete beams with timber piles	20	-	20	-	Filled foundation - Masonry with timber piles	-	-	-	-	Filled foundation, with concrete beams (in situ)	20	-	20	-	Filled foundation, with concrete beams (prefab)	-	-	-	-	tot.	40	0	40	0	tot. 100 100 100 100					
Shallow	Masonry/Concrete Pad foundation	5	5	5	15																																																												
	Concrete raft foundation	10	20	5	15																																																												
	Concrete strip foundation	40	70	40	60																																																												
	Masonry strip foundation	5	5	10	10																																																												
	tot.	60	100	60	100																																																												
Deep	Filled foundation - concrete beams with timber piles	20	-	20	-																																																												
	Filled foundation - Masonry with timber piles	-	-	-	-																																																												
	Filled foundation, with concrete beams (in situ)	20	-	20	-																																																												
	Filled foundation, with concrete beams (prefab)	-	-	-	-																																																												
	tot.	40	0	40	0																																																												
tot. 100 100 100 100																																																																	

Figure 3.14 Foundation inference rules for 'unit' structural layouts

Figure 3.15 Foundation inference rules for 'block' structural layouts

Figure 3.16 Foundation inference rules for 'barn' structural layouts

Table 3.4 Modal foundation types and spring properties for URM structural systems

Structural System	Foundation Type	Horiz. Stiffness (kN/m)	Horiz. Damping (kN/m/s)
MUR/LH/MUR/LH/EWN/FW/HBET:1,2	Shallow masonry	2.25E+05	11280
MUR/LWAL/MUR/LN/EWN/FW/HBET:1,2	Shallow masonry	2.45E+05	13340
MUR/LWAL/MUR/LN/EW/FC/HBET:1,2	Shallow concrete	1.80E+05	8894
MUR/LWAL/MUR/LN/EW/FC/HBET:1,2/IRIR+IRVP:CHV	Shallow concrete	1.89E+05	8796
MUR/LWAL/MUR/LN/EW/FC/HBET:3,20	Shallow concrete	2.15E+05	7914
MUR/LWAL/MUR/LWAL/EWN/FW/HBET:1,2	Shallow masonry	1.33E+05	6028
MUR/LWAL/MUR/LWAL/EW/FC/HBET:1,2	Shallow concrete	9.42E+04	4350
MUR/LWAL/MUR/LWAL/EW/FC/HBET:3,20	Shallow concrete	2.06E+05	8577
MUR/LWAL/MUR/LWAL/EW/FW/HBET:1,2	Shallow masonry	1.22E+05	6166

3.3 Nonlinear Dynamic 'Cloud' Analysis

For the development of fragility functions, which describe the probability of exceeding a given damage or collapse state under increasing levels of ground shaking intensity, a model for the probabilistic relationship between ground motion intensity and the nonlinear structural response of the SDOF system is needed. The approaches that are commonly used for estimating this probabilistic relationship include the cloud method (Jalayer, 2003), the multiple-stripe method (Jalayer, 2003) and Incremental Dynamic Analysis (IDA) (Vamvatsikos and Cornell, 2002). The cloud method has been selected for the derivation of fragility functions herein due to its simplicity.

The cloud method is typically applied using an assumption of linear variation in the logarithmic space of the structural response with the intensity measure (IM) and homoscedasticity of the residuals (see e.g. Baker, 2007). As this method traditionally does not account for the changing earthquake events that contribute to the hazard at different intensity levels (as can be employed with multiple stripe methods), independence of the selected IM to various other properties of the accelerograms needs to be ensured (so-called "sufficiency" of the IM). Admittedly, it would also be possible to use hazard-dependent record selection together with the cloud method, but given that this would require the output of the seismic hazard model to be available *a priori* (whereas instead all components of the risk assessment are currently developed in parallel), the simpler approach of using a wide range of records, and ensuring sufficiency, has instead been chosen herein.

The cloud method has hence been employed using a large suite of records to reduce the effort required to select/scale the records that would be appropriate to capture the nonlinear response of each different structural system. Thus, by applying the same large number of records to all structures, a wide range of nonlinear structural response (from pre-yield to collapse) can be captured for all typologies, together with an adequate modelling of the record-to-record variability.

3.3.1 Selection of records

A database of over 4000 accelerograms has been set up for the nonlinear dynamic analyses, by combining recordings from the NGA1 (Chiou et al., 2008), European (Akkar et al., 2014) and Groningen databases (Bommer et al., 2016). The magnitude, epicentral distance and 5-75% significant duration for each accelerogram have been obtained/calculated, and it has been ensured that they cover the range of these parameters used in the probabilistic risk assessment for the Groningen field. In particular, the magnitude range has been taken to be between 3.5 and 6.5, and epicentral distances up to 60 km have been used.

The latest ground-motion prediction equation (GMPE) for the risk assessment (Bommer et al., 2017) predicts the arbitrary component of spectral acceleration. This choice of component, as opposed to the geometric mean, has allowed the spectral acceleration at a

given period of vibration for a given horizontal component of ground shaking to be directly plotted against its predicted nonlinear dynamic response, thus requiring less dynamic analyses to predict the dispersion in response with a given level of confidence (see e.g. Baker and Cornell, 2006). For this reason, it has been possible to separately use both horizontal components of recordings in the aforementioned databases. The records have been scaled by a maximum factor of 2 only when most of the original records were not strong enough to push the structure beyond the yield displacement (which only occurred for one steel structural system).

3.3.2 Multivariate linear regression

The nonlinear dynamic analyses of each SDOF system have been undertaken in OpenSees (McKenna et al., 2000). Given that the focus is currently on predicting the nonlinear behavior after structural damage, the response data below 80% of the yield displacement has been removed; the aleatory variability in the pre-yield response is much lower than its post-yield counterpart (and is zero when the same damping is considered in the SDOF system and spectral ordinates), and so removing these points helps to create a set of data that is more likely to be homoscedastic (i.e. with constant variance, regardless of the intensity of the ground motion). Furthermore, the aforementioned assumption of a linear relationship between the logarithm of response and the IM is also more reasonable when the data is focused only on the nonlinear response. Nevertheless, for each SDOF model, it has been checked that the hypotheses of a linear relationship and homoscedasticity were reasonable.

Once the maximum nonlinear dynamic displacement response of a given SDOF (S_d) is obtained from all n ground-motion records, each response (d_i) is plotted against a scalar/vector intensity measure ($IM=[IM_i, i=1:m]$ where m indicates the number of variables that define the vector) and the statistical parameters corresponding to the lognormal distribution of $S_d | IM$ can be extracted. In particular, the expected value, $E[\ln S_d | IM]$, is modelled by a linear regression equation (Equation 3.5) with parameters b_0 and b_i ($i=1, \dots, m$), whilst the standard deviation or dispersion (Equation 3.6) is estimated by the standard error of the regression:

$$E[\ln S_d | IM] = \ln \eta_{S_d | IM} = b_0 + b_1 \ln(IM_1) + b_2 \ln(IM_2) + \dots + b_m \ln(IM_m) \quad (3.5)$$

$$\beta_{S_d | IM} \approx \sqrt{\frac{\sum_i^n (\ln(d_i) - \ln \eta_{S_d | IM})^2}{n - (m + 1)}} \quad (3.6)$$

As mentioned above, the parameters b_0 and b_i are the estimated regression coefficients obtained by performing a multivariate linear regression. In order to correctly treat the results of the nonlinear dynamic analyses where the displacement response exceeds the expected ultimate displacement capacity (and thus these SDOF systems are deemed to

have exceeded the collapse limit state and the estimated displacement response is no longer reliable), a censored regression has been undertaken when estimating the coefficients of Equation 3.5 (see Stafford, 2008). In these cases, the value of displacement demand from the nonlinear dynamic analysis is not trusted, but it is known to exceed a given limiting value, and is thus referred to as a censored observation. If all censored observations were set to the limiting value, and a normal linear regression analysis were to be applied as above, the fitted model would be biased. To obtain an unbiased model, maximum likelihood technique is used. The likelihood function for a model with n observations, where $\ln S_d|IM$ is given by Equation 3.5 is:

$$Likelihood = \prod_i^n \phi\left(\frac{\ln(d_i) - \ln \eta_{S_d|IM}}{\beta_{S_d|IM}}\right) \quad (3.7)$$

where $\phi(z)$ is the probability density function for the standard normal distribution. However, rather than finding the values of the coefficients of Equation 3.5 that maximize L , it is necessary to minimize the negative of the log-likelihood function, given by:

$$\ln(Likelihood) = \sum_i^n \ln \phi\left(\frac{\ln(d_i) - \ln \eta_{S_d|IM}}{\beta_{S_d|IM}}\right) \quad (3.8)$$

With the presence of censored variables the likelihood function becomes:

$$Likelihood = \prod_j^{n_c} \left[1 - \Phi\left(\frac{\ln(d_i) - \ln \eta_{S_d|IM}}{\beta_{S_d|IM}}\right)\right] \prod_i^{n_0} \phi\left(\frac{\ln(d_i) - \ln \eta_{S_d|IM}}{\beta_{S_d|IM}}\right) \quad (3.9)$$

where there are n_c censored observations and n_0 observed (uncensored) values and $n_c + n_0 = n$. The $\Phi(z)$ function is the cumulative standard normal distribution function. Taking the logarithm of this expression, as before, gives:

$$\ln(Likelihood) = \sum_j^{n_c} \ln \left[1 - \Phi\left(\frac{\ln(d_i) - \ln \eta_{S_d|IM}}{\beta_{S_d|IM}}\right)\right] + \sum_i^{n_0} \ln \phi\left(\frac{\ln(d_i) - \ln \eta_{S_d|IM}}{\beta_{S_d|IM}}\right) \quad (3.10)$$

An example cloud data plot with censored regression is shown in Figure 3.17, where the censored observations have been plotted at the limiting displacement capacity value. The cloud plots for all structural systems are presented in Appendix C.

Although it is common to check the sufficiency of the IM with respect to magnitude and distance (see e.g. Luco and Cornell, 2007), the dependence on a measure of ground shaking duration has also been considered herein, given the evidence from previous studies that the response of unreinforced masonry structures (and other strength and stiffness degrading systems) is dependent on the duration of strong ground shaking (e.g. Bommer et al., 2004). In order to define the best duration definition to adopt to describe the nonlinear response

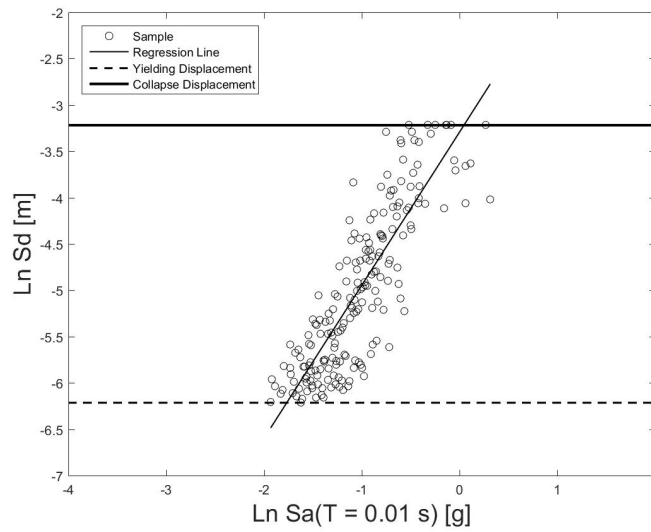


Figure 3.17 Example cloud data plot with censored regression

of Groningen buildings, a sensitivity study has been carried out using 27 different duration definitions (including bracketed, uniform and significant durations). This study has shown that, as expected (see e.g. Bommer et al., 2004), the uniform duration correlates the best to the displacement demand, usually providing the lowest standard deviation of residuals (even if the results obtained using the other definitions were not considerably different). However, its inclusion in the IM vector did not often guarantee the sufficiency with respect to the seismological parameters of interest, a condition that was usually achieved when a significant duration (for any of the various percentages of Arias Intensity used in the study) was adopted instead. For these reasons, the significant duration definition D_{S5-75} (i.e. the time interval between the attainment of 5% and 75% Arias Intensity) is used herein, given that a duration model for this metric has already been developed for the Groningen gas field (Bommer et al., 2017).

Four different scalars/vectors of intensity measures have been checked for sufficiency: $IM=[Sa(T_1)]$; $IM=[Sa(T_1) D_{S5-75}]$; $IM=[Sa(T_1) Sa(T_2)]$ and $IM=[Sa(T_1) Sa(T_2) D_{S5-75}]$; where Sa is the spectral acceleration, T_1 is the period selected from all potential periods in the application-specific GMPE which leads to the highest “efficiency” (i.e. lowest standard deviation according to Equation 3.6), T_2 is a second period selected according to the same approach, and D_{S5-75} is the 5-75% significant duration. It is important to note that when cloud analysis is used together with a vector IM, it can be difficult to separate the effects of each IM parameter when they are highly correlated, a condition referred to as collinearity (see e.g. Baker, 2007). For this reason, the Pearson coefficient (an index measuring the correlation between the IM parameters) has also been calculated and vectors where the parameters were characterised by a high correlation have been excluded. Where more than one of the four IM scalars/vectors represented sufficient IMs, and since they usually provided similar efficiency, the selected IM scalar/vector was the one with the least parameters and, in the case of an IM vector, the lowest Pearson coefficient.

3.3.3 Influence of building-to-building variability

The cloud plots discussed in the previous Section and included in Appendix C have been developed considering a single index building that is assumed to represent a median building within the population (also because, as described in Section 2.1.2, the characteristics of the selected index buildings were typically representative of the modal parameters found in the building exposure model).

The variation in stiffness and strength across the buildings of a given structural system is assumed to increase the dispersion of the cloud response. An additional dispersion of 0.1 has been added to the cloud response to account for this building-to-building variability when producing the fragility functions, as described further in Chapter 4.

In order to check this assumption, cloud plots for Type C and Julianalaan 52 have been compared. These buildings both have the same structural system, but Type C has one storey and Julianalaan has two storeys. The backbone curves of these index buildings were presented previously in Figure 3.4. The base shear coefficient of Julianalaan is 1.5 times that of Type C and the initial stiffness of Julianalaan is 40% of Type C. The cloud plots and regression analysis of the two models have been plotted on top of each other in Figure 3.18. The linear regression is seen to be very similar, and dispersion values of 0.44 (Julianalaan) and 0.45 (Type C) were found, respectively. By randomly selecting half of the response points of each building, and redoing the regression analysis, the dispersion is found to be 0.45. Hence it is clear that the influence of stiffness and strength is much lower than the record-to-record variability and it seems reasonable to add a small additional component of dispersion to account for the influence of stiffness and strength variation on the regression. Furthermore, the difference in ultimate collapse capacity (not considered here) will have a much higher influence on the fragility than the difference in stiffness and strength. This variability is accounted for in the dispersion of the damage/collapse state thresholds, as discussed further in Chapter 4.

3.3.4 Model Uncertainty

In addition to the aleatory variability in the displacement response due to record-to-record and building-to-building variability described above, an epistemic (model) uncertainty has also been included in the analyses. This model uncertainty accounts for inaccuracies in the structural models used to represent the response of a 'real' median building of a given structural system. The values of model uncertainty recommended in FEMA P-58 (FEMA, 2012) have been used herein. The two main sources of model uncertainty there are considered comprise 'level of building definition and construction quality assurance', β_c , which represents the fact that the actual properties of the structural elements might differ from those that have been assumed, and 'quality and completeness of the analytical model', β_q , which recognises that hysteretic models may not accurately capture the behaviour of structural components.

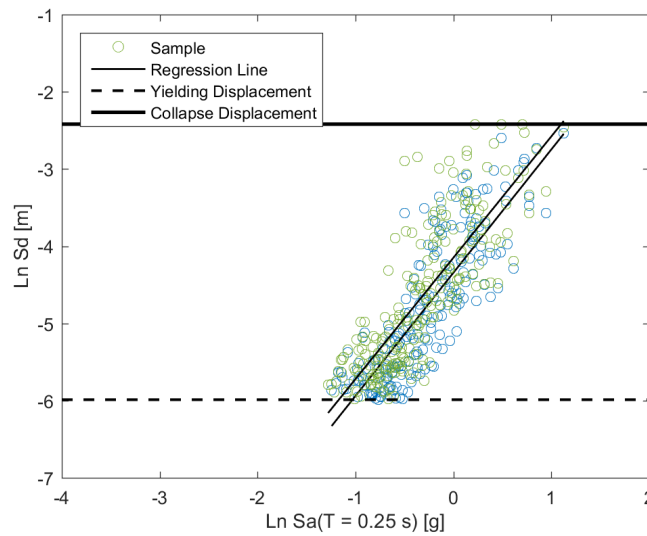


Figure 3.18 Cloud plots of two index buildings with the same structural system but different number of storeys, strength and stiffness: Julianalaan 52 (blue) and Type C (green)

URM Buildings

For URM structures, documents defining the building design are available and have been used in the models and these have been confirmed by visual inspection. Furthermore, the material properties have been confirmed by material testing. However, this high quality data is available for specific index buildings whereas the fragility functions presented herein are not being applied just to these structures, hence β_c will be larger for the class of buildings than the index buildings. The model uncertainty due to construction quality assurance is thus assessed as 'average' and the value of dispersion is taken as 0.25, as suggested in FEMA P-58.

For what concerns the quality of the analytical model, due to the extensive cross validation of the LS-DYNA and ELS software (see Section 2.2), the quality of the analytical model has been assessed as 'superior' and a value of dispersion of 0.1 is assigned, as recommended in FEMA P-58.

The total model uncertainty for URM buildings, β_m , is then given by the SRSS of 0.1 and 0.25, which is equal to 0.27.

Non-URM Buildings

Knowledge of the non-URM structures in Groningen is based on limited field investigations and material properties are based on default values typical for buildings of the type, location and age of construction, and so the construction quality assurance has been herein assessed as 'limited', leading to a value of dispersion of 0.4.

As discussed in Section 2.2, an evaluation of the software used to assess non-URM buildings (SeismoStruct) against numerous experimental tests has been carried out (Mosayk, 2014), and this demonstrates the reliability of the software to predict the response of these types of

structures. However, not all non-structural elements are included in the models and some failure modes are simulated indirectly. According to FEMA P-58, the quality of the analytical model would thus be assessed as 'average' and hence a value of dispersion of 0.25 has been assigned.

The total model uncertainty for non-URM buildings, β_m , is then given by the SRSS of 0.25 and 0.4, which is equal to 0.47.

Logic Tree

Given that inaccuracies in the structural models used to represent the response of a 'real' median building will introduce a bias in the response of all the buildings belonging to a given structural system, the model uncertainty is not modelled as an aleatory variable (as instead were the record-to-record and building-to-building uncertainties), but rather through the use of a logic tree. For computational efficiency, only three branches have been considered on the logic tree, and hence the model uncertainty has been modelled as a discrete three-point distribution.

The values of modelling uncertainty dispersion for URM and non-URM buildings described above, have been used to produce a three-point discrete distribution (in terms of number of standard deviations and associated probabilities) following the approach given in Miller and Rice (1983). These three levels of model uncertainty (corresponding to standard deviations of -1.73, 0 and 1.73) have then been added to Equation 3.5 to produce lower, middle and upper fragility models with associated weights (w) given by the discrete probabilities of each level (i.e. 0.17, 0.66 and 0.17), as illustrated in Figure 3.19.

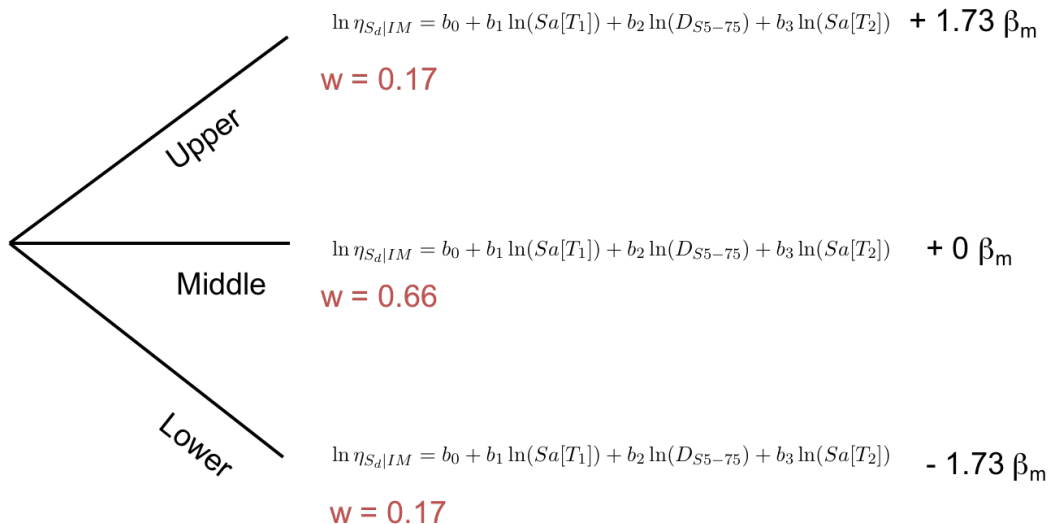


Figure 3.19 Fragility model logic tree for each structural system

Chapter 4

Damage and Collapse Fragility Functions

4.1 Introduction

The regression analyses described in the previous chapter allow equations to be derived that relate the level of shaking with an estimate of the displacement response of an equivalent SDOF system (S_d). By identifying the thresholds to damage or collapse in terms of SDOF displacements (or drifts, obtained by dividing the SDOF displacement by the effective height of the SDOF), it is possible to produce fragility functions that describe the probability of exceeding a number of distinct damage/collapse states. The variability in these damage/collapse state thresholds (β_{DL}) should be accounted for in the dispersion of the response, and can be combined with the the record-to-record variability (β_R) and the building-to-building variability in terms of the stiffness and strength of the backbone curve (β_{BB}):

$$\beta_s = \sqrt{\beta_R^2 + \beta_{BB}^2 + \beta_{DL}^2} \quad (4.1)$$

The damage/collapse state threshold variability has been assumed constant here for the simplification of the risk engine ¹, with a value of 0.3 has been assumed herein, based on studies in the literature (e.g. Dymiotis et al., 1999; Borzi et al., 2008).

The probability of exceeding the limit displacement to each structural damage or collapse state i under a given level of ground shaking is calculated as follows:

$$P_{eDLDSi} = 1 - \Phi\left(\frac{\ln(DLDSi) - \ln \eta_{S_d|IM}}{\beta_s}\right) \quad (4.2)$$

$$P_{eDLCSi} = 1 - \Phi\left(\frac{\ln(DLCSi) - \ln \eta_{S_d|IM}}{\beta_s}\right) \quad (4.3)$$

¹In future versions of the engine, the variation of dispersion with damage state may be considered

where

$$\ln \eta_{S_d|IM} = b_0 + b_1 \ln(Sa[T_1]) + b_2 \ln(D_{S5-75}) + b_3 \ln(Sa[T_2]) \quad (4.4)$$

and $\Phi()$ is the cumulative distribution function of the standard normal distribution, b_0 to b_3 are coefficients obtained from multivariate linear regression, DL is the displacement limit of each damage or collapse state (provided in metres), T_1 and T_2 are periods of vibration, and β_s is the total dispersion (due to record-to-record variability, backbone stiffness and strength variability and damage/collapse state threshold variability). $Sa(T)$ is the spectral acceleration (in g) for a given period of vibration (T_1 or T_2) and D_{S5-75} is the 5-75% significant duration (in seconds), as provided by the hazard calculations of the risk engine.

The damage and collapse states presented herein are sequential. Only the collapse states are used in the fatality risk calculations, whereas, as discussed in Section 1.3, only damage states DS2 and DS3 are used in the group damage curves (though DS4 is also provided for completeness). The following two sections present the definition of the damage and collapse states.

4.2 Damage Limit States

The damage states considered herein have mainly been defined considering damage observed in experimental tests, but they are consistent with the EMS98 damage scale (Grunthal et al., 1998) where damage state 1 (DS1) refers to slight non-structural damage comprising hairline cracks in plaster and partition walls, DS2 refers to slight structural damage, DS3 to moderate damage, DS4 to extensive damage. The main difference with respect to EMS98 is that collapse states are not considered as part of these standard damage scales, and are treated separately, as discussed in Section 4.3 below. The current efforts to identify damage thresholds have not yet enabled a robust evaluation of the threshold to DS1, and thus only structural damage states (from DS2 to DS4) are considered in this report.

4.2.1 Unreinforced Masonry (URM) Buildings

The drift levels at which damage occurs in the URM buildings has been informed by the large testing campaign that has been carried out on components and structures that match the construction practices and materials used in the Groningen field. A specific report focusing on the damage observed in the numerous tests has been compiled (Graziotti et al., 2017b), and the results in terms of the damage descriptions and levels of attic displacement have been used to identify SDOF drift limits to damage ($\theta_{SDOF_{DLi}}$).

The damage states for URM buildings are defined as follows:

DS2: minor structural damage. It has been determined a the onset of cracking in primary resisting elements. The observed damage could be easily repaired.

DS3: significant structural damage. This level of performance was associated with a damage observed in all the piers contributing to the in-plane response of the building.

DS4: severe damage (leading to demolition) associated to loss of stiffness and strength of the structural elements contributing to the lateral resistance.

After each stage of the shake-table testing sequence, detailed surveys were carried out and have allowed the maximum achieved top floor (attic) drift (%) at which a given level of damage was *not* observed to be obtained. These values have been used to identify the attic limit state displacements for each damage state (DL_i), which have then been transformed to SDOF drift levels by dividing by the transformation factor and the effective height, using Equations 3.1 and 3.4, respectively. It is noted that the values reported in Table 4.1 are slightly different to those reported in Graziotti et al.(2017b) as the SDOF system calculations used herein assume that the roof mass is located at the attic height.

Table 4.1 SDOF drift limits for each damage state, as observed in the URM shake-table tests

Shake-table Test	$\theta_{SDOF,DL2}$ (%)	$\theta_{SDOF,DL3}$ (%)	$\theta_{SDOF,DL4}$ (%)
EUC-BUILD1	0.09	0.26	0.77
LNEC-BUILD1	0.13	0.30	0.59
EUC-BUILD2	0.01	0.25	0.94
Average	0.08	0.27	0.77

In order to calculate the threshold SDOF displacements (S_{di}) for each building typology, the average SDOF drifts reported in Table 4.1 have been multiplied by the effective height of each building typology.

4.2.2 Reinforced Concrete (RC) Buildings

The drift levels at which damage is predicted to occur in reinforced concrete buildings has been informed by the recent cyclic and dynamic tests on cast-in-place and precast RC specimens (see Brunesi et al., 2017a; 2017b; 2017c). The results in terms of the damage descriptions and levels of attic displacement and associated SDOF drift have been used to identify the appropriate damage limits for the fragility functions.

The damage states are defined for the cast-in-place specimen as follows:

DS2: full-depth hairline cracks at base of walls, and also cracks appearing at wall-slab joints.

DS3: Hairline cracks lengthen and extend, though with limited opening. Strength degradation begins.

DS4: Wider cracks have appeared and spread, and the strength drop is of the order of 20%.

The damage states are defined for the precast specimen as follows:

DS2: narrow cracks initiate around the wall connectors.

DS3: sliding of the slabs above walls and permanent flexural deformation in the connectors leading to residual displacements. Strength degradation initiates.

DS4: Heavy damage with permanent crack opening of 1 cm between transverse and stability walls. The structure is considered to be near collapse.

The values of SDOF drift at which each of the aforementioned damage states were reached in the EUC-BUILD 3 and EUC-BUILD4 cyclic tests are presented in Table 4.2.

Table 4.2 SDOF drift limits for each damage state, as observed in the RC cyclic tests

Shake Table Test	$\theta_{SDOF,DL2}$ (%)	$\theta_{SDOF,DL3}$ (%)	$\theta_{SDOF,DL4}$ (%)
EUC-BUILD3 (cast-in-place)	0.8	1.25	3.0
EUC-BUILD4 (pre-cast)	0.14	0.50	1.15

The values presented in Table 4.2 have been used for the low-rise precast wall-slab-wall and low-rise and mid-to-high rise cast-in-place wall-slab-wall structural systems in the v5 exposure model. For all other structural systems, the recommendations of HAZUS (FEMA, 2004) for pre-code RC buildings have been used, as presented in Table 4.3.

Table 4.3 SDOF drift limits for each damage state, based on values in HAZUS (FEMA, 2004)

Structural System	$\theta_{SDOF,DL2}$ (%)	$\theta_{SDOF,DL3}$ (%)	$\theta_{SDOF,DL4}$ (%)
Cast-in-place wall-slab-wall mid-rise	0.54	0.84	2.0
Cast-in-place frame low-rise	0.4	0.64	1.6
Cast-in-place frame mid to high-rise	0.27	0.43	1.1
Cast-in-place post and beam low-rise	0.4	0.64	1.6
Cast-in-place post and beam mid to high-rise	0.27	0.43	1.1
Precast post and beam low-rise	0.4	0.64	1.6
Precast post and beam mid to high-rise	0.27	0.43	1.1

4.2.3 Timber and Steel Buildings

Unlike the URM and RC Groningen building types, which require bespoke damage limit states (as they feature a number of construction details that are not typically found in other parts of the world), standard limit state definitions are assumed to apply to the timber and steel constructions. The SDOF drift limit states to damage recommended by HAZUS (FEMA, 2004) have been adopted herein. The following descriptions of the damage states are provided in HAZUS, whilst the damage limits/thresholds to each damage state are provided in Table 4.4 in terms of SDOF drift.

Wood, Light Frame

DS2: Small plaster or gypsum-board cracks at corners of door and window openings and wall-ceiling intersections; small cracks in masonry chimneys and masonry veneer.

DS3: Large plaster or gypsum-board cracks at corners of door and window openings; small diagonal cracks across shear wall panels exhibited by small cracks in stucco and gypsum wall panels; large cracks in brick chimneys; toppling of tall masonry chimneys.

Table 4.4 SDOF drift limits to damage for steel and timber systems, based on values in HAZUS (FEMA, 2004)

Structural System	$\theta_{SDOF,DL2}$ (%)	$\theta_{SDOF,DL3}$ (%)	$\theta_{SDOF,DL4}$ (%)
Wood, Light Frame	0.32	0.79	2.45
Steel, Light Braced Frame	0.4	0.64	1.6
Steel, Moment Frame low-rise	0.48	0.76	1.62
Steel, Moment Frame mid to high-rise	0.32	0.51	1.1
Steel, Braced Frame low-rise	0.4	0.64	1.6
Steel, Braced Frame mid to high-rise	0.27	0.43	1.1

DS4: Large diagonal cracks across shear wall panels or large cracks at plywood joints; permanent lateral movement of floors and roof; toppling of most brick chimneys; cracks in foundations; splitting of wood sill plates and/or slippage of structure over foundations; partial collapse of “room-over-garage” or other “soft-story” configurations; small foundations cracks.

Steel, Light Braced Frame

These structures are mostly single storey structures combining rod-braced frames in one direction and moment frames in the other. Due to the repetitive nature of the structural systems, the type of damage to structural members is expected to be rather uniform throughout the structure.

DS2: Few steel rod braces have yielded which may be indicated by minor sagging of rod braces. Minor cracking at welded connections or minor deformations at bolted connections of moment frames may be observed.

DS3: Most steel braces have yielded exhibiting observable significantly sagging rod braces; few brace connections may be broken. Some weld cracking may be observed in the moment frame connections.

DS4: Significant permanent lateral deformation of the structure due to broken brace rods, stretched anchor bolts and permanent deformations at moment frame members. Some screw or welded attachments of roof and wall siding to steel framing may be broken. Some purlin and girt connections may be broken.

Steel, Moment Frame

DS2: Minor deformations in connections or hairline cracks in few welds.

DS3: Some steel members have yielded exhibiting observable permanent rotations at connections; few welded connections may exhibit major cracks through welds or few bolted connections may exhibit broken bolts or enlarged bolt holes.

DS4: Most steel members have exceeded their yield capacity, resulting in significant permanent lateral deformation of the structure. Some of the structural members or connections may have exceeded their ultimate capacity exhibited by major permanent member rotations at connections, buckled flanges and failed connections. Partial collapse of portions of structure is possible due to failed critical elements and/or connections.

4.2.4 Summary of damage limit states

Table 4.5 presents the final SDOF drift limits to damage that have been assigned to all models.

4.3 Collapse Limit States

4.3.1 Collapse states from dynamic analysis of URM buildings

A detailed description of the collapse mechanisms observed in each of the nonlinear dynamic analyses that have been run in either LS-DYNA or ELS, described in Chapter 2, has been produced. The time in the analysis at which the collapse mechanism was initiated has been identified, and the maximum attic displacement up until that point in the analysis has been reported. It has been possible to identify a weaker direction of the building in all models; this is the direction that has a lower base shear capacity and in which global collapse is initiated. This direction has thus been used for the development of the fragility functions, and so the attic displacement in this weaker direction has been extracted in all cases.

Three collapse states per building (with the third being global collapse) have been selected for the development of fragility functions. The collapse states have been assumed to be sequential, with increased consequences from one collapse state to the next (similar to the damage states). The observed collapse states, and associated SDOF drifts, are presented for each index building in detail in Appendix E.

4.3.2 Collapse states for non-URM buildings

For non-URM (light steel frame, light timber frames, concrete wall/slab) collapse is not explicitly modelled. Instead, collapse mechanisms are defined in terms of unseating (for some timber/RC buildings) or exceedance of joint rotations, and these have been associated to a given value of attic displacement and SDOF drift for each model, as discussed further in Mosayk (2015a). Only one collapse state has been considered for non-URM structures.

Table 4.5 SDOF drift limits to damage for all models

Index Building	Structural System	$\theta_{SDOF,DL2}$	$\theta_{SDOF,DL3}$	$\theta_{SDOF,DL4}$
Precast RC post and beam	CR+PC/LPB/CR+PC/LPB/EWN/FN/HBET:1,2	0.40	0.64	1.60
Precast RC wall-slab-wall	CR+PC/LWAL/CR+PC/LN/EWN/FC/HBET:1,2	0.14	0.50	1.15
Cast-in-place RC post and beam	CR+CIP/LPB/CR+CIP/LPB/EWN/FN/HBET:1,2	0.40	0.64	1.60
Cast-in-place RC wall-slab-wall	CR+CIP/LWAL/CR+CIP/LN/EWN/FC/HBET:1,2	0.80	1.25	3.00
De Haver	MUR/LH/MUR/LH/EWN/FW/HBET:1,2	0.08	0.27	0.31
De Haver (no house)	W/LPB/W/LPB/EW/FW/HBET:1,2	0.08	0.27	0.31
Solwerderstraat 55	MUR/LWAL/MUR/LN/EWN/FW/HBET:1,2	0.08	0.27	0.77
Julianalaan 52	MUR/LWAL/MUR/LN/EW/FC/HBET:1,2	0.08	0.27	0.77
Zijlvest 25	MUR/LWAL/MUR/LN/EW/FC/HBET:1,2/IRIR+IRVP:CHV	0.08	0.27	0.77
Koeriersterweg 20-21	MUR/LWAL/MUR/LN/EW/FC/HBET:3,20	0.08	0.27	0.48
Nieuwstraat 8	MUR/LWAL/MUR/LWAL/EWN/FW/HBET:1,2	0.08	0.27	0.77
Kwelder 1	MUR/LWAL/MUR/LWAL/EW/FC/HBET:1,2	0.08	0.27	0.77
Schuitenzandflat 2-56	MUR/LWAL/MUR/LWAL/EW/FC/HBET:3,20	0.08	0.27	0.67
Badweg 12	MUR/LWAL/MUR/LWAL/EW/FW/HBET:1,2	0.08	0.27	0.34
Kwelder 8	W/LWAL/W/LWAL/EW/FW/HBET:1,2	0.32	0.79	2.45
Steenweg 19	S/LFM/S/LFM/EWN/FC/HBET:1,2	0.48	0.76	1.62
Glulam portal frame	S/LFBR/W/LPB/EWN/FN/HBET:1,2	0.32	0.79	2.45
Beneluxweg 15	S/LFBR/S/LPB/EWN/FN/HBET:1,2	0.40	0.64	1.60
HAZUS S2L	S/LFBR/S/LFBR/EWN/FN/HBET:1,2	0.40	0.64	1.60
Precast RC wall-slab-wall + HAZUS	CR+PC/LWAL/CR+PC/LN/EWN/FC/HBET:3,20	0.14	0.50	1.15
Cast-in-place RC wall-slab-wall + HAZUS	CR+CIP/LWAL/CR+CIP/LN/EWN/FC/HBET:3,20	0.05	0.18	0.23
HAZUS S2M	S/LFBR/S/LFBR/EWN/FC/HBET:3,20	0.27	0.43	1.07
Steenweg 19 + HAZUS	S/LFM/S/LFM/EWN/FC/HBET:3,20	0.32	0.51	1.08
HAZUS C1L	CR+CIP/LFM/CR+CIP/LFM/EWN/FC/HBET:1,2	0.40	0.64	1.60
HAZUS C1M	CR+CIP/LFM/CR+CIP/LFM/EWN/FC/HBET:3,20	0.27	0.43	1.07
Cast-in-place RC post and beam + HAZUS	CR+CIP/LPB/CR+CIP/LPB/EWN/FN/HBET:3,20	0.27	0.43	1.07
Precast RC post and beam + HAZUS	CR+PC/LPB/CR+PC/LPB/EWN/FN/HBET:3,20	0.21	0.34	0.72

4.3.3 Global Collapse Capacity

The global collapse drift values obtained from the dynamic analyses of URM buildings might overestimate the actual displacement capacity at global collapse, as only a limited number of records have been used for each structure, and an iterative approach to identify the lowest displacement at which global collapse occurs was not undertaken. In order to attempt to correct for what could be an under- or over-estimation of the global collapse capacity, the SDOF drift for the global collapse limit state (where this occurs) has been calculated using the average of the maximum attic displacement obtained in the records where global collapse does not occur and the lowest displacement at which global collapse was instead identified. The collapse debris associated with the collapse states of each index building is discussed in Chapter 5, and it is noted that given the aforementioned correction, global collapse is not associated with 100% debris, but with a corrected value of 75% to avoid being overly conservative in the estimation of the consequences of global collapse.

4.3.4 Summary of collapse limit states

Table 4.6 presents the final SDOF collapse state drift limits for each model.

4.4 Fragility Functions

4.4.1 Structural Fragility Functions

The structural fragility functions for each model are calculated using Equations 4.2 and 4.3 and the parameters of the multivariate linear regression (discussed in Chapter 3), the total dispersion, β_s , and the displacement limit of each damage or collapse state, as presented in Tables 4.7, 4.8 and 4.9 for the middle, lower and upper branches of the logic tree, respectively. Fragility functions for all models, in terms of just the scalar intensity measure ($S_a [T_1]$), are plotted in Appendix D.

4.4.2 Chimney Fragility Functions

The fragility functions for chimneys have been taken from the study by Taig and Pickup (2016), which used the observed damage and collapse of chimneys from a number of earthquakes including those of Liege (1983) and Roermond (1992). Taig and Pickup (2016) propose lower and upper bound step functions in terms of bands of PGA (g) for buildings constructed before and after 1920 (see Figure 4.1).

Table 4.6 SDOF drift limits to collapse for all models

Index Building	Structural System	$\theta_{SDOF,CS1}$	$\theta_{SDOF,CS2}$	$\theta_{SDOF,CS3}^*$
Precast RC post and beam	CR+PC/LPB/CR+PC/LPB/EWN/FN/HBET:1,2	-	-	3.40
Precast RC wall-slab-wall	CR+PC/LWAL/CR+PC/LN/EWN/FC/HBET:1,2	-	-	2.90
Cast-in-place RC post and beam	CR+CIP/LPB/CR+CIP/LPB/EWN/FN/HBET:1,2	-	-	3.40
Cast-in-place RC wall-slab-wall	CR+CIP/LWAL/CR+CIP/LN/EWN/FC/HBET:1,2	-	-	5.00
De Haver	MUR/LH/MUR/LH/EWN/FW/HBET:1,2	0.15	0.31	0.63
De Haver (no house)	W/LPB/W/LPB/EW/FW/HBET:1,2	-	-	0.90
Solwerderstraat 55	MUR/LWAL/MUR/LN/EWN/FW/HBET:1,2	1.78	2.46	2.56
Julianalaan 52	MUR/LWAL/MUR/LN/EW/FC/HBET:1,2	-	1.23	1.25
Zijlvest 25	MUR/LWAL/MUR/LN/EW/FC/HBET:1,2/IRIR+IRVP:CHV	0.99	2.45	2.88
Koeriersterweg 20-21	MUR/LWAL/MUR/LN/EW/FC/HBET:3,20	0.25	0.48	1.55
Nieuwstraat 8	MUR/LWAL/MUR/LWAL/EWN/FW/HBET:1,2	0.88	1.18	2.60
Kwelder 1	MUR/LWAL/MUR/LWAL/EW/FC/HBET:1,2	0.77	1.00	4.30
Schuitenzandflat 2-56	MUR/LWAL/MUR/LWAL/EW/FC/HBET:3,20	0.30	0.67	1.19
Badweg 12	MUR/LWAL/MUR/LWAL/EW/FW/HBET:1,2	0.09	0.34	0.59
Kwelder 8	W/LWAL/W/LWAL/EW/FW/HBET:1,2	-	-	4.40
Steenweg 19	S/LFB/S/LFB/EWN/FC/HBET:1,2	-	-	7.70
Glulam portal frame	S/LFB/W/LPB/EWN/FN/HBET:1,2	-	-	16.0
Beneluxweg 15	S/LFB/S/LPB/EWN/FN/HBET:1,2	-	-	7.80
HAZUS S2L	S/LFB/S/LFB/EWN/FN/HBET:1,2	-	-	4.00
Precast RC wall-slab-wall + HAZUS	CR+PC/LWAL/CR+PC/LN/EWN/FC/HBET:3,20	-	-	1.50
Cast-in-place RC wall-slab-wall + HAZUS	CR+CIP/LWAL/CR+CIP/LN/EWN/FC/HBET:3,20	-	-	3.40
HAZUS S2M	S/LFB/S/LFB/EWN/FC/HBET:3,20	-	-	2.67
Steenweg 19 + HAZUS	S/LFB/S/LFB/EWN/FC/HBET:3,20	-	-	5.10
HAZUS C1L	CR+CIP/LFM/CR+CIP/LFM/EWN/FC/HBET:1,2	-	-	4.00
HAZUS C1M	CR+CIP/LFM/CR+CIP/LFM/EWN/FC/HBET:3,20	-	-	2.67
Cast-in-place RC post and beam + HAZUS	CR+CIP/LPB/CR+CIP/LPB/EWN/FN/HBET:3,20	-	-	2.20
Precast RC post and beam + HAZUS	CR+PC/LPB/CR+PC/LPB/EWN/FN/HBET:3,20	-	-	2.20

* Note that non-URM models only have one collapse state

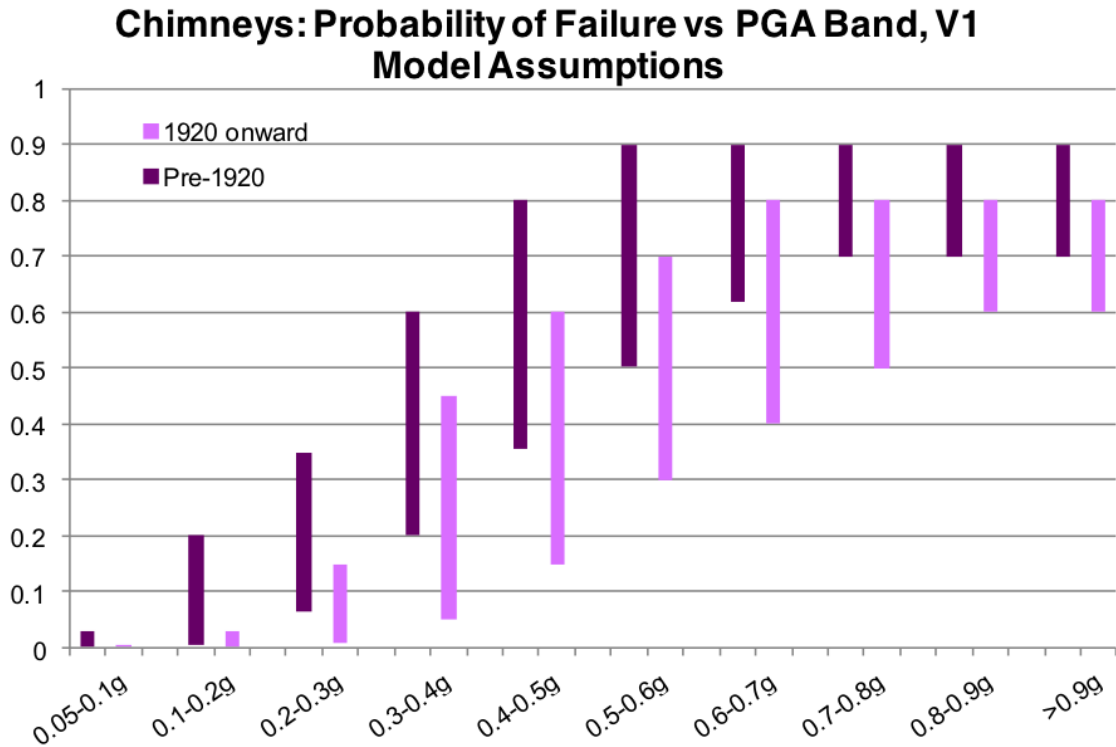


Figure 4.1 Empirical chimney fragility functions (Taig and Pickup, 2006)

Upper, middle and lower values of the probability of collapse for each PGA band have been used to fit lognormal fragility functions for the upper, middle and lower branches of the logic tree, leading to the functions presented in Figure 4.2 and tabulated in Table 4.10.

The probability of chimney collapse (P_{ChC}) is calculated using the data in Table 4.10 and the following formula:

$$P_{ChC} = \Phi\left(\frac{\ln(PGA) - \ln(\overline{PGA}_{chf})}{\beta_{chf}}\right) \quad (4.5)$$

where $\Phi()$ is the cumulative distribution function of the standard normal distribution, \overline{PGA}_{chf} is the median PGA of the chimney collapse fragility function (in terms of g) and β_{chf} is the standard deviation. PGA is the level of peak ground acceleration (or spectral acceleration at 0.01 seconds) in terms of g, as provided by the hazard calculations of the risk engine.

Table 4.7 Middle branch fragility function inputs for all models

Structural System	T_1 (s)	T_2 (s)	b_0	b_1	b_2	b_3	β_s	DL_{DS2} (m)	DL_{DS3} (m)	DL_{DS4} (m)	DL_{CS1} (m)	DL_{CS2} (m)	DL_{CS3} (m)
CR+PC/LPB/CR+PC/LPB/EWN/FN/HBET:1,2	1.5	-	-1.034	0.856	-0.113	0	0.41	0.026	0.042	0.104	0.218	0.218	0.218
CR+PC/LWAL/CR+PC/LN/EWN/FC/HBET:1,2	0.4	0.7	-2.784	0.621	-0.075	0.41	0.43	0.006	0.021	0.048	0.120	0.120	0.120
CR+CIP/LPB/CR+CIP/LPB/EWN/FN/HBET:1,2	1.5	0.85	-1.136	0.705	0	0.23	0.41	0.026	0.042	0.104	0.218	0.218	0.218
CR+CIP/LWAL/CR+CIP/LN/EWN/FC/HBET:1,2	0.85	-	-1.960	0.909	0	0	0.38	0.036	0.056	0.136	0.226	0.226	0.226
MUR/LH/MUR/LH/EWN/FW/HBET:1,2	0.5	0.01	-3.526	0.914	-0.085	0.80	0.43	0.003	0.009	0.010	0.005	0.010	0.021
W/LPB/W/LPB/EWN/FW/HBET:1,2	0.3	-	-4.230	0.950	0	0	0.42	0.002	0.008	0.009	0.026	0.026	0.026
MUR/LWAL/MUR/LN/EWN/FW/HBET:1,2	0.4	0.25	-3.282	0.803	0	0.40	0.42	0.004	0.015	0.042	0.096	0.133	0.138
MUR/LWAL/MUR/LN/EW/FC/HBET:1,2	0.25	0.5	-4.066	1.315	0	0.39	0.55	0.003	0.011	0.030	0.048	0.048	0.049
MUR/LWAL/MUR/LN/EW/FC/HBET:1,2/IRIR+IRVP:CHV	0.5	-	-2.629	1.192	-0.043	0	0.52	0.003	0.010	0.029	0.037	0.092	0.108
MUR/LWAL/MUR/LN/EW/FC/HBET:3,20	0.6	-	-2.591	1.026	-0.053	0	0.38	0.005	0.017	0.030	0.016	0.030	0.099
MUR/LWAL/MUR/LWAL/EWN/FW/HBET:1,2	0.25	0.5	-4.165	0.952	0	0.23	0.46	0.002	0.008	0.023	0.026	0.035	0.078
MUR/LWAL/MUR/LWAL/EW/FC/HBET:1,2	0.01	0.3	-3.901	1.651	0	0.98	0.54	0.002	0.007	0.021	0.021	0.028	0.118
MUR/LWAL/MUR/LWAL/EW/FC/HBET:3,20	0.6	0.01	-2.666	1.577	0	0.19	0.43	0.010	0.033	0.083	0.037	0.083	0.147
MUR/LWAL/MUR/LWAL/EW/FW/HBET:1,2	0.01	-	-3.094	2.147	-0.054	0	0.54	0.002	0.008	0.010	0.002	0.010	0.017
W/LWAL/W/LWAL/EW/FW/HBET:1,2	0.01	0.4	-3.344	0.938	0	0.41	0.46	0.009	0.022	0.067	0.120	0.120	0.120
S/LFM/S/LFM/EWN/FC/HBET:1,2	1.5	-	-1.161	0.662	0	0	0.43	0.030	0.048	0.102	0.480	0.480	0.480
S/LFBR/W/LPB/EWN/FN/HBET:1,2	0.3	-	-3.735	0.724	0.025	0	0.35	0.013	0.032	0.098	0.640	0.640	0.640
S/LFBR/S/LPB/EWN/FN/HBET:1,2	0.01	-	-4.016	0.989	0.045	0	0.42	0.015	0.024	0.061	0.296	0.296	0.296
S/LFBR/S/LFBR/EWN/FN/HBET:1,2	0.6	-	-2.795	0.745	0	0	0.47	0.022	0.035	0.088	0.220	0.220	0.220
CR+PC/LWAL/CR+PC/LN/EWN/FC/HBET:3,20	0.6	-	-2.531	0.828	0	0	0.40	0.012	0.041	0.095	0.120	0.120	0.120
CR+CIP/LWAL/CR+CIP/LN/EWN/FC/HBET:3,20	1	-	-1.507	0.925	0.017	0	0.40	0.048	0.076	0.182	0.303	0.303	0.303
S/LFBR/S/LFBR/EWN/FC/HBET:3,20	0.85	-	-1.940	0.813	0.048	0	0.38	0.037	0.059	0.147	0.366	0.366	0.366
S/LFM/S/LFM/EWN/FC/HBET:3,20	3	-	0.537	0.874	0.065	0	0.37	0.040	0.064	0.135	0.643	0.643	0.643
CR+CIP/LFM/CR+CIP/LFM/EWN/FC/HBET:1,2	0.6	-	-2.801	0.684	-0.061	0	0.46	0.018	0.029	0.074	0.184	0.184	0.184
CR+CIP/LFM/CR+CIP/LFM/EWN/FC/HBET:3,20	0.85	2	-1.903	0.680	0	0.09	0.40	0.031	0.049	0.122	0.304	0.304	0.304
CR+CIP/LPB/CR+CIP/LPB/EWN/FN/HBET:3,20	2	-	-0.635	0.798	-0.036	0	0.38	0.035	0.056	0.139	0.292	0.292	0.292
CR+PC/LPB/CR+PC/LPB/EWN/FN/HBET:3,20	2.5	-	-0.015	0.870	-0.047	0	0.36	0.035	0.056	0.139	0.292	0.292	0.292

Table 4.8 Lower branch fragility function inputs for all models

Structural System	T_1 (s)	T_2 (s)	b_0	b_1	b_2	b_3	β_s	DL_{DS2} (m)	DL_{DS3} (m)	DL_{DS4} (m)	DL_{CS1} (m)	DL_{CS2} (m)	DL_{CS3} (m)
CR+PC/LPB/CR+PC/LPB/EWN/FN/HBET:1,2	1.5	-	-0.221	0.856	-0.113	0	0.41	0.026	0.042	0.104	0.218	0.218	0.218
CR+PC/LWAL/CR+PC/LN/EWN/FC/HBET:1,2	0.4	0.7	-1.971	0.621	-0.075	0.41	0.43	0.006	0.021	0.048	0.120	0.120	0.120
CR+CIP/LPB/CR+CIP/LPB/EWN/FN/HBET:1,2	1.5	0.85	-0.323	0.705	0	0.23	0.41	0.026	0.042	0.104	0.218	0.218	0.218
CR+CIP/LWAL/CR+CIP/LN/EWN/FC/HBET:1,2	0.85	-	-1.147	0.909	0	0	0.38	0.036	0.056	0.136	0.226	0.226	0.226
MUR/LH/MUR/LH/EWN/FW/HBET:1,2	0.5	0.01	-3.059	0.914	-0.085	0.80	0.43	0.003	0.009	0.010	0.005	0.010	0.021
W/LPB/W/LPB/EWN/FW/HBET:1,2	0.3	-	-3.417	0.950	0	0	0.42	0.002	0.008	0.009	0.026	0.026	0.026
MUR/LWAL/MUR/LN/EWN/FW/HBET:1,2	0.4	0.25	-2.815	0.803	0	0.40	0.42	0.004	0.015	0.042	0.096	0.133	0.138
MUR/LWAL/MUR/LN/EW/FC/HBET:1,2	0.25	0.5	-3.599	1.315	0	0.39	0.55	0.003	0.011	0.030	0.048	0.048	0.049
MUR/LWAL/MUR/LN/EW/FC/HBET:1,2/IRIR+IRVP:CHV	0.5	-	-2.162	1.192	-0.043	0	0.52	0.003	0.010	0.029	0.037	0.092	0.108
MUR/LWAL/MUR/LN/EW/FC/HBET:3,20	0.6	-	-2.124	1.026	-0.053	0	0.38	0.005	0.017	0.030	0.016	0.030	0.099
MUR/LWAL/MUR/LWAL/EWN/FW/HBET:1,2	0.25	0.5	-3.698	0.952	0	0.23	0.46	0.002	0.008	0.023	0.026	0.035	0.078
MUR/LWAL/MUR/LWAL/EW/FC/HBET:1,2	0.01	0.3	-3.434	1.651	0	0.98	0.54	0.002	0.007	0.021	0.021	0.028	0.118
MUR/LWAL/MUR/LWAL/EW/FC/HBET:3,20	0.6	0.01	-2.199	1.577	0	0.19	0.43	0.010	0.033	0.083	0.037	0.083	0.147
MUR/LWAL/MUR/LWAL/EW/FW/HBET:1,2	0.01	-	-2.627	2.147	-0.054	0	0.54	0.002	0.008	0.010	0.002	0.010	0.017
W/LWAL/W/LWAL/EW/FW/HBET:1,2	0.01	0.4	-2.531	0.938	0	0.41	0.46	0.009	0.022	0.067	0.120	0.120	0.120
S/LFM/S/LFM/EWN/FC/HBET:1,2	1.5	-	-0.348	0.662	0	0	0.43	0.030	0.048	0.102	0.480	0.480	0.480
S/LFBR/W/LPB/EWN/FN/HBET:1,2	0.3	-	-2.922	0.724	0.025	0	0.35	0.013	0.032	0.098	0.640	0.640	0.640
S/LFBR/S/LPB/EWN/FN/HBET:1,2	0.01	-	-3.203	0.989	0.045	0	0.42	0.015	0.024	0.061	0.296	0.296	0.296
S/LFBR/S/LFBR/EWN/FN/HBET:1,2	0.6	-	-1.982	0.745	0	0	0.47	0.022	0.035	0.088	0.220	0.220	0.220
CR+PC/LWAL/CR+PC/LN/EWN/FC/HBET:3,20	0.6	-	-1.718	0.828	0	0	0.40	0.012	0.041	0.095	0.120	0.120	0.120
CR+CIP/LWAL/CR+CIP/LN/EWN/FC/HBET:3,20	1	-	-0.694	0.925	0.017	0	0.40	0.048	0.076	0.182	0.303	0.303	0.303
S/LFBR/S/LFBR/EWN/FC/HBET:3,20	0.85	-	-1.127	0.813	0.048	0	0.38	0.037	0.059	0.147	0.366	0.366	0.366
S/LFM/S/LFM/EWN/FC/HBET:3,20	3	-	1.350	0.874	0.065	0	0.37	0.040	0.064	0.135	0.643	0.643	0.643
CR+CIP/LFM/CR+CIP/LFM/EWN/FC/HBET:1,2	0.6	-	-1.988	0.684	-0.061	0	0.46	0.018	0.029	0.074	0.184	0.184	0.184
CR+CIP/LFM/CR+CIP/LFM/EWN/FC/HBET:3,20	0.85	2	-1.090	0.680	0	0.09	0.40	0.031	0.049	0.122	0.304	0.304	0.304
CR+CIP/LPB/CR+CIP/LPB/EWN/FN/HBET:3,20	2	-	0.178	0.798	-0.036	0	0.38	0.035	0.056	0.139	0.292	0.292	0.292
CR+PC/LPB/CR+PC/LPB/EWN/FN/HBET:3,20	2.5	-	0.798	0.870	-0.047	0	0.36	0.035	0.056	0.139	0.292	0.292	0.292

Table 4.9 Upper branch fragility function inputs for all models

Structural System	T_1 (s)	T_2 (s)	b_0	b_1	b_2	b_3	β_s	DL_{DS2} (m)	DL_{DS3} (m)	DL_{DS4} (m)	DL_{CS1} (m)	DL_{CS2} (m)	DL_{CS3} (m)
CR+PC/LPB/CR+PC/LPB/EWN/FN/HBET:1,2	1.5	-	-1.848	0.856	-0.113	0	0.41	0.026	0.042	0.104	0.218	0.218	0.218
CR+PC/LWAL/CR+PC/LN/EWN/FC/HBET:1,2	0.4	0.7	-3.597	0.621	-0.075	0.41	0.43	0.006	0.021	0.048	0.120	0.120	0.120
CR+CIP/LPB/CR+CIP/LPB/EWN/FN/HBET:1,2	1.5	0.85	-1.949	0.705	0	0.23	0.41	0.026	0.042	0.104	0.218	0.218	0.218
CR+CIP/LWAL/CR+CIP/LN/EWN/FC/HBET:1,2	0.85	-	-2.773	0.909	0	0	0.38	0.036	0.056	0.136	0.226	0.226	0.226
MUR/LH/MUR/LH/EWN/FW/HBET:1,2	0.5	0.01	-3.993	0.914	-0.085	0.80	0.43	0.003	0.009	0.010	0.005	0.010	0.021
W/LPB/W/LPB/EWN/FW/HBET:1,2	0.3	-	-5.044	0.950	0	0	0.42	0.002	0.008	0.009	0.026	0.026	0.026
MUR/LWAL/MUR/LN/EWN/FW/HBET:1,2	0.4	0.25	-3.749	0.803	0	0.40	0.42	0.004	0.015	0.042	0.096	0.133	0.138
MUR/LWAL/MUR/LN/EW/FC/HBET:1,2	0.25	0.5	-4.533	1.315	0	0.39	0.55	0.003	0.011	0.030	0.048	0.048	0.049
MUR/LWAL/MUR/LN/EW/FC/HBET:1,2/IRIR+IRVP:CHV	0.5	-	-3.096	1.192	-0.043	0	0.52	0.003	0.010	0.029	0.037	0.092	0.108
MUR/LWAL/MUR/LN/EW/FC/HBET:3,20	0.6	-	-3.058	1.026	-0.053	0	0.38	0.005	0.017	0.030	0.016	0.030	0.099
MUR/LWAL/MUR/LWAL/EWN/FW/HBET:1,2	0.25	0.5	-4.632	0.952	0	0.23	0.46	0.002	0.008	0.023	0.026	0.035	0.078
MUR/LWAL/MUR/LWAL/EW/FC/HBET:1,2	0.01	0.3	-4.368	1.651	0	0.98	0.54	0.002	0.007	0.021	0.021	0.028	0.118
MUR/LWAL/MUR/LWAL/EW/FC/HBET:3,20	0.6	0.01	-3.133	1.577	0	0.19	0.43	0.010	0.033	0.083	0.037	0.083	0.147
MUR/LWAL/MUR/LWAL/EW/FW/HBET:1,2	0.01	-	-3.561	2.147	-0.054	0	0.54	0.002	0.008	0.010	0.002	0.010	0.017
W/LWAL/W/LWAL/EW/FW/HBET:1,2	0.01	0.4	-4.157	0.938	0	0.41	0.46	0.009	0.022	0.067	0.120	0.120	0.120
S/LFM/S/LFM/EWN/FC/HBET:1,2	1.5	-	-1.974	0.662	0	0	0.43	0.030	0.048	0.102	0.480	0.480	0.480
S/LFBR/W/LPB/EWN/FN/HBET:1,2	0.3	-	-4.548	0.724	0.025	0	0.35	0.013	0.032	0.098	0.640	0.640	0.640
S/LFBR/S/LPB/EWN/FN/HBET:1,2	0.01	-	-4.829	0.989	0.045	0	0.42	0.015	0.024	0.061	0.296	0.296	0.296
S/LFBR/S/LFBR/EWN/FN/HBET:1,2	0.6	-	-3.608	0.745	0	0	0.47	0.022	0.035	0.088	0.220	0.220	0.220
CR+PC/LWAL/CR+PC/LN/EWN/FC/HBET:3,20	0.6	-	-3.344	0.828	0	0	0.40	0.012	0.041	0.095	0.120	0.120	0.120
CR+CIP/LWAL/CR+CIP/LN/EWN/FC/HBET:3,20	1	-	-2.320	0.925	0.017	0	0.40	0.048	0.076	0.182	0.303	0.303	0.303
S/LFBR/S/LFBR/EWN/FC/HBET:3,20	0.85	-	-2.753	0.813	0.048	0	0.38	0.037	0.059	0.147	0.366	0.366	0.366
S/LFM/S/LFM/EWN/FC/HBET:3,20	3	-	-0.277	0.874	0.065	0	0.37	0.040	0.064	0.135	0.643	0.643	0.643
CR+CIP/LFM/CR+CIP/LFM/EWN/FC/HBET:1,2	0.6	-	-3.614	0.684	-0.061	0	0.46	0.018	0.029	0.074	0.184	0.184	0.184
CR+CIP/LFM/CR+CIP/LFM/EWN/FC/HBET:3,20	0.85	2	-2.717	0.680	0	0.09	0.40	0.031	0.049	0.122	0.304	0.304	0.304
CR+CIP/LPB/CR+CIP/LPB/EWN/FN/HBET:3,20	2	-	-1.448	0.798	-0.036	0	0.38	0.035	0.056	0.139	0.292	0.292	0.292
CR+PC/LPB/CR+PC/LPB/EWN/FN/HBET:3,20	2.5	-	-0.828	0.870	-0.047	0	0.36	0.035	0.056	0.139	0.292	0.292	0.292

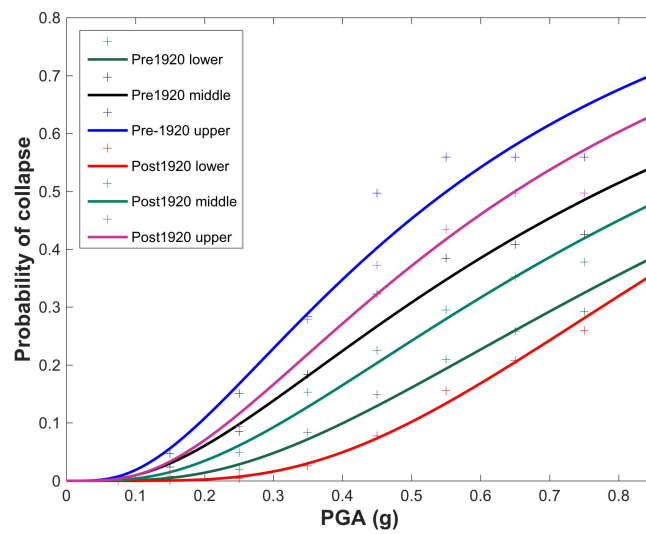


Figure 4.2 Lognormal chimney fragility functions for each branch of the logic tree for buildings constructed before and after 1920

Table 4.10 Input parameters of chimney fragility functions

Building Age	Logic Tree Branch	\overline{PGA}_{chf}	β_{chf}
Pre-1920	Lower	0.585	0.62
	Middle	0.412	0.78
	Upper	0.285	0.73
Post-1920	Lower	0.765	0.52
	Middle	0.583	0.69
	Upper	0.427	0.67

Chapter 5

Fatality Consequence Model

This chapter describes the consequence model that has been developed to estimate the fatality risk.

5.1 Methodology

The following assumptions are made when calculating fatality risk:

- Structural collapse states are sequential.
- Chimney collapse only contributes to the probability of dying outside the building.
- Chimney collapse and structural collapse are assumed to be independent.

The probability of dying inside the building, under a given level of ground shaking, due to structural collapse is calculated as follows:

$$P_{d_{inside}} = (P_{eDLCS1} - P_{eDLCS2}) \times P_{d_{inside}|CS1} + (P_{eDLCS2} - P_{eDLCS3}) \times P_{d_{inside}|CS2} + P_{eDLCS3} \times P_{d_{inside}|CS3} \quad (5.1)$$

where $P_{d_{inside}|CSi}$ refers to the probability of dying inside given structural collapse state i .

The probability of dying outside the building, under a given level of ground shaking, is calculated as follows

$$P_{d_{outside}} = (P_{eDLCS1} - P_{eDLCS2}) \times P_{d_{outside}|CS1} + (P_{eDLCS2} - P_{eDLCS3}) \times P_{d_{outside}|CS2} + P_{eDLCS3} \times P_{d_{outside}|CS3} + (1 - P_{eDLCS1}) \times P_{d_{outside}ChC} \quad (5.2)$$

where $P_{d_{outside}|CSi}$ refers to the probability of dying outside given structural collapse state i and $P_{d_{outside}ChC}$ refers to the probability of dying outside due to chimney collapse.

For the calculation of Local Personal Risk, the inside local personal risk (ILPR) and the outside local personal risk (OLPR) are combined based on the following weights, which assume that the hypothetical person that is permanently located in or near the building (where 'near' is defined as being within 5 metres of the perimeter of the building) has a 99% probability of being inside and a 1% probability of being outside at the time of the earthquake:

$$LPR = 0.99 \times ILPR + 0.01 \times OLPR \quad (5.3)$$

For the calculation of group risk, the average number of people inside and outside the building during the day and night are provided within the exposure model.

5.2 Probability of dying, given collapse

5.2.1 Inside the building

Coburn and Spence (2002) present a casualty model that considers a number of factors (M1 to M5) to calculate the number of human casualties (N) in a given building, following ground shaking:

$$N = M1 \times M2 \times M3 \times [M4 + M5 \times (1 - M4)] \quad (5.4)$$

Factors M1 and M2 are used to estimate the number of people within the building at the time of the earthquake, which are not needed for the estimation of inside local personal risk (where a single person is assumed to be permanently located within the building and spread uniformly across the total internal floor area of the building, or with some distribution across the floors where some floors, such as attics, are infrequently accessed) and are already accounted for in the exposure model for group risk.

The M3 factor defines the percentage of the occupants that are trapped by collapse and are unable to escape. Coburn and Spence (2002) have estimated average percentages for masonry and reinforced concrete buildings separately, considering the intensity and characteristics of the earthquake. Given that trapped people have to be located within the portion of the structure that collapses, this factor was herein replaced with the probability that the fictional person is trapped, which can be represented by the percentage of total floor area inside the building that is impacted by collapsed debris (given by the area of inside debris, $A_{debris_{inside}}$, divided by the total floor area, A_{floor}). This latter percentage is estimated as a function of the collapse mechanism (which could be either partial or complete) and the average floor area of each building typology, and is calculated by combining the collapse observations of the nonlinear dynamic analyses (Appendix E) and the footprint area data included in the exposure model.

The M4 factor identifies the percentage of trapped occupants that are killed instantaneously. This number is typically less than 1 as there are a number of features of the building that can provide shelter for occupants (such as furniture, doorways, roof frames etc.). This factor has been estimated by Coburn and Spence (2002), based on past observations from earthquakes, as being 20% for timber and masonry buildings and 40% for reinforced concrete and steel buildings.

The percentage of the surviving trapped occupants who subsequently die is given by factor M5, and depends on the building material and the effectiveness of search and rescue (SAR) efforts. It is assumed that a damaging earthquake in Groningen would trigger SAR efforts from the community, emergency squads and SAR experts up to 36 hours after the event. In this situation, the percentage of trapped survivors in collapsed buildings that subsequently die has been estimated by Coburn and Spence as 45% for masonry buildings and 70% for reinforced concrete buildings. For timber buildings they note that the value would be about 10%.

The proposed casualty model to estimate the probability of loss of life inside collapsed buildings, for a given collapse state (CSi), is thus as follows, where M4 and M5 depend on the material of the structural system, as discussed above:

$$P_{d_{inside}|CSi} = \alpha_{inCSi}[M4 + M5 \times (1 - M4)] \quad (5.5)$$

where

$$\alpha_{inCSi} = \frac{A_{debris_{inside}}}{A_{floor}} \quad (5.6)$$

In order to compare this model with empirical data, use was made of the study by So and Pomonis (2012) on the probability of death given collapse for European URM buildings with timber floors. So and Pomonis (2012) report that the volume loss for such buildings is typically 30% (according to a number of Italian earthquakes from the 1970s to the 1990s), and the fatality ratio (percentage of occupants that died) varied from 9 to 12%. According to Equation 12, and assuming that the volume loss is equivalent to the area of debris divided by the floor area, the probability of death inside a building would be 16.8%. It is feasible that observed fatality ratios could be lower than the probability of death inside a building, as the available data could be biased by the location of the people within the building at the time of the event, and thus might not sample all possible locations. Hence, whilst it is difficult to validate the methodology using existing data, the comparison shows that proposed framework gives figures that are in line with observed casualty data.

5.2.2 Outside the building

For outside risk, it has been shown in Taig and Pickup (2016) that the probability of dying when being hit by falling debris outside of a building is close to 1, and hence the probability of dying outside buildings for each collapse mechanism (which could be due to collapse of the structure or small non-structural elements such as chimneys and parapets) is simply calculated from the ratio of the area of debris outside the building (for each collapse mechanism/element) and the outside area at risk ¹:

$$P_{d_{outside}|CSi} = \alpha_{outCSi} = \frac{A_{debris_{outside}}}{A_{exposed}} \quad (5.7)$$

The fatality risk from chimney collapse is treated slightly differently to structural failure, as rather than combining the probability of chimney collapse and the probability of dying given chimney collapse, the probability of dying outside due to chimney collapse is calculated directly:

$$P_{d_{outside}_{ChC}} = \Phi\left(\frac{\ln(PGA) - \ln(\overline{PGA}_{chd})}{\beta_{chd}}\right), \quad PGA < 0.75g \quad (5.8)$$

$$P_{d_{outside}_{ChC}} = \Phi\left(\frac{\ln(0.75) - \ln(\overline{PGA}_{chd})}{\beta_{chd}}\right), \quad PGA \geq 0.75g \quad (5.9)$$

where $\Phi()$ is the cumulative distribution function of the standard normal distribution, PGA is the level of peak ground acceleration (or spectral acceleration at 0.01 seconds) in terms of g , \overline{PGA}_{chd} is the median PGA of the chimney collapse vulnerability function (in terms of g) and β_{chd} is the standard deviation. The parameters of this equation have been fit using the fragility function data as well as the area of collapsed debris for chimney collapse (from Taig and Pickup, 2016) and the average outside area for each structural system (available from the exposure model).

5.2.3 Final model

Tables ?? and 5.2 report the middle branch values of inside and outside collapse debris ratios (α_{inCSi} and α_{outCSi} , respectively) for each collapse state, for all structural systems. It is noted that for two of these systems the area of debris has been weighted by a probability of being within a given portion of the building, as in one index building (Koeriersterweg) collapse occurs in an attic which is unlikely to be frequently accessed, and in the other case (De Haver) there is a higher probability of being inside the house than in the barn. The lower and upper branch models are presented in Tables 5.3 to 5.6. These collapse debris ratios (for the three logic tree branches) are based on a combination of the values observed in the

¹The outside area at risk is estimated using the exposed perimeter of the building, available in the v5 EDB, and a distance of 5 metres from the perimeter of the building.

collapse analyses (see Appendix E), proposed values given in HAZUS (FEMA, 2004) and expert judgment.

Each branch of the logic tree for inside probabilities of dying, given collapse, is calculated using the debris ratios from Tables ?? to 5.6 and Equation 5.5. As presented previously in Equation 5.7, the probability of dying outside, given collapse is given directly by the outside debris ratios. The weights of the logic tree branches are 0.25 for the lower and upper branches, and 0.5 for the middle branch.

Table 5.1 Middle branch inside and outside collapse debris ratios per collapse state

Structural system	M4+M5(1-M4)	α_{inCS1}	α_{inCS2}	α_{inCS3}	α_{outCS1}	α_{outCS2}	α_{outCS3}
CR+PC/LPB/CR+PC/LPB/EWN/FN/HBET:1,2	0.82	-	-	0.150	-	-	0.030
CR+PC/LPB/CR+PC/LPB/EWN/FN/HBET:3,20	0.82	-	-	0.150	-	-	0.025
CR+PC/LWAL/CR+PC/LN/EWN/FC/HBET:1,2	0.82	-	-	0.500	-	-	0.125
CR+PC/LWAL/CR+PC/LN/EW/FC/HBET:1,2	0.82	-	-	0.500	-	-	0.125
CR+PC/LWAL/CR+PC/LN/EW/FC/HBET:3,20	0.82	-	-	0.500	-	-	0.125
CR+PC/LWAL/CR+PC/LWAL/EWN/FC/HBET:1,2	0.82	-	-	0.250	-	-	0.050
CR+PC/LWAL/CR+PC/LWAL/EWN/FC/HBET:3,20	0.82	-	-	0.250	-	-	0.050
CR+PC/LWAL/CR+PC/LWAL/EW/FC/HBET:1,2	0.82	-	-	0.250	-	-	0.063
CR+CIP/LPB/CR+CIP/LPB/EWN/FN/HBET:1,2	0.82	-	-	0.150	-	-	0.030
CR+CIP/LPB/CR+CIP/LPB/EWN/FN/HBET:3,20	0.82	-	-	0.150	-	-	0.025
CR+CIP/LFM/CR+CIP/LFM/EWN/FC/HBET:1,2	0.82	-	-	0.130	-	-	0.026
CR+CIP/LFM/CR+CIP/LFM/EWN/FC/HBET:3,20	0.82	-	-	0.100	-	-	0.020
CR+CIP/LWAL/CR+CIP/LN/EW/FC/HBET:1,2	0.82	-	-	0.300	-	-	0.075
CR+CIP/LWAL/CR+CIP/LN/EW/FC/HBET:3,20	0.82	-	-	0.300	-	-	0.075
CR+CIP/LWAL/CR+CIP/LWAL/EWN/FC/HBET:1,2	0.82	-	-	0.150	-	-	0.030
CR+CIP/LWAL/CR+CIP/LWAL/EWN/FC/HBET:3,20	0.82	-	-	0.150	-	-	0.030
MUR/LH/MUR/LH/EWN/FW/HBET:1,2	0.56	0.036	0.175	0.400	0.0000	0.0000	0.150
MUR/LH/MUR/LH/EWN/FW/HBET:3,20	0.56	0.036	0.175	0.400	0.0000	0.0000	0.150
MUR/LWAL/MUR/LN/EWN/FW/HBET:1,2	0.56	0.000	0.540	0.750	0.033	0.0667	0.500
MUR/LWAL/MUR/LN/EWN/FW/HBET:3,20	0.56	0.000	0.540	0.750	0.050	0.1000	0.500
MUR/LWAL/MUR/LN/EW/FC/HBET:1,2	0.56	0.040	0.040	0.750	0.048	0.0480	0.500
MUR/LWAL/MUR/LN/EW/FC/HBET:1,2/IRIR+IRVP:CHV	0.56	0.006	0.013	0.750	0.006	0.0090	0.500
MUR/LWAL/MUR/LN/EW/FC/HBET:3,20	0.56	0.002	0.102	0.750	0.050	0.1000	0.750
MUR/LWAL/MUR/LN/EW/FW/HBET:1,2	0.56	0.000	0.500	0.750	0.100	0.1667	0.500
MUR/LWAL/MUR/LN/EW/FW/HBET:3,20	0.56	0.000	0.500	0.750	0.150	0.2500	0.500
MUR/LWAL/MUR/LWAL/EWN/FW/HBET:1,2	0.56	0.450	0.450	0.750	0.000	0.0037	0.250
MUR/LWAL/MUR/LWAL/EWN/FW/HBET:3,20	0.56	0.000	0.540	0.750	0.026	0.0513	0.500

Table 5.2 Middle branch inside and outside collapse debris ratios per collapse state (continued)

Structural system	M4+M5(1-M4)	α_{inCS1}	α_{inCS2}	α_{inCS3}	α_{outCS1}	α_{outCS2}	α_{outCS3}
MUR/LWAL/MUR/LWAL/EW/FC/HBET:1,2	0.56	0.000	0.030	0.750	0.011	0.0111	0.250
MUR/LWAL/MUR/LWAL/EW/FC/HBET:3,20	0.56	0.000	0.121	0.250	0.038	0.0750	0.125
MUR/LWAL/MUR/LWAL/EW/FW/HBET:1,2	0.56	0.000	0.500	0.750	0.056	0.0926	0.250
MUR/LWAL/MUR/LWAL/EW/FW/HBET:3,20	0.56	0.000	0.500	0.750	0.100	0.1667	0.500
MUR/LWAL/W/LPB/EWN/FN/HBET:1,2	0.56	-	-	0.030	-	-	0.006
MUR/LWAL/W/LPB/EWN/FN/HBET:3,20	0.56	-	-	0.030	-	-	0.005
W/LPB/W/LPB/EW/FN/HBET:1,2	0.28	-	-	0.750	-	-	0.150
W/LPB/W/LPB/EW/FN/HBET:3,20	0.28	-	-	0.750	-	-	0.125
W/LWAL/W/LN/EWN/FW/HBET:1,2	0.28	-	-	0.030	-	-	0.008
W/LWAL/W/LN/EW/FW/HBET:1,2	0.28	-	-	0.030	-	-	0.008
W/LWAL/W/LN/EW/FW/HBET:3,20	0.28	-	-	0.030	-	-	0.008
W/LWAL/W/LWAL/EWN/FW/HBET:1,2	0.28	-	-	0.030	-	-	0.008
W/LWAL/W/LWAL/EWN/FW/HBET:3,20	0.28	-	-	0.030	-	-	0.008
W/LWAL/W/LWAL/EW/FW/HBET:1,2	0.28	-	-	0.030	-	-	0.008
W/LWAL/W/LWAL/EW/FW/HBET:3,20	0.28	-	-	0.030	-	-	0.008
S/LPB/S/LPB/EWN/FN/HBET:1,2	0.82	-	-	0.150	-	-	0.030
S/LPB/S/LPB/EWN/FN/HBET:3,20	0.82	-	-	0.150	-	-	0.025
S/LFM/S/LFM/EWN/FC/HBET:1,2	0.82	-	-	0.080	-	-	0.016
S/LFM/S/LFM/EWN/FC/HBET:3,20	0.82	-	-	0.050	-	-	0.010
S/LFBR/W/LPB/EWN/FN/HBET:1,2	0.82	-	-	0.030	-	-	0.006
S/LFBR/W/LPB/EWN/FN/HBET:3,20	0.28	-	-	0.030	-	-	0.005
S/LFBR/S/LPB/EWN/FN/HBET:1,2	0.82	-	-	0.030	-	-	0.006
S/LFBR/S/LPB/EWN/FN/HBET:3,20	0.82	-	-	0.050	-	-	0.008
S/LFBR/S/LFBR/EWN/FN/HBET:1,2	0.82	-	-	0.080	-	-	0.016
S/LFBR/S/LFBR/EWN/FN/HBET:3,20	0.82	-	-	0.050	-	-	0.008
S/LFBR/S/LFBR/EWN/FC/HBET:1,2	0.82	-	-	0.080	-	-	0.016
S/LFBR/S/LFBR/EWN/FC/HBET:3,20	0.82	-	-	0.050	-	-	0.010

Table 5.3 Lower branch inside and outside collapse debris ratios per collapse state

Structural system	M4+M5(1-M4)	α_{inCS1}	α_{inCS2}	α_{inCS3}	α_{outCS1}	α_{outCS2}	α_{outCS3}
CR+PC/LPB/CR+PC/LPB/EWN/FN/HBET:1,2	0.82	-	-	0.100	-	-	0.020
CR+PC/LPB/CR+PC/LPB/EWN/FN/HBET:3,20	0.82	-	-	0.100	-	-	0.017
CR+PC/LWAL/CR+PC/LN/EWN/FC/HBET:1,2	0.82	-	-	0.400	-	-	0.100
CR+PC/LWAL/CR+PC/LN/EW/FC/HBET:1,2	0.82	-	-	0.400	-	-	0.100
CR+PC/LWAL/CR+PC/LN/EW/FC/HBET:3,20	0.82	-	-	0.400	-	-	0.100
CR+PC/LWAL/CR+PC/LWAL/EWN/FC/HBET:1,2	0.82	-	-	0.200	-	-	0.040
CR+PC/LWAL/CR+PC/LWAL/EWN/FC/HBET:3,20	0.82	-	-	0.200	-	-	0.040
CR+PC/LWAL/CR+PC/LWAL/EW/FC/HBET:1,2	0.82	-	-	0.200	-	-	0.050
CR+CIP/LPB/CR+CIP/LPB/EWN/FN/HBET:1,2	0.82	-	-	0.100	-	-	0.020
CR+CIP/LPB/CR+CIP/LPB/EWN/FN/HBET:3,20	0.82	-	-	0.100	-	-	0.017
CR+CIP/LFM/CR+CIP/LFM/EWN/FC/HBET:1,2	0.82	-	-	0.100	-	-	0.020
CR+CIP/LFM/CR+CIP/LFM/EWN/FC/HBET:3,20	0.82	-	-	0.080	-	-	0.016
CR+CIP/LWAL/CR+CIP/LN/EW/FC/HBET:1,2	0.82	-	-	0.200	-	-	0.050
CR+CIP/LWAL/CR+CIP/LN/EW/FC/HBET:3,20	0.82	-	-	0.200	-	-	0.050
CR+CIP/LWAL/CR+CIP/LWAL/EWN/FC/HBET:1,2	0.82	-	-	0.100	-	-	0.020
CR+CIP/LWAL/CR+CIP/LWAL/EWN/FC/HBET:3,20	0.82	-	-	0.100	-	-	0.020
MUR/LH/MUR/LH/EWN/FW/HBET:1,2	0.56	0.027	0.140	0.335	0.000	0.000	0.100
MUR/LH/MUR/LH/EWN/FW/HBET:3,20	0.56	0.027	0.140	0.335	0.000	0.000	0.100
MUR/LWAL/MUR/LN/EWN/FW/HBET:1,2	0.56	0.000	0.480	0.650	0.017	0.050	0.400
MUR/LWAL/MUR/LN/EWN/FW/HBET:3,20	0.56	0.000	0.480	0.650	0.025	0.075	0.400
MUR/LWAL/MUR/LN/EW/FC/HBET:1,2	0.56	0.020	0.020	0.650	0.024	0.024	0.400
MUR/LWAL/MUR/LN/EW/FC/HBET:1,2/IRIR+IRVP:CHV	0.56	0.003	0.007	0.650	0.003	0.005	0.400
MUR/LWAL/MUR/LN/EW/FC/HBET:3,20	0.56	0.001	0.090	0.650	0.025	0.075	0.650
MUR/LWAL/MUR/LN/EW/FW/HBET:1,2	0.56	0.000	0.400	0.650	0.083	0.133	0.400
MUR/LWAL/MUR/LN/EW/FW/HBET:3,20	0.56	0.000	0.400	0.650	0.125	0.200	0.400
MUR/LWAL/MUR/LWAL/EWN/FW/HBET:1,2	0.56	0.400	0.400	0.650	0.000	0.003	0.150
MUR/LWAL/MUR/LWAL/EWN/FW/HBET:3,20	0.56	0.000	0.480	0.650	0.013	0.038	0.400

Table 5.4 Lower branch inside and outside collapse debris ratios per collapse state (continued)

Structural system	M4+M5(1-M4)	α_{inCS1}	α_{inCS2}	α_{inCS3}	α_{outCS1}	α_{outCS2}	α_{outCS3}
MUR/LWAL/MUR/LWAL/EW/FC/HBET:1,2	0.56	0.000	0.015	0.650	0.007	0.007	0.150
MUR/LWAL/MUR/LWAL/EW/FC/HBET:3,20	0.56	0.000	0.100	0.200	0.025	0.063	0.100
MUR/LWAL/MUR/LWAL/EW/FW/HBET:1,2	0.56	0.000	0.400	0.650	0.046	0.074	0.150
MUR/LWAL/MUR/LWAL/EW/FW/HBET:3,20	0.56	0.000	0.400	0.650	0.083	0.133	0.400
MUR/LWAL/W/LPB/EWN/FN/HBET:1,2	0.56	-	-	0.010	-	-	0.002
MUR/LWAL/W/LPB/EWN/FN/HBET:3,20	0.56	-	-	0.010	-	-	0.002
W/LPB/W/LPB/EW/FN/HBET:1,2	0.28	-	-	0.650	-	-	0.130
W/LPB/W/LPB/EW/FN/HBET:3,20	0.28	-	-	0.650	-	-	0.108
W/LWAL/W/LN/EWN/FW/HBET:1,2	0.28	-	-	0.010	-	-	0.003
W/LWAL/W/LN/EW/FW/HBET:1,2	0.28	-	-	0.010	-	-	0.003
W/LWAL/W/LN/EW/FW/HBET:3,20	0.28	-	-	0.010	-	-	0.003
W/LWAL/W/LWAL/EWN/FW/HBET:1,2	0.28	-	-	0.010	-	-	0.003
W/LWAL/W/LWAL/EWN/FW/HBET:3,20	0.28	-	-	0.010	-	-	0.003
W/LWAL/W/LWAL/EW/FW/HBET:1,2	0.28	-	-	0.010	-	-	0.003
W/LWAL/W/LWAL/EW/FW/HBET:3,20	0.28	-	-	0.010	-	-	0.003
S/LPB/S/LPB/EWN/FN/HBET:1,2	0.82	-	-	0.100	-	-	0.020
S/LPB/S/LPB/EWN/FN/HBET:3,20	0.82	-	-	0.100	-	-	0.017
S/LFM/S/LFM/EWN/FC/HBET:1,2	0.82	-	-	0.060	-	-	0.012
S/LFM/S/LFM/EWN/FC/HBET:3,20	0.82	-	-	0.030	-	-	0.006
S/LFBR/W/LPB/EWN/FN/HBET:1,2	0.82	-	-	0.010	-	-	0.002
S/LFBR/W/LPB/EWN/FN/HBET:3,20	0.28	-	-	0.010	-	-	0.002
S/LFBR/S/LPB/EWN/FN/HBET:1,2	0.82	-	-	0.010	-	-	0.002
S/LFBR/S/LPB/EWN/FN/HBET:3,20	0.82	-	-	0.030	-	-	0.005
S/LFBR/S/LFBR/EWN/FN/HBET:1,2	0.82	-	-	0.060	-	-	0.012
S/LFBR/S/LFBR/EWN/FN/HBET:3,20	0.82	-	-	0.030	-	-	0.005
S/LFBR/S/LFBR/EWN/FC/HBET:1,2	0.82	-	-	0.060	-	-	0.012
S/LFBR/S/LFBR/EWN/FC/HBET:3,20	0.82	-	-	0.030	-	-	0.006

Table 5.5 Upper branch inside and outside collapse debris ratios per collapse state

Structural system	M4+M5(1-M4)	α_{inCS1}	α_{inCS2}	α_{inCS3}	α_{outCS1}	α_{outCS2}	α_{outCS3}
CR+PC/LPB/CR+PC/LPB/EWN/FN/HBET:1,2	0.82	-	-	0.200	-	-	0.040
CR+PC/LPB/CR+PC/LPB/EWN/FN/HBET:3,20	0.82	-	-	0.200	-	-	0.033
CR+PC/LWAL/CR+PC/LN/EWN/FC/HBET:1,2	0.82	-	-	0.600	-	-	0.150
CR+PC/LWAL/CR+PC/LN/EW/FC/HBET:1,2	0.82	-	-	0.600	-	-	0.150
CR+PC/LWAL/CR+PC/LN/EW/FC/HBET:3,20	0.82	-	-	0.600	-	-	0.150
CR+PC/LWAL/CR+PC/LWAL/EWN/FC/HBET:1,2	0.82	-	-	0.300	-	-	0.060
CR+PC/LWAL/CR+PC/LWAL/EWN/FC/HBET:3,20	0.82	-	-	0.300	-	-	0.060
CR+PC/LWAL/CR+PC/LWAL/EW/FC/HBET:1,2	0.82	-	-	0.300	-	-	0.075
CR+CIP/LPB/CR+CIP/LPB/EWN/FN/HBET:1,2	0.82	-	-	0.200	-	-	0.040
CR+CIP/LPB/CR+CIP/LPB/EWN/FN/HBET:3,20	0.82	-	-	0.200	-	-	0.033
CR+CIP/LFM/CR+CIP/LFM/EWN/FC/HBET:1,2	0.82	-	-	0.150	-	-	0.030
CR+CIP/LFM/CR+CIP/LFM/EWN/FC/HBET:3,20	0.82	-	-	0.100	-	-	0.020
CR+CIP/LWAL/CR+CIP/LN/EW/FC/HBET:1,2	0.82	-	-	0.400	-	-	0.100
CR+CIP/LWAL/CR+CIP/LN/EW/FC/HBET:3,20	0.82	-	-	0.400	-	-	0.100
CR+CIP/LWAL/CR+CIP/LWAL/EWN/FC/HBET:1,2	0.82	-	-	0.200	-	-	0.040
CR+CIP/LWAL/CR+CIP/LWAL/EWN/FC/HBET:3,20	0.82	-	-	0.200	-	-	0.040
MUR/LH/MUR/LH/EWN/FW/HBET:1,2	0.56	0.045	0.210	0.465	0.000	0.000	0.200
MUR/LH/MUR/LH/EWN/FW/HBET:3,20	0.56	0.045	0.210	0.465	0.000	0.000	0.100
MUR/LWAL/MUR/LN/EWN/FW/HBET:1,2	0.56	0.000	0.600	0.850	0.050	0.083	0.600
MUR/LWAL/MUR/LN/EWN/FW/HBET:3,20	0.56	0.000	0.600	0.850	0.075	0.125	0.600
MUR/LWAL/MUR/LN/EW/FC/HBET:1,2	0.56	0.060	0.060	0.850	0.072	0.072	0.600
MUR/LWAL/MUR/LN/EW/FC/HBET:1,2/IRIR+IRVP:CHV	0.56	0.011	0.027	0.850	0.012	0.018	0.600
MUR/LWAL/MUR/LN/EW/FC/HBET:3,20	0.56	0.002	0.113	0.850	0.075	0.125	0.850
MUR/LWAL/MUR/LN/EW/FW/HBET:1,2	0.56	0.000	0.600	0.850	0.117	0.200	0.600
MUR/LWAL/MUR/LN/EW/FW/HBET:3,20	0.56	0.000	0.600	0.850	0.175	0.300	0.600
MUR/LWAL/MUR/LWAL/EWN/FW/HBET:1,2	0.56	0.500	0.500	0.850	0.000	0.005	0.350
MUR/LWAL/MUR/LWAL/EWN/FW/HBET:3,20	0.56	0.000	0.600	0.850	0.038	0.064	0.600

Table 5.6 Upper branch inside and outside collapse debris ratios per collapse state (continued)

Structural system	M4+M5(1-M4)	α_{inCS1}	α_{inCS2}	α_{inCS3}	α_{outCS1}	α_{outCS2}	α_{outCS3}
MUR/LWAL/MUR/LWAL/EW/FC/HBET:1,2	0.56	0.000	0.046	0.850	0.015	0.015	0.350
MUR/LWAL/MUR/LWAL/EW/FC/HBET:3,20	0.56	0.000	0.150	0.300	0.050	0.088	0.150
MUR/LWAL/MUR/LWAL/EW/FW/HBET:1,2	0.56	0.000	0.600	0.850	0.065	0.111	0.350
MUR/LWAL/MUR/LWAL/EW/FW/HBET:3,20	0.56	0.000	0.600	0.850	0.117	0.200	0.600
MUR/LWAL/W/LPB/EWN/FN/HBET:1,2	0.56	-	-	0.050	-	-	0.010
MUR/LWAL/W/LPB/EWN/FN/HBET:3,20	0.56	-	-	0.050	-	-	0.008
W/LPB/W/LPB/EW/FN/HBET:1,2	0.28	-	-	0.850	-	-	0.170
W/LPB/W/LPB/EW/FN/HBET:3,20	0.28	-	-	0.850	-	-	0.142
W/LWAL/W/LN/EWN/FW/HBET:1,2	0.28	-	-	0.050	-	-	0.013
W/LWAL/W/LN/EW/FW/HBET:1,2	0.28	-	-	0.050	-	-	0.013
W/LWAL/W/LN/EW/FW/HBET:3,20	0.28	-	-	0.050	-	-	0.013
W/LWAL/W/LWAL/EWN/FW/HBET:1,2	0.28	-	-	0.050	-	-	0.013
W/LWAL/W/LWAL/EWN/FW/HBET:3,20	0.28	-	-	0.050	-	-	0.013
W/LWAL/W/LWAL/EW/FW/HBET:1,2	0.28	-	-	0.050	-	-	0.013
W/LWAL/W/LWAL/EW/FW/HBET:3,20	0.28	-	-	0.050	-	-	0.013
S/LPB/S/LPB/EWN/FN/HBET:1,2	0.82	-	-	0.200	-	-	0.040
S/LPB/S/LPB/EWN/FN/HBET:3,20	0.82	-	-	0.200	-	-	0.033
S/LFM/S/LFM/EWN/FC/HBET:1,2	0.82	-	-	0.100	-	-	0.020
S/LFM/S/LFM/EWN/FC/HBET:3,20	0.82	-	-	0.070	-	-	0.014
S/LFBR/W/LPB/EWN/FN/HBET:1,2	0.82	-	-	0.050	-	-	0.010
S/LFBR/W/LPB/EWN/FN/HBET:3,20	0.28	-	-	0.050	-	-	0.008
S/LFBR/S/LPB/EWN/FN/HBET:1,2	0.82	-	-	0.050	-	-	0.010
S/LFBR/S/LPB/EWN/FN/HBET:3,20	0.82	-	-	0.070	-	-	0.012
S/LFBR/S/LFBR/EWN/FN/HBET:1,2	0.82	-	-	0.100	-	-	0.020
S/LFBR/S/LFBR/EWN/FN/HBET:3,20	0.82	-	-	0.070	-	-	0.012
S/LFBR/S/LFBR/EWN/FC/HBET:1,2	0.82	-	-	0.100	-	-	0.020
S/LFBR/S/LFBR/EWN/FC/HBET:3,20	0.82	-	-	0.070	-	-	0.014

Chapter 6

Conclusions and Future Plans

The v5 fragility and consequence models presented herein build upon an extensive modelling and experimental testing campaign that has been presented in a number of NAM reports and peer-reviewed publications (as cited herein and included in the references of this report). This report has explained how the outcomes of such studies have been utilised for the development of damage and collapse fragility and fatality functions for the most important structural systems that are present in the Groningen field. These functions have been used in NAM'S Monte Carlo risk engine to estimate Local Personal Risk (LPR), group risk (Maatschappelijk Risico) and group damage plots (so-called Maatschappelijk Risico (Schade)) for all buildings in the field.

The work presented herein (and all of the studies that feed these analyses) will be assessed by a number of international and national experts during an assurance workshop that is planned for February/March 2018. In the meantime, a number of developments on the numerical modelling, experimental testing and exposure model fronts are planned, and any new data arising from these efforts will be fed into the methodology presented herein, and updated fragility and consequence inputs for the risk engine will be produced. On the other hand, the methodology for developing fragility and consequence models is unlikely to undergo major changes in the near future. There may, however, be a need to also estimate economic losses due to damage in the future, and in this case a consequence model related to repair costs for different damage states will need to be developed.

Chapter 7

References

- Akkar S., Sandikkaya M.A., Senyurt M., Azari Sisi A., Ay B.O., Traversa P., Douglas J., Cotton F., Luzi L., Hernandez B. and Godey S. (2014) "Reference database for seismic ground-motion in Europe (RESORCE)," *Bulletin of Earthquake Engineering*, 12, 311-339.
- Arup (2017a) "EDB V5 data documentation," 229746_052.0_REP2014, November 2017.
- Arup (2017b) "EDB V5 post-analysis documentation," 229746_052.0_REP2018c, November 2017.
- Arup (2017c) "Typology modelling: Analysis results in support of fragility functions - 2017 batch results," 229746_031.0_REP2005, November 2017.
- Arup, TU Delft, Eucentre (2015) "Eucentre shake-table test of terraced house modelling predictions and analysis cross validation," November 2015.
- Arup, TU Delft, Eucentre and Arcadis (2016a) "EUC-BUILD2: Modelling predictions and analysis cross validation of detached single-storey URM building," September 2016.
- Arup, TU Delft and Eucentre (2016b) "Laboratory component testing: Modelling post-test predictions and analysis cross validation," February 2016.
- Arup, TU Delft, Eucentre and Mosayk (2017) "LNEC-BUILD1: Modelling predictions and analysis cross validation," September 2017.
- ASI (2017) *Extreme Loading for Structures v5*, Applied Science International LLC, Durham (NC), USA.
- Baker J.W. (2007) "Probabilistic structural response assessment using vector-valued intensity measures," *Earthquake Engineering and Structural Dynamics*, 36, pp. 1861-1883.
- Baker J.W. and Cornell C.A. (2006) "Which spectral acceleration are you using?" *Earthquake Spectra*, 22(2), pp. 293-312.
- Bommer J.J., Magenes G., Hancock J. and Penazzo P. (2004) "The influence of strong-motion duration on the seismic response of masonry structures," *Bulletin of Earthquake Engineering*, 2(1), pp. 1-26.
- Bommer J.J., Stafford P.J., Edwards B., Dost B., van Dedem E., Rodriguez-Marek A., Kruiver P.P., van Elk J., Doornhof D. and Ntinalexis M. (2016) "Framework for a Ground-Motion Model for Induced Seismic Hazard and Risk Analysis in the Groningen Gas Field, The Netherlands," *Earthquake Spectra*, 33(2), pp. 481-498.

- Bommer J.J., Edwards B., Kruiver P.P., Rodriguez-Marek A., Stafford P.J., Dost B., Ntinalexis M., Ruigrok E. and Spetzler J. (2017) "V5 ground-motion model for the Groningen Field," October 2017.
- Borzi B., Crowley H. and Pinho R. (2008) "Simplified pushover-based earthquake loss assessment (SP-BELA) method for masonry buildings," *International Journal of Architectural Heritage*, 2:4, 353-376.
- Brunesi E., Peloso S., Pinho R. and Nascimbene R. (2017a) "Cyclic testing of a full-scale RC cast-in-place wall-slab-wall structure representative of the Groningen building stock (EUC-BUILD3)," Eucentre Foundation, Pavia, Italy, May 2017, Available from URL: www.eucentre.it/nam-project.
- Brunesi E., Peloso S., Pinho R. and Nascimbene R. (2017b) "Cyclic testing of a full-scale RC precast wall-slab-wall structure representative of the Groningen building stock (EUC-BUILD4)," Eucentre Foundation, Pavia, Italy, May 2017, Available from URL: www.eucentre.it/nam-project.
- Brunesi E., Peloso S., Pinho R. and Nascimbene R. (2017c) "Dynamic testing of a full scale two-storey RC precast wall-slab-wall structure representative of the Groningen building stock (EUC-BUILD5)," Eucentre Foundation, Pavia, Italy, May 2017, Available from URL: www.eucentre.it/nam-project.
- Brzez S., Scawthorn C., Charleson A.W., Allen L., Greene M., Jaiswal K. ad Silva V. (2013) "GEM Building Taxonomy Version 2.0," GEM Technical Report 2013-02 V1.0.0, 188 pp., GEM Foundation, Pavia, Italy, doi: 10.13117/GEM.EXT-MOD.TR2013.02
- Casarotti C. and Pinho R. (2007) "An adaptive capacity spectrum method for assessment of bridges subjected to earthquake action," *Bulletin of Earthquake Engineering*, 5, pp. 377-390.
- Calvi G.M., Pinho R., Magenes G., Bommer J.J., Restrepo-Velez L.F. and Crowley H. (2006), "Development of seismic vulnerability assessment methodologies over the past 30 years," *ISET Journal of Earthquake Technology*, Paper no. 472, 43 (3), pp. 75-104.
- Chiou B., Darragh R., Gregor N. and Silva W. (2008) NGA Project Strong-Motion Database, *Earthquake Spectra*, 24(1), pp. 23-44.
- Coburn A. and Spence R. (2002) *Earthquake Protection*, 2nd Edition, John Wiley & Sons Ltd, Chichester.
- Coburn A.W., Spence R.J.S. and Pomonis, A. (1992) "Factors Determining Casualty Levels in Earthquakes: Mortality Prediction in Building Collapse," *Proceedings of the 10th World Conference on Earthquake Engineering*, Madrid, Spain
- Correia A.A., Marques A.I., Bernardo V., Grottoli L., Tomassetti U. and Graziotti F. (2017) "Shake-table test up to collapse on a roof substructure of a Dutch terraced house (LNEC-BUILD2)," October 2017.
- Crowley H., Pinho R., Polidoro B. and Stafford P. (2015) "Development of v2 partial collapse fragility and consequence functions for the Groningen field," November 2015.
- Crowley H., Polidoro B., Pinho R., van Elk J. (2017) "Framework for developing fragility and consequence models for local personal risk," *Earthquake Spectra*, in press.

- D'Ayala, D., Meslem, A., Vamvatsikos, D., Porter, K. and Rossetto, T. (2014). Guidelines for analytical vulnerability assessment of low/mid-rise buildings. GEM Technical Report 2014-12, GEM Foundation, Pavia, Italy. DOI: 10.13117/GEM.VULN-MOD.TR2014.12.
- Dymiotis C., Kappos A.J. and Chryssanthopoulos M.K. (1999) "Seismic reliability of RC frame with uncertain drift and member capacity," *Journal of Structural Engineering*, 125(9), pp. 1038–1047.
- Eucentre, P&P, TU-Delft, TU-Eindhoven (2015) "Material Characterisation," Version 1.3, October 2015.
- FEMA (2004) "HAZUS-MH Technical Manual," Federal Emergency Management Agency, Washington D.C.
- FEMA (2012) "Seismic performance assessment of buildings. Volume 1 - Methodology," FEMPA P-58-1, Federal Emergency Management Agency, Washington D.C.
- Graziotti F, Tomassetti U., Rossi A., Marchesi B., Kallioras S., Mandirola M, Fragomeli A., Mellia E., Peloso S., Cuppari F, Guerrini G., Penna A., Magenes G. (2015) "Experimental campaign on cavity wall systems representative of the Groningen building stock", Report n. EUC318/2015U, Eucentre Foundation, Pavia, Italy. Available from URL: www.eucentre.it/nam-project
- Graziotti F., Rossi A., Mandirola M., Penna A., and Magenes G. (2016a) "Experimental characterization of calcium-silicate brick masonry for seismic assessment," *Proceedings of the 16th International Brick and Block Masonry Conference (IBMAC)*, Padua, Italy, 1619-1627.
- Graziotti F, Tomassetti U., Rossi A., Marchesi B., Kallioras S., Mandirola M., Fragomeli A., Mellia E., Peloso S., Cuppari F, Guerrini G., Penna A. and Magenes G. (2016b) "Experimental campaign on a clay URM full-scale specimen representative of the Groningen building stock (EUC-BUILD2)," July 2016.
- Graziotti F, Tomassetti U., Penna A., Magenes G. (2016c) "Out-of-plane shaking table tests on URM single leaf and cavity walls," *Engineering Structures* 125, 455–470.
- Graziotti F, Tomassetti U., Kallioras S., Penna A., and Magenes G. (2017a) "Shaking table test on a full scale URM cavity wall building," *Bulletin of Earthquake Engineering*, doi: 10.1007/s10518-017-0185-8.
- Graziotti F, Tomassetti U., Penna A., Magenes M. (2017b) "Tests on URM clay and calcium-silicate masonry structures: identification of damage states," Eucentre Foundation, Pavia, Italy. Working Version of October 2017. Available from URL: www.eucentre.it/nam-project
- Graziotti F, Tomassetti U., Sharma S., Grottoli L., Dainotti S., Scherini S., Penna A. and Magenes G. (2017c) "Out-of-plane two-way bending shaking table tests on single leaf and cavity walls," Eucentre Foundation, Pavia Italy. Working Version of October 2017. Available from URL: www.eucentre.it/nam-project
- GRC - Geotechnical Research Centre of Western Ontario University (2015) DYNA6.1 – A program for the computation of the response of rigid foundations to all types of dynamic loads. Ontario, Canada.
- Grunthal G., Musson R.M.W., Schwarz J. and Stucchi M. (1998) "European Macroseismic Scale 1998," Centre Europeen de Geodynamique et de Seismologie, ISBN No2-87977-008-4.
- Jaiswal K., Wald D.J. and Hearne M. (2009) "Estimating Casualties for Large Worldwide Earthquakes using an Empirical Approach," US Geological Survey Open-File Report 1136

- Jalayer F. (2003) Direct probabilistic seismic analysis: Implementing non-linear dynamic assessments, Ph.D. Dissertation, Stanford University.
- Jonkman S.N., van Gelder P.H.A.J.M and Vrijling J.K. (2003) "An overview of quantitative risk measures for loss of life and economic damage," *Journal of Hazardous Materials A99*, pp. 1-30.
- Kruiver P.P., van Dedem E., Romijn R., de Lange G.L., Korff M., Stafleu J., Gunnick J.L., Rodriguez-Marek A., Bommer J.J., van Elk J. and Doornhof D. (2016) "An integrated shear-wave velocity model for the Groningen gas field, The Netherlands," submitted to *Bulletin of Earthquake Engineering*.
- LSTC - Livermore Software Technology Corporation (2013) LS-DYNA - A general-purpose finite element program capable of simulating complex problems. Livermore, California.
- Luco N. and Cornell C.A. (2007) "Structure-Specific Scalar Intensity Measures for Near-Source and Ordinary Earthquake Ground Motions," *Earthquake Spectra*, 23(2), pp. 357-392.
- McKenna F., Fenves G.L., Scott M.H. and Jeremic, B. (2000) Open System for Earthquake Engineering Simulation (OpenSees), Pacific Earthquake Engineering Research Center, University of California, Berkeley, CA.
- Miller A.C. and Rice T.R. (1983) "Discrete approximations of probability distributions," *Management Science*, 29(3), pp. 352-362
- Mosayk (2014) "Software verification against experimental benchmark data," November 2014.
- Mosayk (2015a) "Structural modelling of non-URM buildings - v2 risk model update," October 2015.
- Mosayk (2015b) "Soil-structure interaction (SSI) impedance functions for SDOF systems," October 2015.
- Mosayk (2016) "Using the Applied Element Method to model URM walls subjected to in-plane cyclic shear-compression," December 2016.
- Mosayk (2017a) "Using the Applied Element Method to model the shake-table testing of two full-scale URM houses," October 2017.
- Mosayk (2017b) "Using the Applied Element Method to model the collapse shake-table testing of a URM cavity wall structure," October 2017.
- Mosayk (2017c) "Using the Applied Element Method to model the collapse shake-table testing of a terraced house roof substructure," October 2017.
- Mosayk (2017d) "Nonlinear dynamic analysis of index buildings for v5 fragility and consequence models," October 2017.
- Mosayk (2017e) "Using the Applied Element Method to model the shake-table out-of-plane testing of full-scale URM wall specimens subjected to one-way bending," November 2017.
- Mylonakis G., Nikolaou S., Gazetas G. (2006). Footings under seismic loading: Analysis and design issues with emphasis on bridge foundations. *Soil Dynamics and Earthquake Engineering* 26, 824–853.
- Samardjieva E. and Badal J. (2002) "Estimation of the expected number of casualties caused by strong earthquakes," *Bulletin of Seismological Society of America*, 92, pp. 2310–2322.

- Seismosoft (2017) SeismoStruct v2016 - A computer program for static and dynamic nonlinear analysis of framed structures, Available from <http://www.seismosoft.com>
- So E.K.M. and Pomonis A. (2012) "Derivation of globally applicable casualty rates for use in earthquake loss estimation models," Proceedings of 15th World Conference on Earthquake Engineering, paper 1164.
- Stafford P.J. (2008) "Conditional prediction of absolute durations", Bulletin of Seismological Society of America, 98(3), pp. 1588-1594.
- Takeda T., Sozen M.A. and Nielsen N.N. (1970) "Reinforced concrete response to simulated earthquakes," ASCE Journal of the Structural Division, 96, 12.
- Taig A.R. and Pickup F.E. (2016) "Risk Assessment of Falling Hazards in Earthquakes in the Groningen region," Arup Report 229746_32.0_{REP}1008, Available from URL: <http://www.nam.nl/feiten-en-cijfers/onderzoeksrapporten.html>
- Tomasetti U., Correia A.A., Graziotti F., Marques A.I., Mandirola M., and Candeias P.X. (2017) "Collapse shaking table test on a URM cavity wall building representative of a Dutch terraced house (LNEC-BUILD1)," Eucentre Foundation, Pavia, Italy and LNEC, Lisbon, Portugal, September 2017.
- Vamvatsikos D. and Cornell C.A. (2002) "Incremental dynamic analysis," Earthquake Engineering and Structural Dynamics, 31(3), pp. 491–514.

Appendix A

Explanation of Structural System and Layout Attributes

The following table explains the GEM Building Taxonomy codes that have been used herein.

Table A.1 Explanation of GEM Building Taxonomy codes

Attribute	Value	GEM taxonomy code
Material of lateral load-resisting system	Precast concrete	CR+PC
	Cast-in-place concrete	CR+CIP
	Masonry	MUR
	Wood	W
	Steel	S
Type of lateral load-resisting system	No lateral load-resisting system	LN
	Post and beam	LPB
	Moment frame	LFM
	Braced frame	LFBR
	Hybrid lateral load-resisting system	LH
	Walls	LWAL
Presence of exterior wall	No outer leaf cavity wall	EWN
	Presence of outer leaf	EW
Material of floor system	No elevated floor material	FN
	Concrete	FC
	Timber	FW
Height	Range of number of storeys above ground (a = upper bound, b = lower bound)	HBET:a,b
Structural Irregularity	Irregular structure	IRIR
	Vertical structural irregularity - primary	IRVP
	Change in vertical structure	CHV

The structural layout attribute is defined using a number of codes that are described in the table below.

Table A.2 Explanation of structural layout codes

Attribute	Short description	Geometric grouping
UBH	Block Unit	Medium sized buildings which are touching other similar buildings forming a uniform or homogeneous block
UBA	Aggregated Unit	Medium sized buildings which are touching different buildings, forming a homogeneous block
UH	House	Medium sized buildings with small span which are freestanding
BTN	Block Tall	Buildings without large spans expected to contain horizontal repetitions of unit structures in one direction. 'Tall' is designated where a gutter height is larger than 10 m
WBW	Warehouse	Buildings with flat roof, large span and a single-storey structure
WBH	Barn with House	Buildings which are formed by single storey buildings with a pitched roof with a large span and medium sized buildings with small span

Appendix B

Representativeness of Index Buildings

The following plots present the histograms of various characteristics of the structural systems, based on the data in the v5 exposure model. These histograms can be used to verify the representativeness of the index buildings used herein, and to inform the selection of future index buildings.

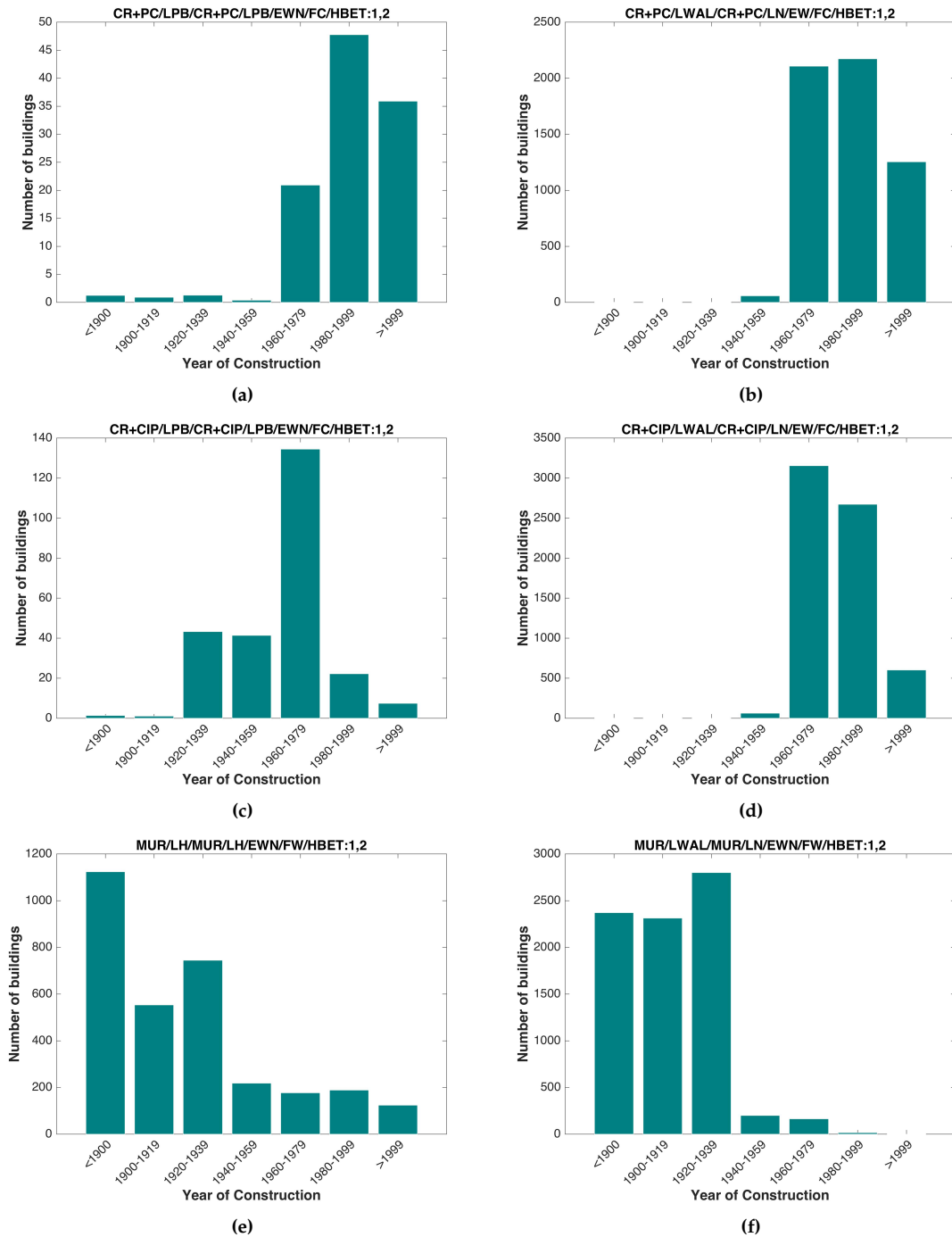


Figure B.1 Histograms of year of construction

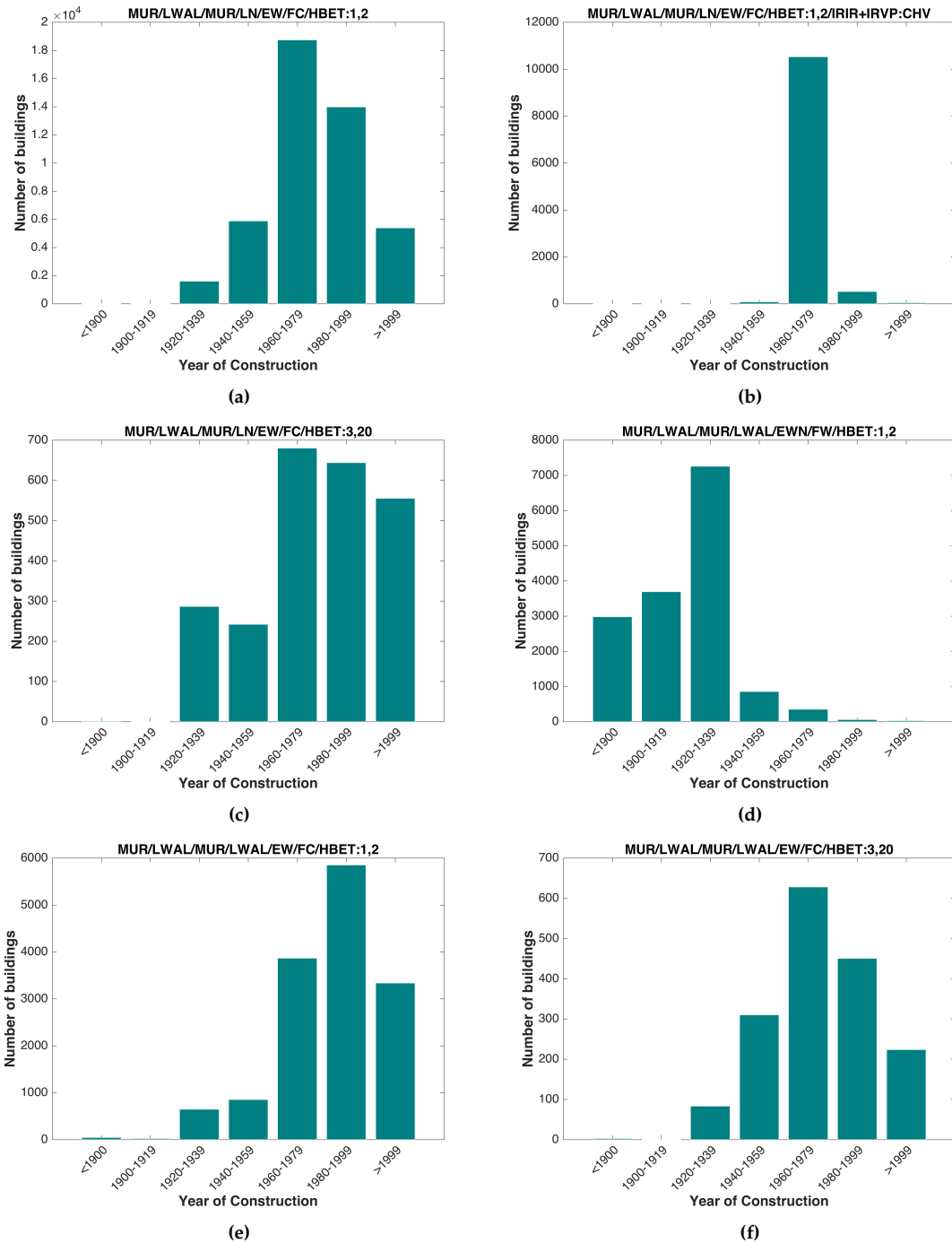


Figure B.2 Histograms of year of construction (continued)

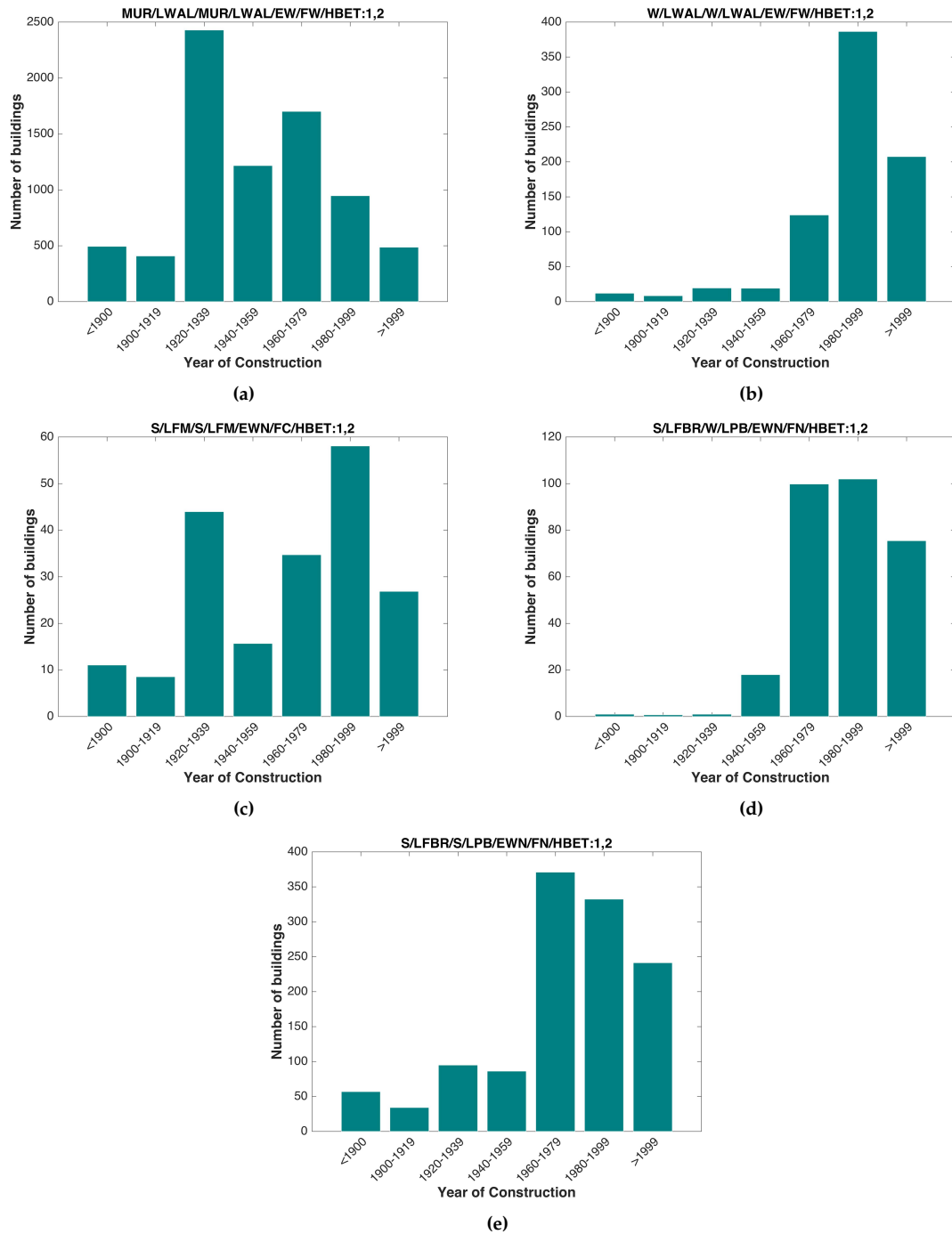


Figure B.3 Histograms of year of construction (continued)

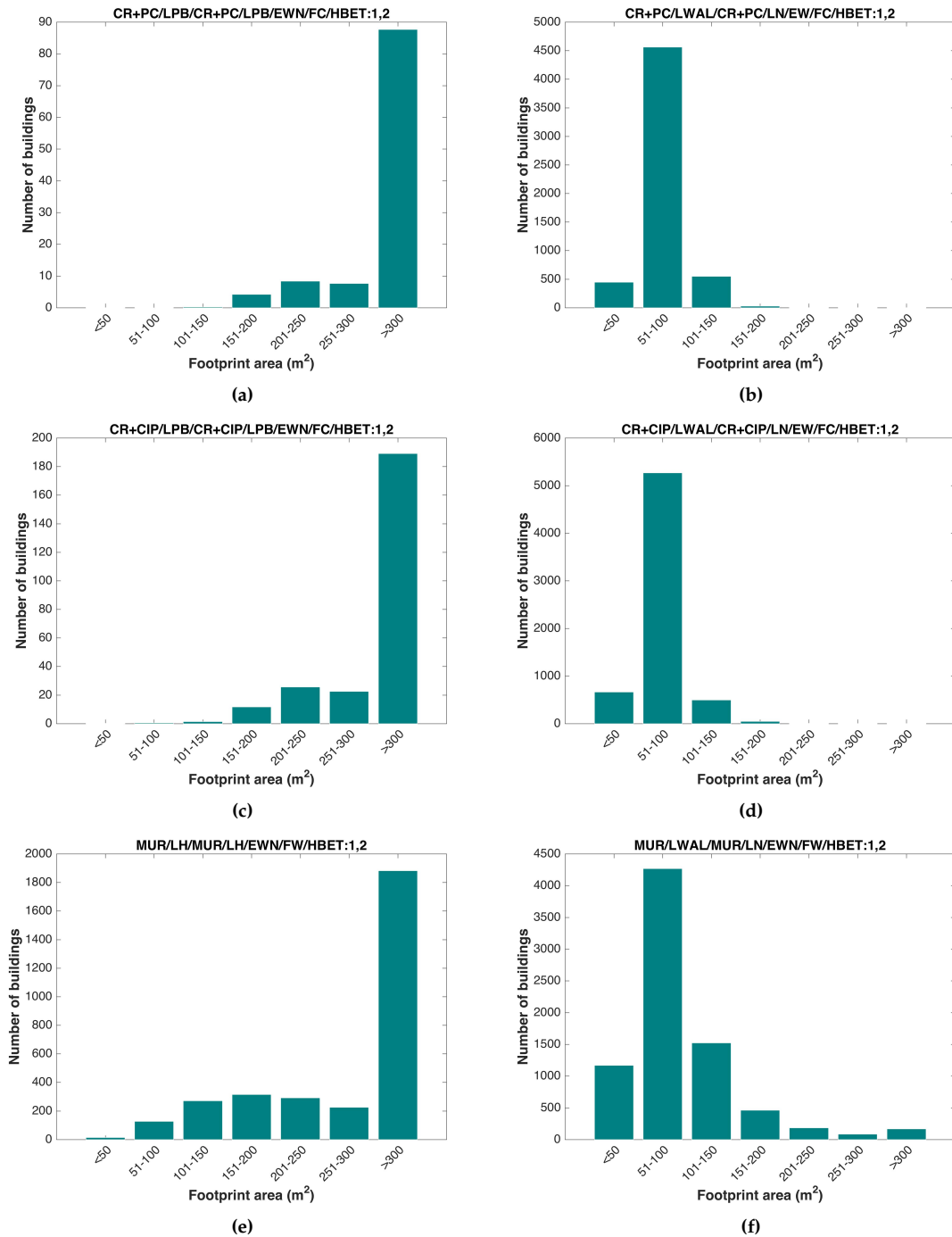


Figure B.4 Histograms of footprint area

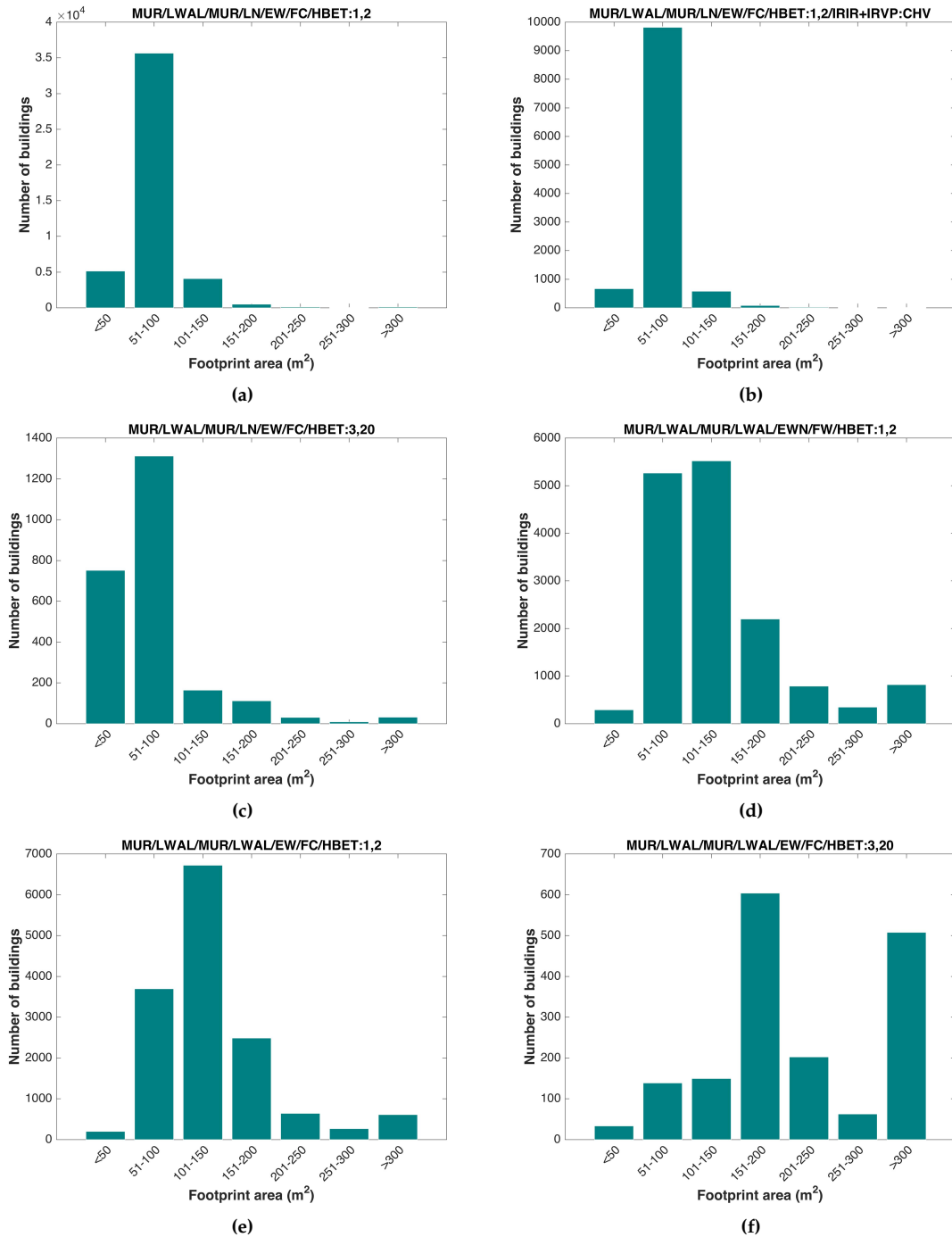


Figure B.5 Histograms of footprint area (continued)

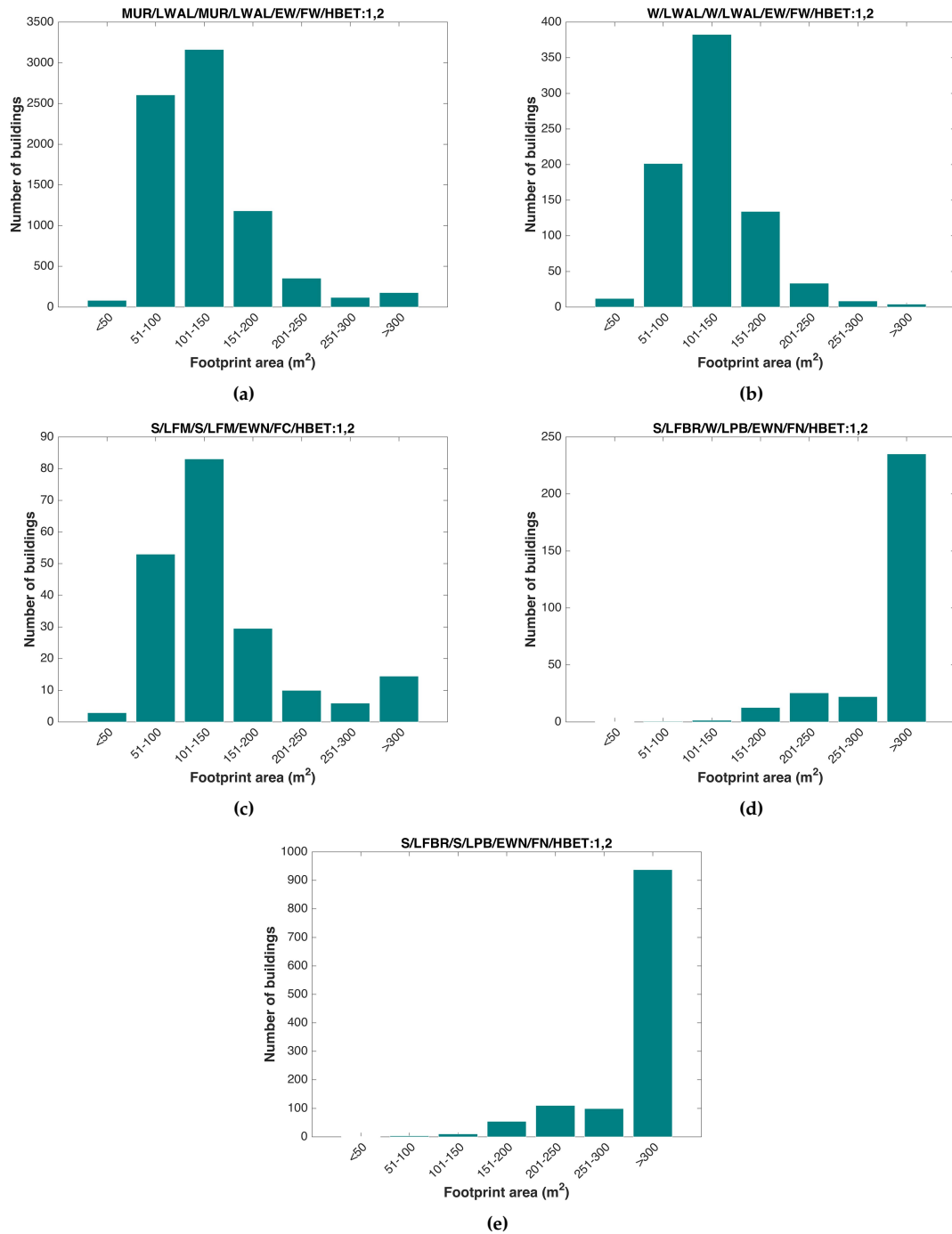


Figure B.6 Histograms of footprint area (continued)

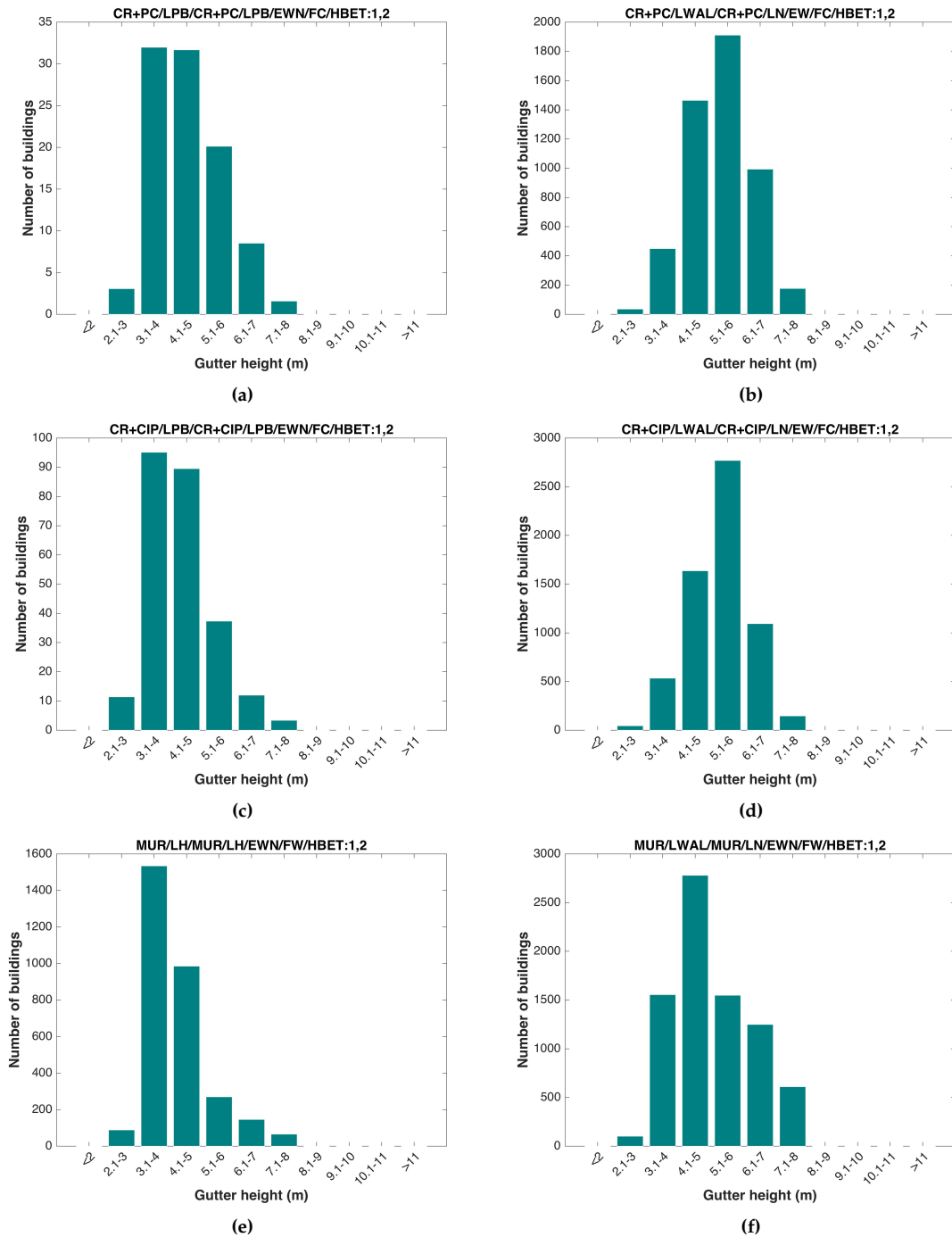


Figure B.7 Histograms of gutter height

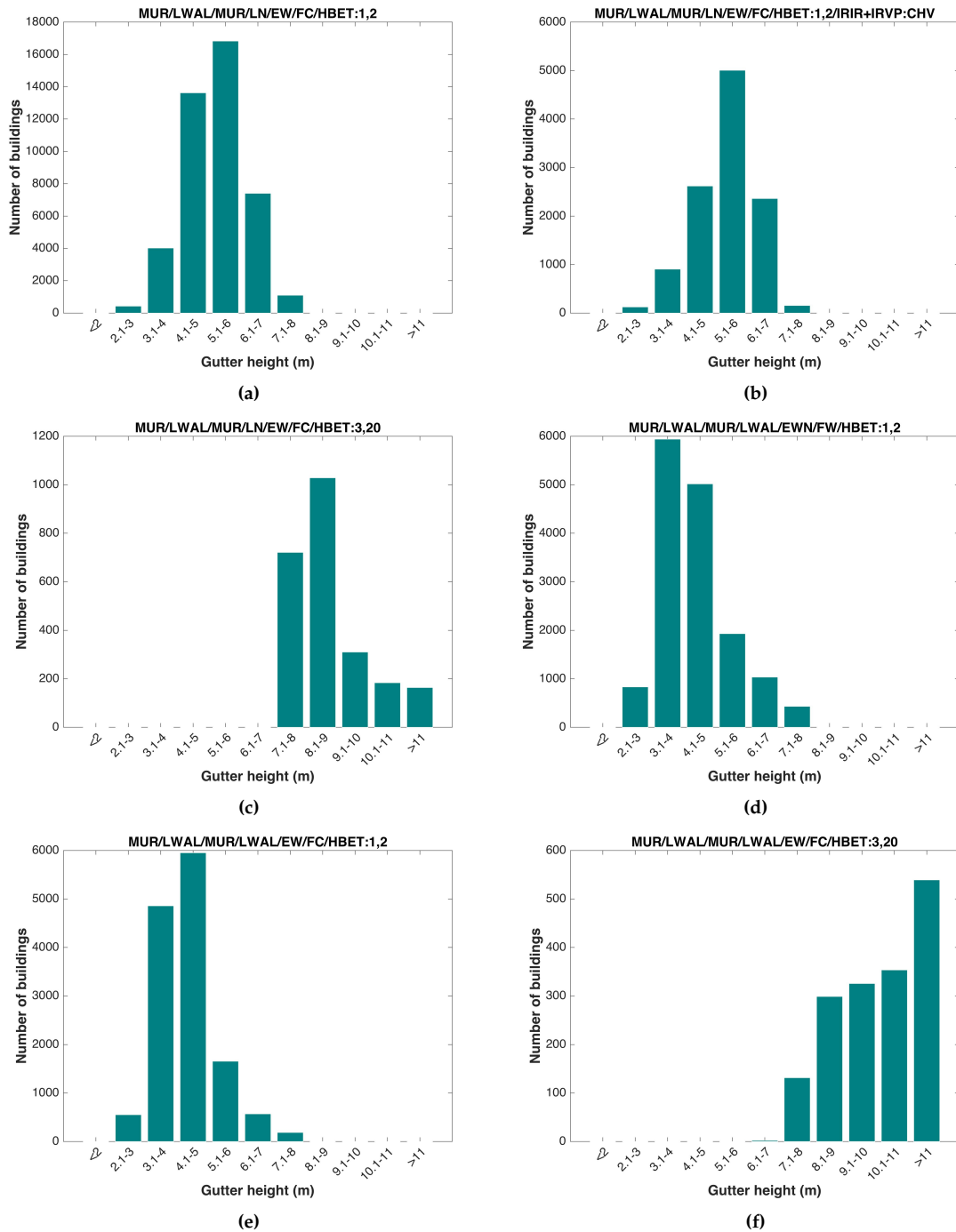


Figure B.8 Histograms of gutter height (continued)

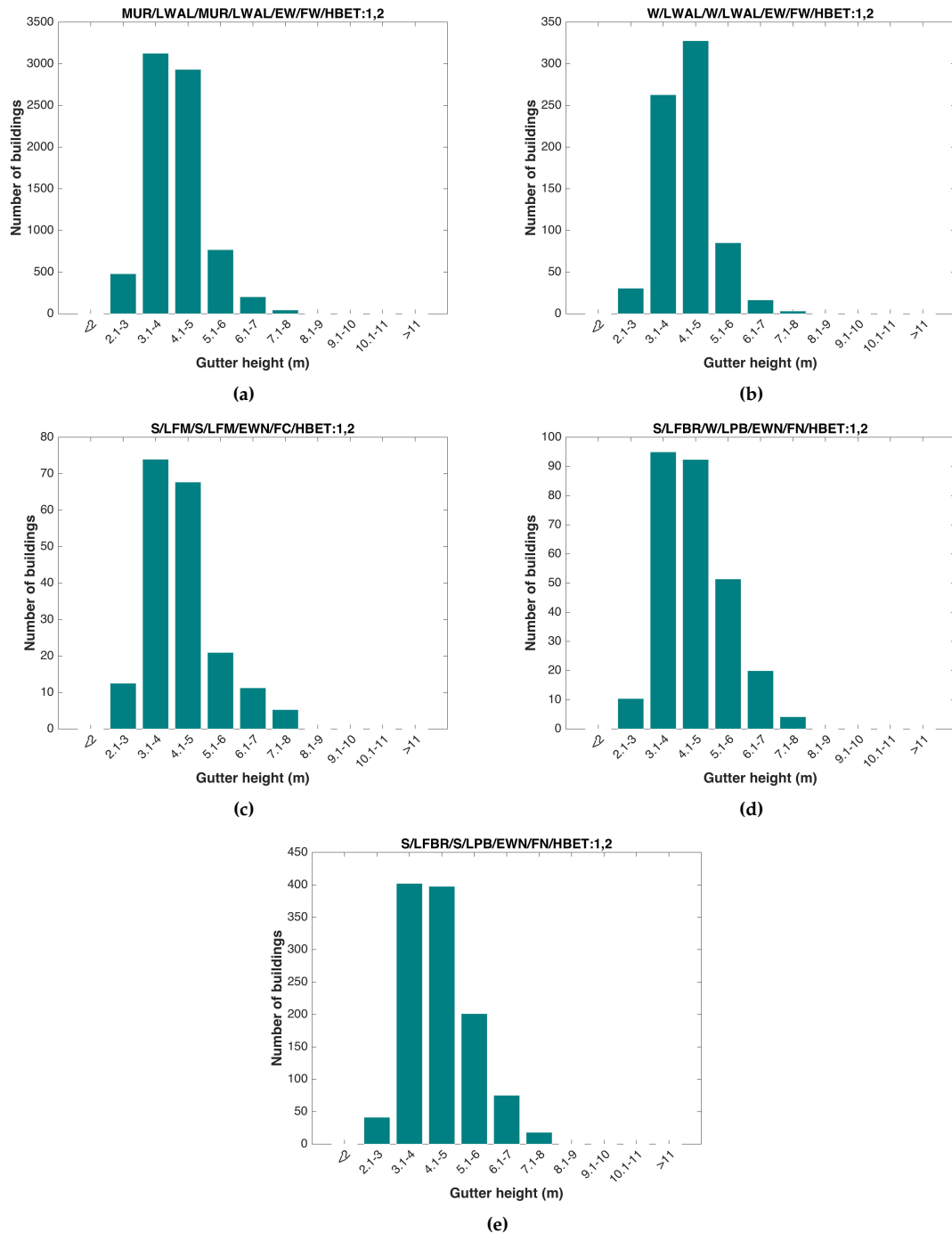


Figure B.9 Histograms of gutter height (continued)

Appendix C

Cloud Plots for all Models

The cloud plots for all OpenSees models (from Tables 3.1 and 3.1) are presented in the following figures. For simplicity of presentation of the results, the structural systems are identified using short codes, as presented in Table C.1.

Table C.1 Short code names for each structural system

Structural System	Short name
CR+PC/LPB/CR+PC/LPB/EWN/FN/HBET:1,2	PC1L
CR+PC/LPB/CR+PC/LPB/EWN/FN/HBET:3,20	PC1M
CR+PC/LWAL/CR+PC/LN/EWN/FC/HBET:1,2	PC2L
CR+PC/LWAL/CR+PC/LN/EW/FC/HBET:1,2	PC3L
CR+PC/LWAL/CR+PC/LN/EW/FC/HBET:3,20	PC3M
CR+PC/LWAL/CR+PC/LWAL/EWN/FC/HBET:1,2	PC4L
CR+PC/LWAL/CR+PC/LWAL/EWN/FC/HBET:3,20	PC4M
CR+PC/LWAL/CR+PC/LWAL/EW/FC/HBET:1,2	PC5L
CR+CIP/LPB/CR+CIP/LPB/EWN/FN/HBET:1,2	RC1L
CR+CIP/LPB/CR+CIP/LPB/EWN/FN/HBET:3,20	RC1M
CR+CIP/LFM/CR+CIP/LFM/EWN/FC/HBET:1,2	RC2L
CR+CIP/LFM/CR+CIP/LFM/EWN/FC/HBET:3,20	RC2M
CR+CIP/LWAL/CR+CIP/LN/EW/FC/HBET:1,2	RC3L
CR+CIP/LWAL/CR+CIP/LN/EW/FC/HBET:3,20	RC3M
CR+CIP/LWAL/CR+CIP/LWAL/EWN/FC/HBET:1,2	RC4L
CR+CIP/LWAL/CR+CIP/LWAL/EWN/FC/HBET:3,20	RC4M
MUR/LH/MUR/LH/EWN/FW/HBET:1,2	URM1L
MUR/LH/MUR/LH/EWN/FW/HBET:3,20	URM1M
MUR/LWAL/MUR/LN/EWN/FW/HBET:1,2	URM2L
MUR/LWAL/MUR/LN/EWN/FW/HBET:3,20	URM2M
MUR/LWAL/MUR/LN/EW/FC/HBET:1,2	URM3L
MUR/LWAL/MUR/LN/EW/FC/HBET:1,2/IRIR+IRVP:CHV	URM4L
MUR/LWAL/MUR/LN/EW/FC/HBET:3,20	URM3M
MUR/LWAL/MUR/LN/EW/FW/HBET:1,2	URM5L
MUR/LWAL/MUR/LN/EW/FW/HBET:3,20	URM5M
MUR/LWAL/MUR/LWAL/EWN/FW/HBET:1,2	URM6L
MUR/LWAL/MUR/LWAL/EWN/FW/HBET:3,20	URM6M
MUR/LWAL/MUR/LWAL/EW/FC/HBET:1,2	URM7L
MUR/LWAL/MUR/LWAL/EW/FC/HBET:3,20	URM7M
MUR/LWAL/MUR/LWAL/EW/FW/HBET:1,2	URM8L
MUR/LWAL/MUR/LWAL/EW/FW/HBET:3,20	URM8M
MUR/LWAL/W/LPB/EWN/FN/HBET:1,2	W1L
MUR/LWAL/W/LPB/EWN/FN/HBET:3,20	W1M
W/LPB/W/LPB/EW/FN/HBET:1,2	W2L
W/LPB/W/LPB/EW/FN/HBET:3,20	W2M
W/LWAL/W/LN/EWN/FW/HBET:1,2	W3L
W/LWAL/W/LN/EW/FW/HBET:1,2	W4L
W/LWAL/W/LN/EW/FW/HBET:3,20	W4M
W/LWAL/W/LWAL/EWN/FW/HBET:1,2	W5L
W/LWAL/W/LWAL/EWN/FW/HBET:3,20	W5M
W/LWAL/W/LWAL/EW/FW/HBET:1,2	W6L
W/LWAL/W/LWAL/EW/FW/HBET:3,20	W6M
S/LPB/S/LPB/EWN/FN/HBET:1,2	S1L
S/LPB/S/LPB/EWN/FN/HBET:3,20	S1M
S/LFM/S/LFM/EWN/FC/HBET:1,2	S2L
S/LFM/S/LFM/EWN/FC/HBET:3,20	S2M
S/LFBR/W/LPB/EWN/FN/HBET:1,2	W7L
S/LFBR/W/LPB/EWN/FN/HBET:3,20	W7M
S/LFBR/S/LPB/EWN/FN/HBET:1,2	S3L
S/LFBR/S/LPB/EWN/FN/HBET:3,20	S3M
S/LFBR/S/LFBR/EWN/FN/HBET:1,2	S4L
S/LFBR/S/LFBR/EWN/FN/HBET:3,20	S4M
S/LFBR/S/LFBR/EWN/FC/HBET:1,2	S5L
S/LFBR/S/LFBR/EWN/FC/HBET:3,20	S5M

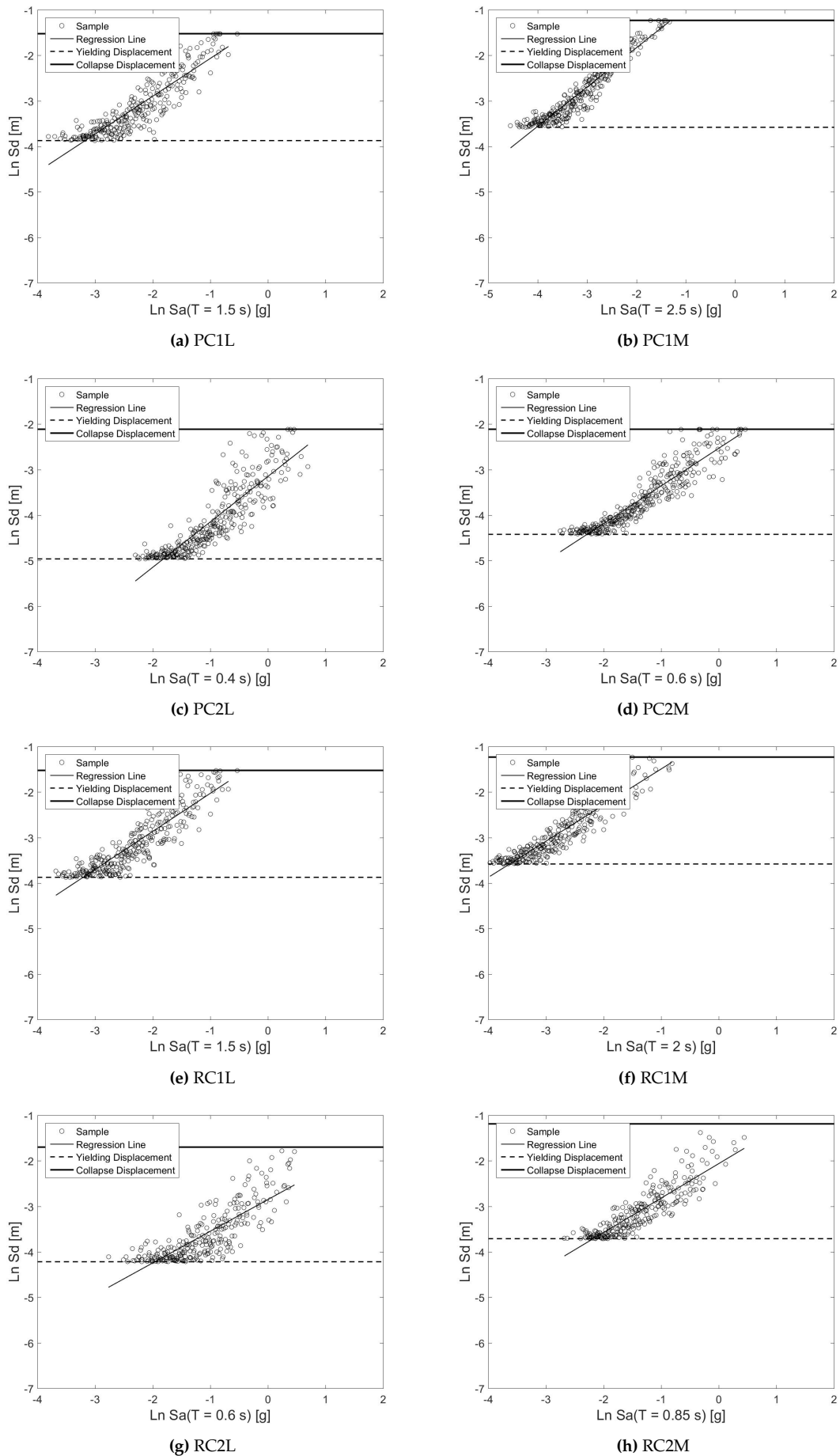


Figure C.1 Cloud plots for each structural system

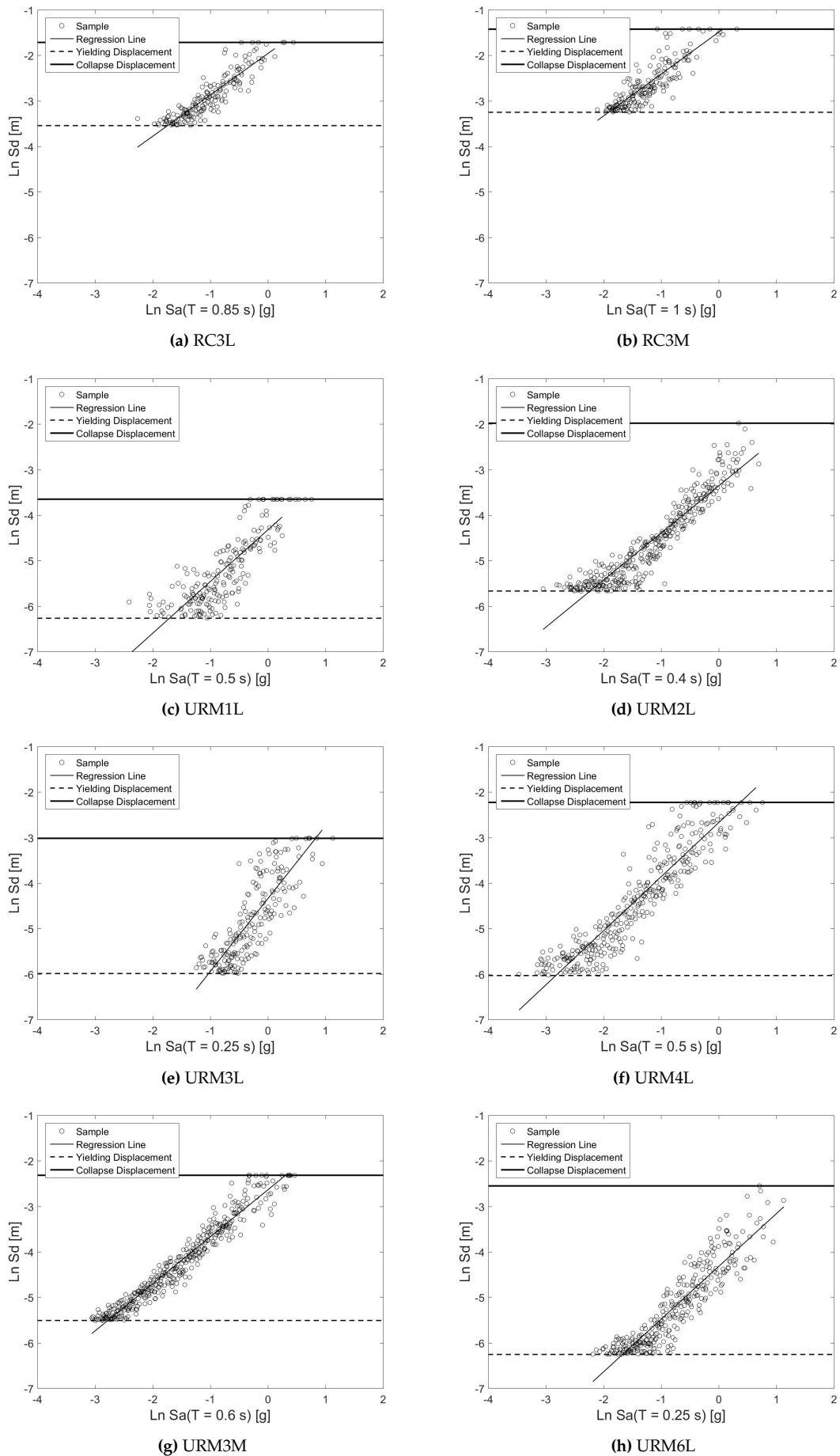
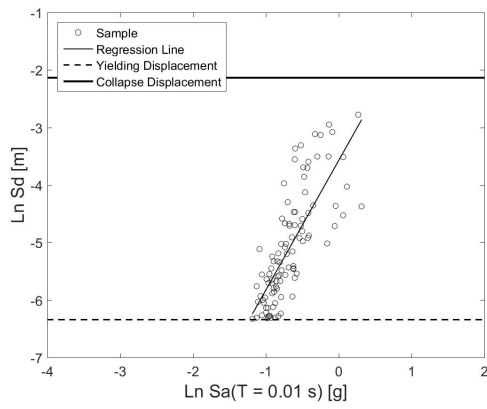
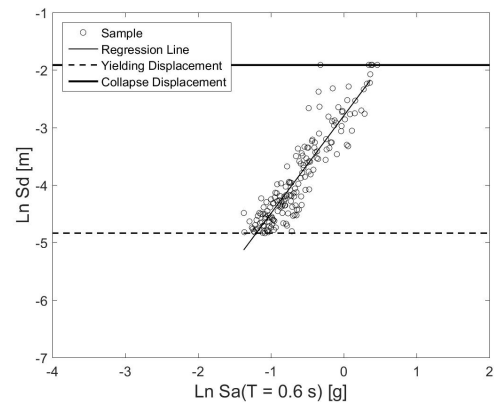


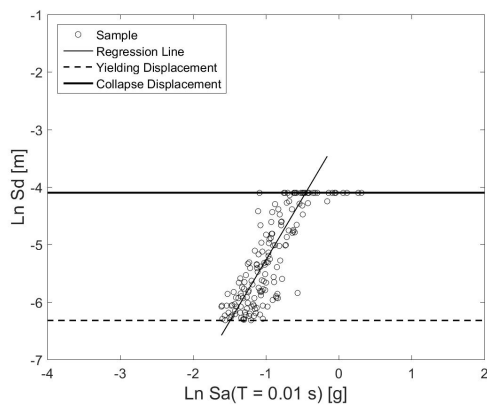
Figure C.2 Cloud plots for each structural system (cont.)



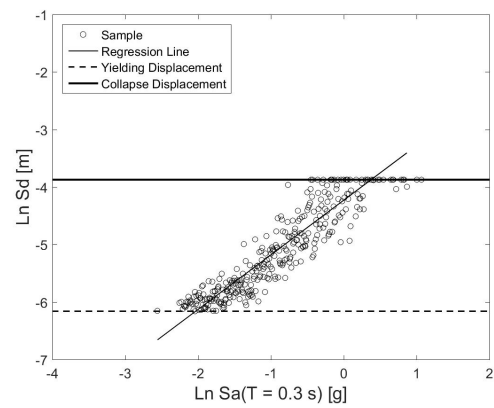
(a) URM7L



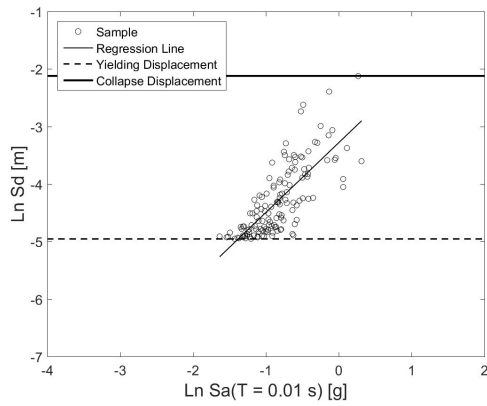
(b) URM7M



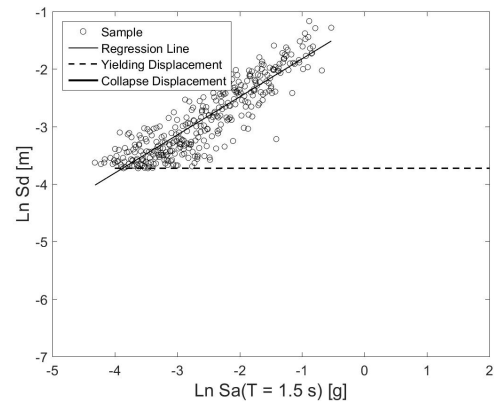
(c) URM8L



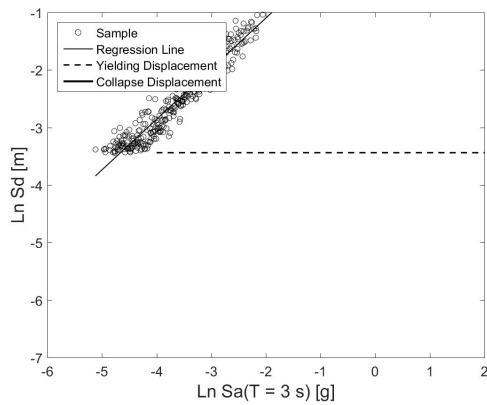
(d) W2L



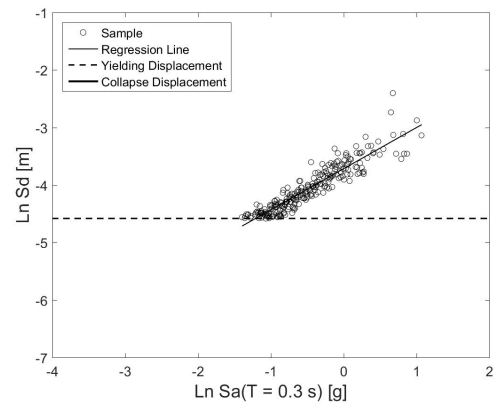
(e) W6L



(f) S2L

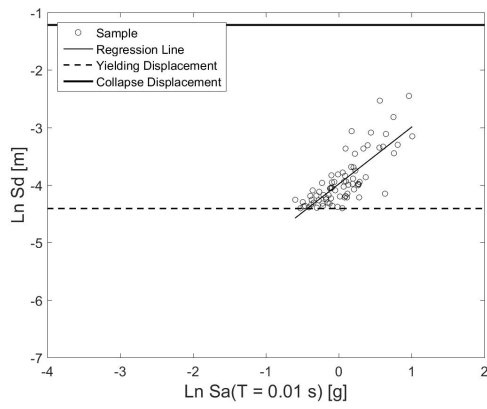


(g) S2M

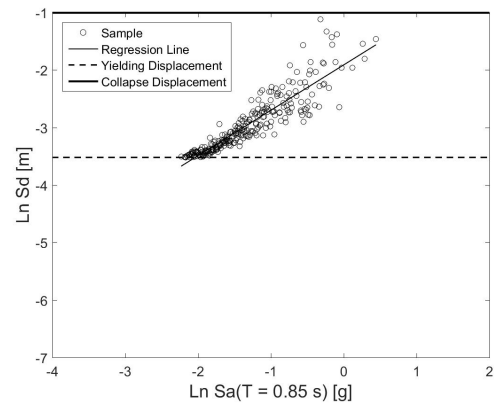


(h) W7L

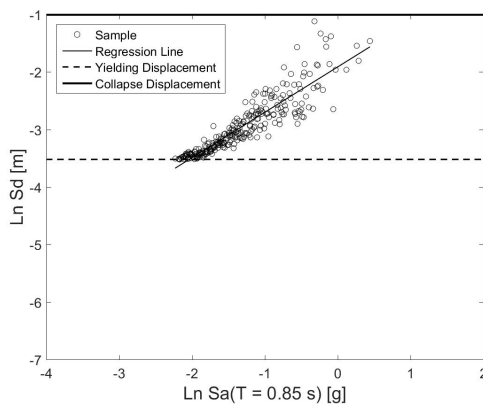
Figure C.3 Cloud plots for each structural system (cont.)



(a) S3L



(b) S5L



(c) S5M

Figure C.4 Cloud plots for each structural system (cont.)

Appendix D

Collapse Mechanisms of URM Index Buildings

The nonlinear dynamic analyses described in Chapter 2 have been undertaken using subsets of the records summarised in Table D.1 below. More details on these records are provided in Arup (2017c) and Mosyak (2017d). The different collapse mechanisms/states, and the records that produced them, are summarised for each URM index building in the following sections.

Table D.1 Records used in the nonlinear dynamic analyses

Record no.	Record name	PGA (g) in weak direction
1	N-00356	0.09
2	E-00137	0.19
3	N-00694	0.23
4	N-00616	0.24
5	N-00147	0.25
6	N-00250	0.88
7	E-17167	0.53
8	N-00415	0.70
9	N-00569	0.52
10	N-00407	0.82
11	N-00451	1.25
12	N-03445	0.16
13	N-14717	0.17

D.1 De Haver

The collapse states observed in the LS-DYNA model of De Haver from partial collapse up to global collapse are shown in Figures D.1, D.2 and D.3. It is noted that the roof structure is not rendered in some of these figures to more easily show the damage/collapse. The lowest attic displacements and associated SDOF drift limits observed for each collapse states A to C are reported in Table D.2. All three collapse states are used for the fragility functions.

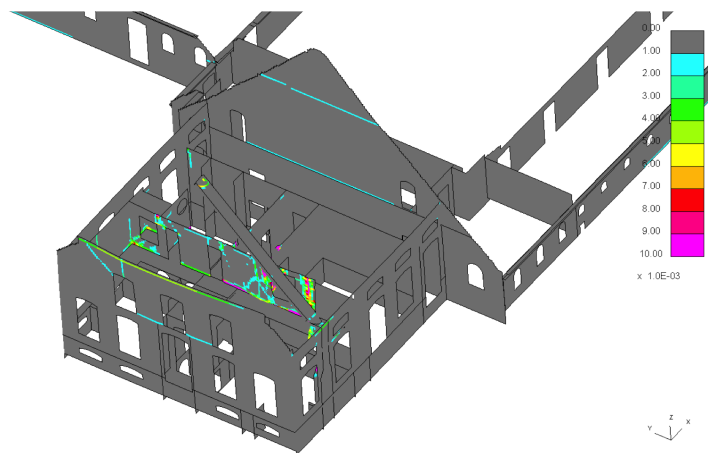


Figure D.1 Collapse state A of LS-DYNA De Haver model (Record 4)

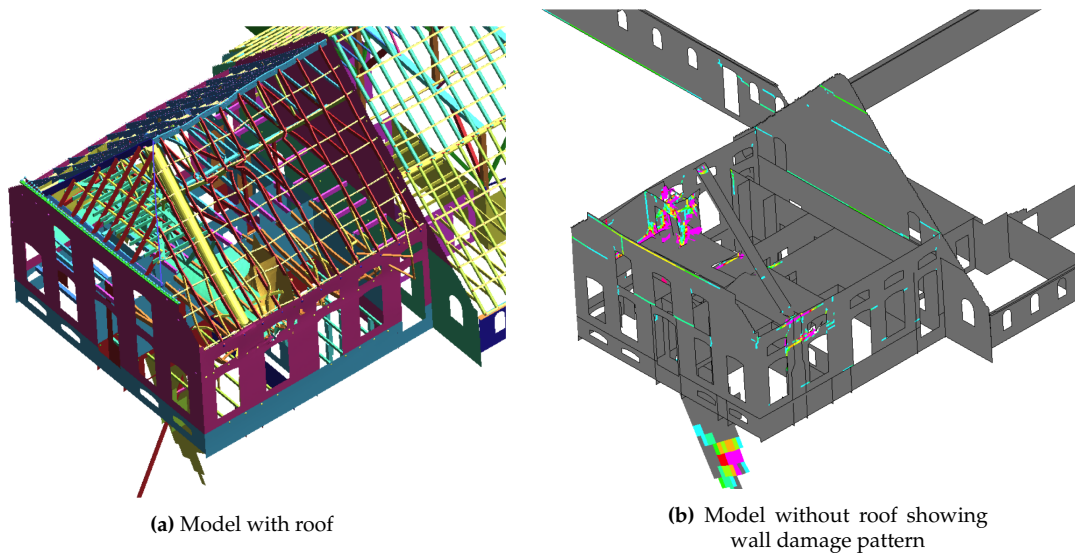


Figure D.2 Collapse state B of LS-DYNA De Haver model (Record 5)

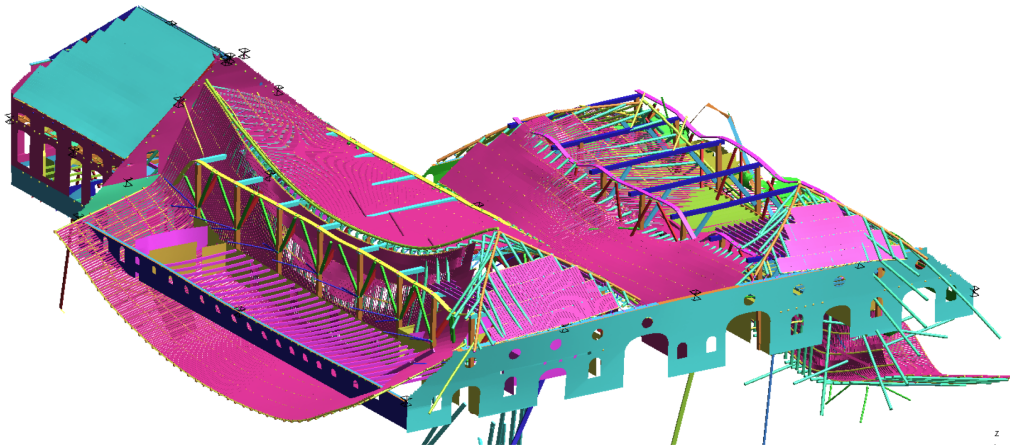


Figure D.3 Global collapse (collapse state C) of LS-DYNA De Haver model (Record 7)

Table D.2 SDOF drift limits for the collapse states of De Haver

Collapse state	Description	Attic displacement (mm)	θ_{SDOF}
A	Roof timber elements and out-of-plane failure of internal wall (house)	4.09	0.15
B	Out-of-plane failure of internal wall and collapse of mezzanine (house)	10.3	0.31
C	Total collapse of barn and collapse states (A) and (B)	22.7	0.69

D.2 Solwerderstraat 55

The collapse states observed in the LS-DYNA model of Solwerderstraat 55 from partial collapse up to global collapse are shown in Figures D.4 and D.5. The lowest attic displacements and associated SDOF drift limits observed for each collapse state are reported in Table D.3. It is noted that the displacement of collapse state C (under record X) is higher than that of collapse state D (which occurred under record Y), but the consequences in terms of collapse debris are similar, and thus the lower displacement is used for global collapse. Hence, collapse states A and B and D are used for the three collapse states in the fragility functions.

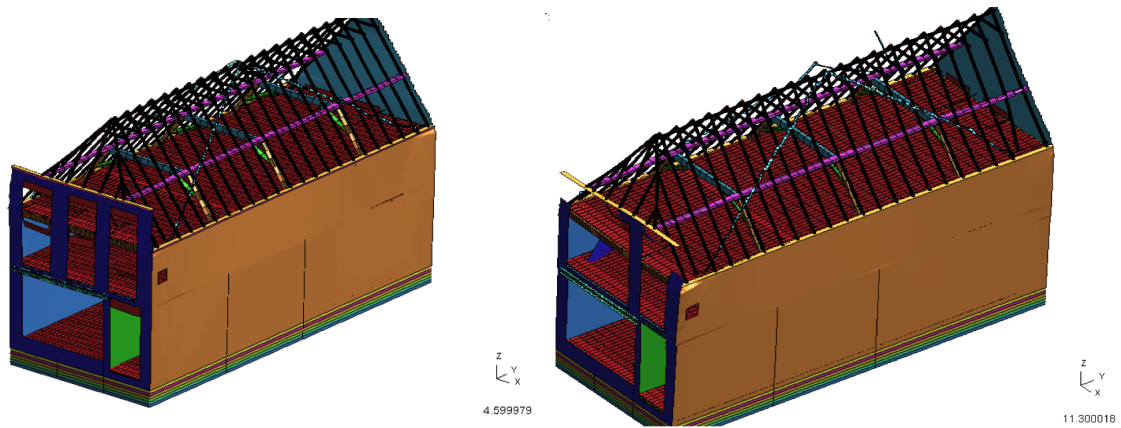


Figure D.4 Collapse states A and B of LS-DYNA Solwerderstraat 55 model (Records 5 and 8)

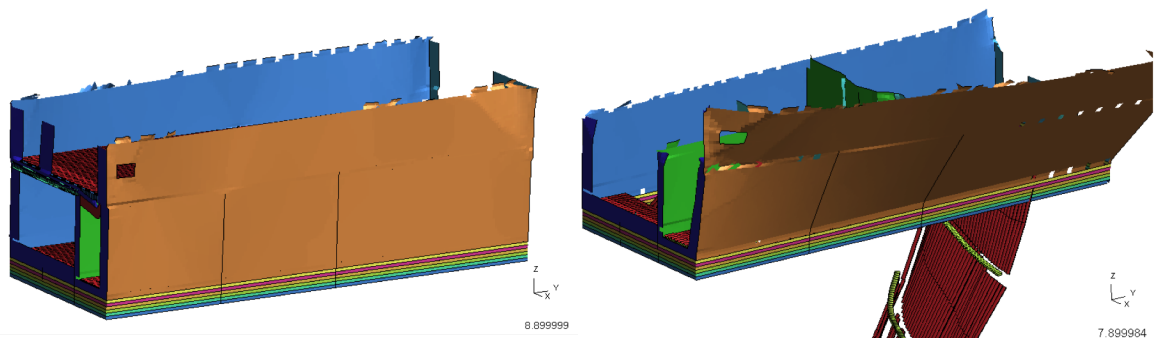


Figure D.5 Collapse states C and D of LS-DYNA Solwerderstraat 55 model (Records 11 and 9)

Table D.3 SDOF drift limits for the collapse states of Solwerderstraat 55

Collapse State	Description	Attic displacement (mm)	θ_{SDOF}
A	Lintel failure on the front façade	47.2	0.67
B	Partial collapse of the front façade	120.6	1.71
C	Onset of roof and second floor collapse, partial collapse of back façade	180.8	2.57
D	Global collapse	166.4	2.36

D.3 Julianalaan 52

The collapse states observed in the LS-DYNA model of Julianalaan 52 from partial collapse up to global collapse are shown in Figures D.6, a and D.7. The lowest attic displacements and associated SDOF drift limits observed for each collapse state are reported in Table D.4. Only these two collapse states are used in the derivation of the fragility and consequence models.



Figure D.6 Collapse state A of LS-DYNA Julianalaan 52 model (Record 8)

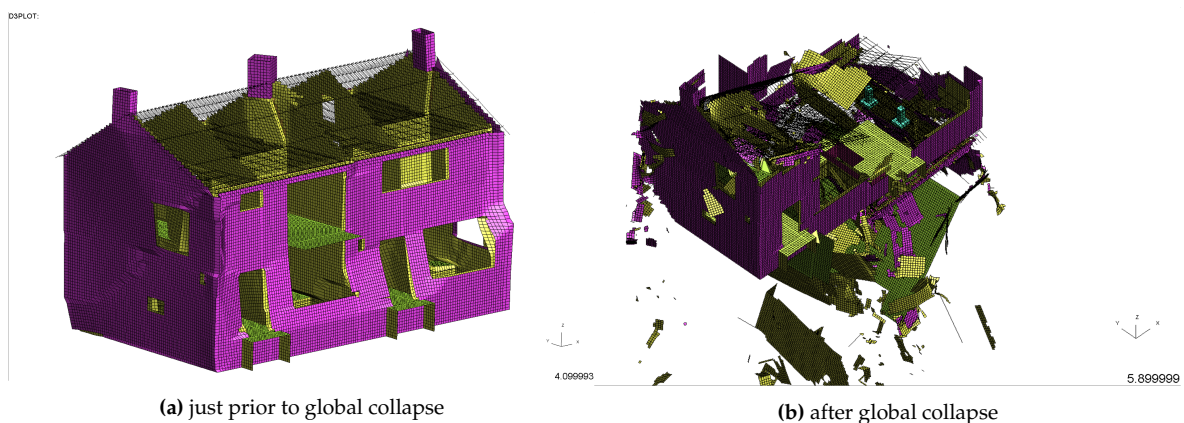


Figure D.7 Collapse state B of LS-DYNA Julianalaan 52 model (Record 11)

Table D.4 SDOF drift limits for the collapse states of Julianalaan 52

Collapse State	Description	Attic displacement (mm)	θ_{SDOF}
A	Both leaves of one gable wall collapse (inside and outside)	55.85	1.23
B	Global collapse	56.64	1.25

D.4 Zijlvest 25

The collapse states observed in the LS-DYNA model of Zijlvest 25 from partial collapse up to global collapse are shown in Figures D.8, D.9, D.10 and D.11. The lowest attic displacements and associated SDOF drift limits observed for each collapse state are reported in Table D.5. The three collapse states for the fragility functions have been taken as collapse state A, the average (in terms of drifts and consequences) of collapse states B and C, and collapse state D.

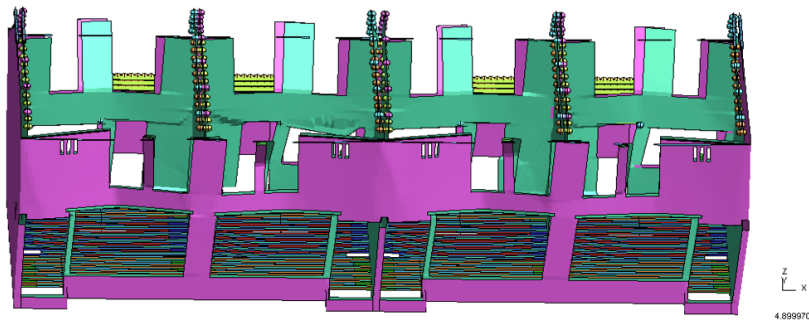


Figure D.8 Collapse state A of LS-DYNA Zijlvest 25 model (Record 6)

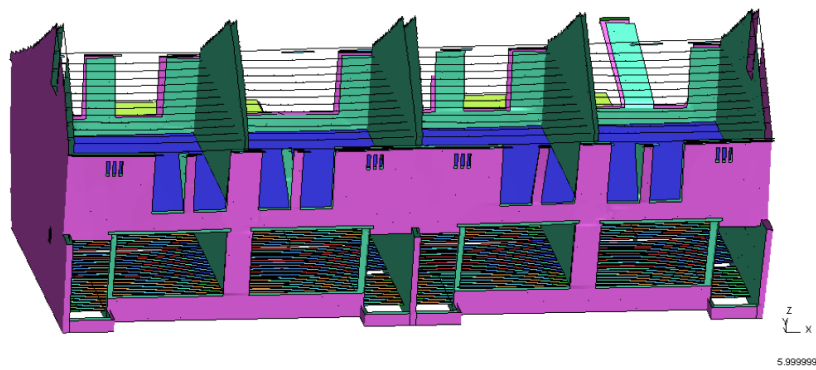


Figure D.9 Collapse state B of LS-DYNA Zijlvest 25 model (Record 10)

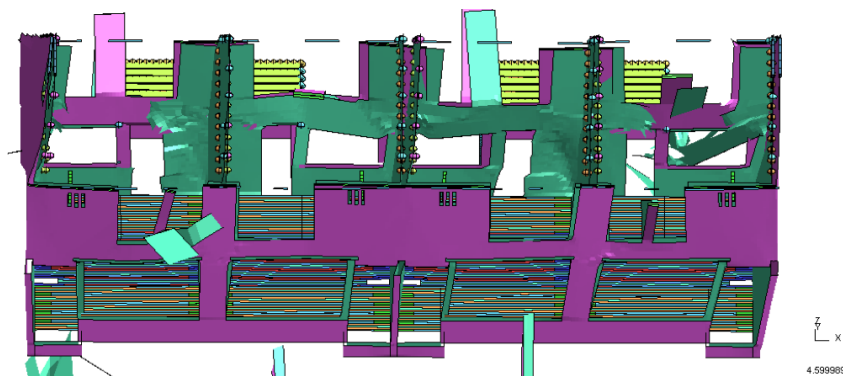


Figure D.10 Collapse state C of LS-DYNA Zijlvest 25 model (Record 8)

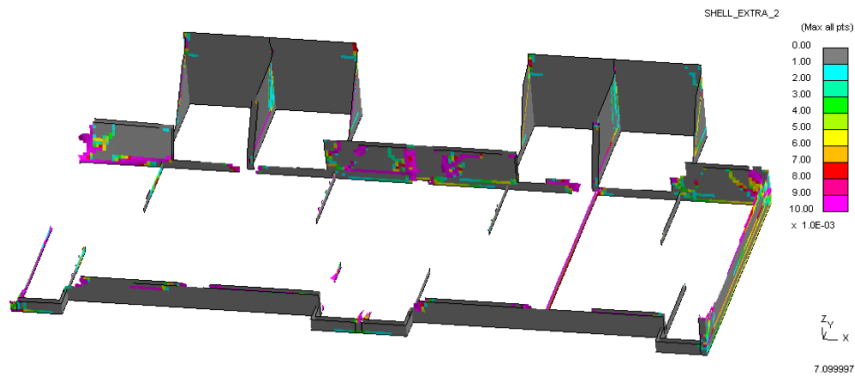


Figure D.11 Collapse state D of LS-DYNA Zijlvest 25 model (Record 9)

Table D.5 SDOF drift limits for the collapse states of Zijlvest 25

Collapse State	Description	Attic displacement (mm)	θ_{SDOF}
A	Masonry columns collapse outwards and lintel collapse	37.8	0.99
B	Masonry columns collapse both inwards and outwards	80.0	2.09
C	Column & lintel collapse inwards and outwards, both floors	107.1	2.80
D	Global collapse	112.9	2.93

D.5 Koeriersterweg 20-21

The collapse states observed in the LS-DYNA model of Koeriersterweg 20-21 from partial collapse to global collapse are shown in Figures D.12, D.13 and D.14. The lowest attic displacements and associated SDOF drift limits observed for each collapse state are reported in Table D.6 ¹. As only three collapse states are being considered in the risk engine, these have been taken as collapse state A, the average (in terms of drifts and consequences) of collapse states B, C and D, and collapse state E.

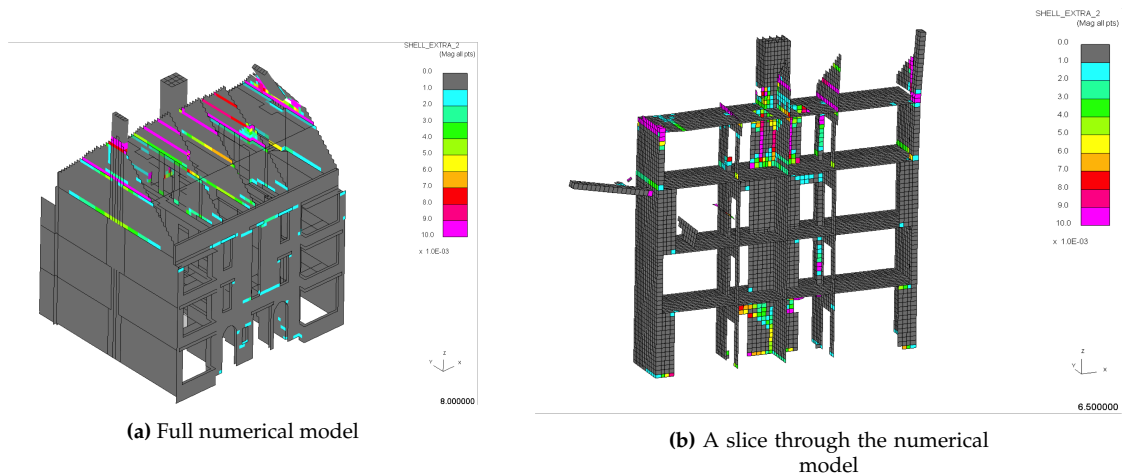


Figure D.12 Collapse states A and B of LS-DYNA Koeriersterweg 20-21 model (Record 12 scaled to 0.2g and 0.3g, respectively)

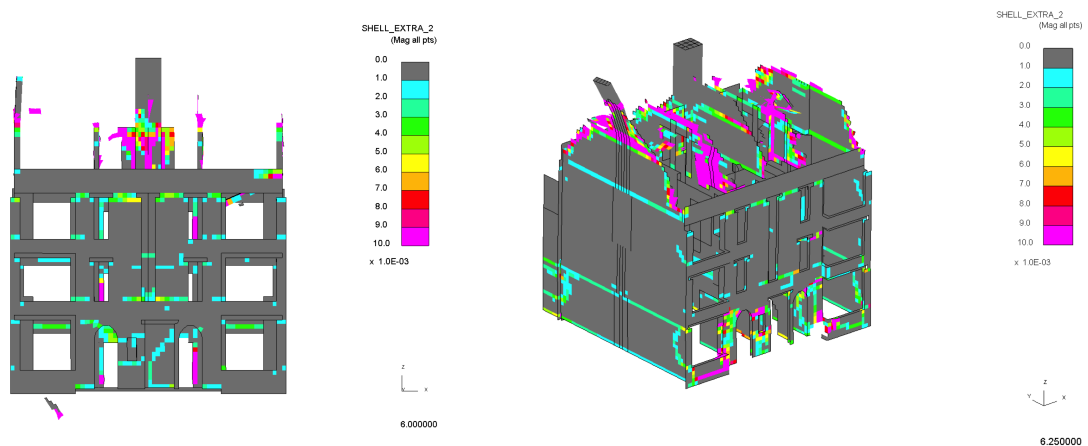


Figure D.13 Collapse states C and D of LS-DYNA Koeriersterweg 20-21 model (Record 13 scaled to 0.4g and Record 12 scaled to 0.4g)

¹As discussed in Arup (2017c), this is an older model that has been run with incremental dynamic analysis (IDA, Vamvatsikos and Cornell, 2002), rather than with a suite of records with increasing levels of intensity. Unusual behaviour has been observed, with a given collapse mechanism occurring much earlier as the IDA progresses, and this is believed to be due to unrealistic ground motions being created through scaling. For this model, the displacement for a given mechanism has been taken from the results of the lowest intensity ground shaking for which it has been observed.

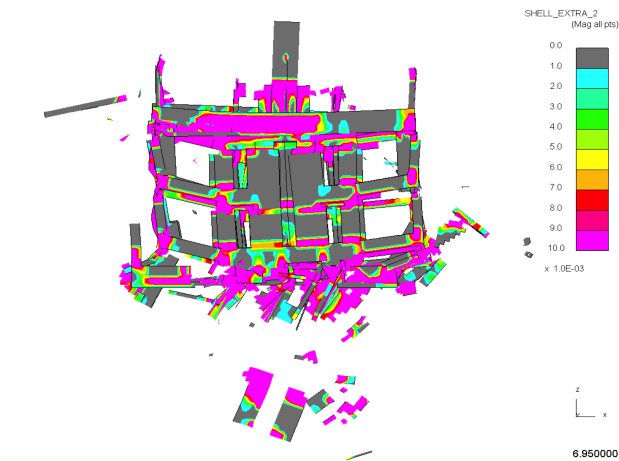


Figure D.14 Collapse state E of LS-DYNA Koeriersterweg 20-21 model (Record 12 scaled to 0.6g)

Table D.6 SDOF drift limits for the collapse states of Koeriersterweg 20-21

Collapse State	Description	Attic displacement (mm)	θ_{SDOF}
A	OOP failure of gable wall on to 30% of attic	16.0	0.25
B	OOP failure of gable wall on to 50% attic & chimney failure	24.3	0.37
C	OOP failure of gable wall on to 100% attic & chimney failure	27.7	0.42
D	OOP failure of gable wall on to 100% attic & 3rd floor & chimney failure	41.9	0.64
E	Global collapse	121.3	1.86

D.6 Nieuwstraat 8

Both ELS and LS-DYNA models have been produced for this index building. The collapse mechanisms observed in both software were related to the unseating of the timber floor from the solid URM walls, however only the ELS model has been used as the LS-DYNA was still being checked at the time of developing the fragility and consequences models. The collapse states observed in the ELS model of Nieuwstraat 8 from partial gable collapse up to global collapse are shown in Figures D.15, D.16 and D.17. The lowest attic displacements and associated SDOF drift limits observed for each collapse state are reported in Table D.7. All three collapse states are used in the derivation of the fragility and consequence models.

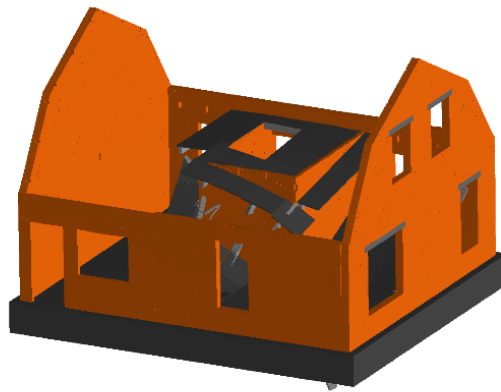


Figure D.15 Collapse state A of ELS Nieuwstraat 8 model (Record 6)

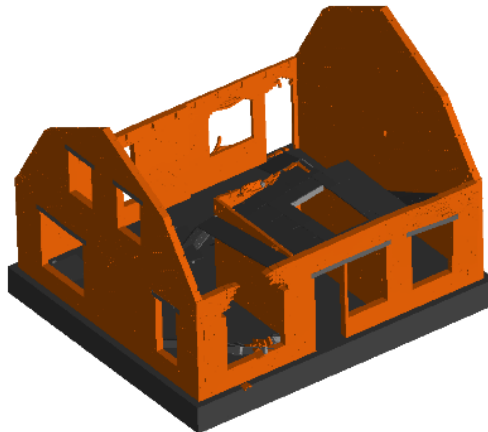


Figure D.16 Collapse state B of ELS Nieuwstraat 8 model (Record 10)

Table D.7 SDOF drift limits for the collapse states of Nieuwstraat 8

Collapse State	Description	Attic displacement (mm)	θ_{SDOF}
A	Almost complete failure of floor	26.4	0.88
B	Almost complete failure of floor and wall collapse around windows	35.4	1.18
C	Global collapse	104	3.47

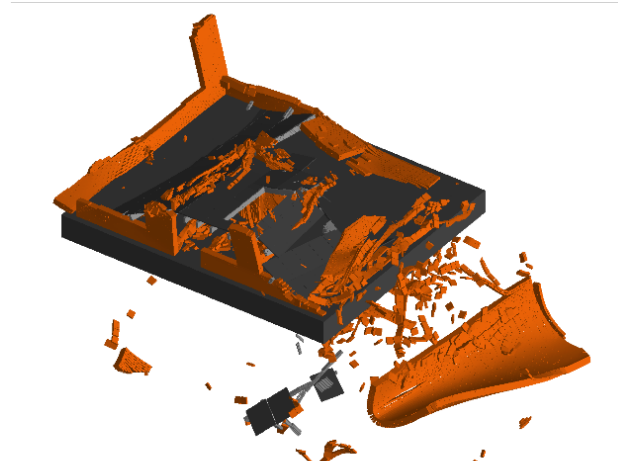


Figure D.17 Collapse state C of ELS Nieuwstraat 8 model (Record 9)

D.7 Kwelder 1

The collapse states observed in the LS-DYNA model of Kwelder 1 from partial collapse to global collapse are shown in Figures D.18, D.19 and D.20. It is noted that in some figures the external rendering has been removed to show more clearly the collapse, especially when this occurs inside the building. The lowest attic displacements and associated SDOF drift limits observed for each collapse state are reported in Table D.8. It is noted that the displacement of collapse state D is higher than that of collapse state E (global collapse), but the consequences in terms of collapse debris are similar, and thus the lower displacement is used for global collapse. Collapse states B and C occur at similar drift levels, and so the average of the drifts and consequences have been used to produce a collapse state. The final three collapse states used in the risk engine are thus collapse state A, the average of collapse states B and C, and collapse state E (global collapse).

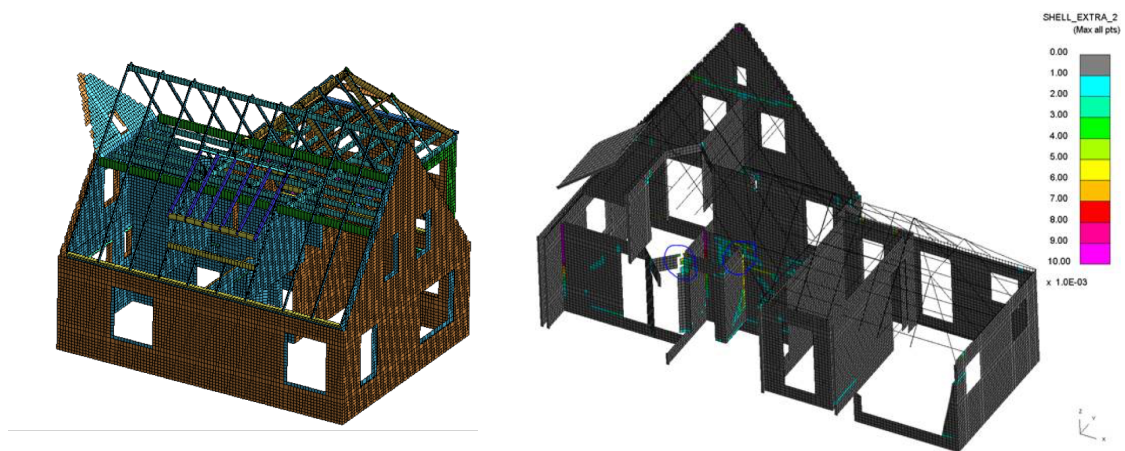


Figure D.18 Collapse states A and B of LS-DYNA Kwelder 1 model (Records 6 and 7)

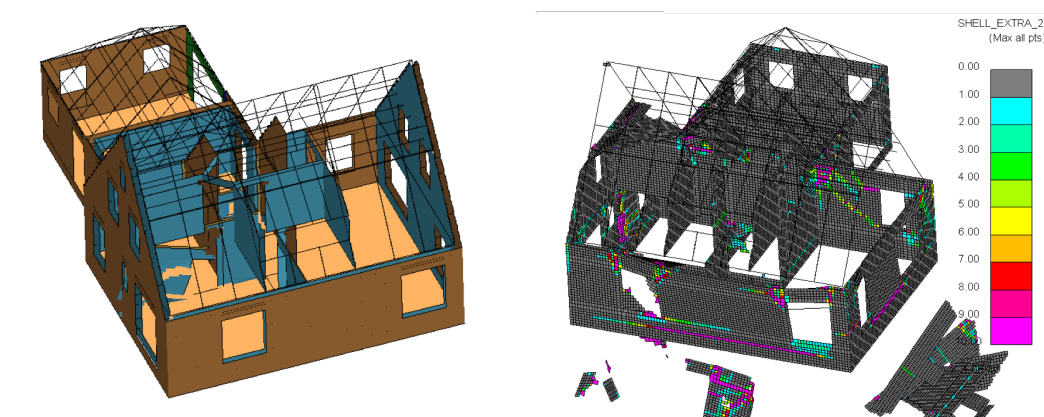


Figure D.19 Collapse states C and D of LS-DYNA Kwelder 1 model (Records 10 and 9)

Table D.8 SDOF drift limits for the collapse states of Kwelder 1

Collapse State	Description	Attic displacement (mm)	θ_{SDOF}
A	OOP failure of part of gable wall	7.52	0.27
B	Minor internal partition wall failure	22.7	0.83
C	Moderate internal partition wall failure	32.1	1.17
D	Gable and extensive partition and main wall failure	56.1	2.04
E	Global collapse	40.3	1.46

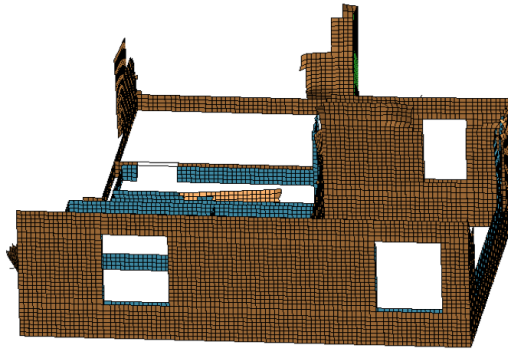


Figure D.20 Collapse state E of LS-DYNA Kwelder 1 model (Record 11)

D.8 Schuitenzandflat 2-56

The collapse states observed in the LS-DYNA model of Schuitenzandflat 2-56 from partial collapse up to global collapse are shown in Figures D.21, D.22, and D.23. Global collapse of the whole structure was not observed in any of the analyses. The three collapse states used in the risk engine have been taken as collapse state A, the average drifts and consequences of collapse states B, C and D and collapse state E².

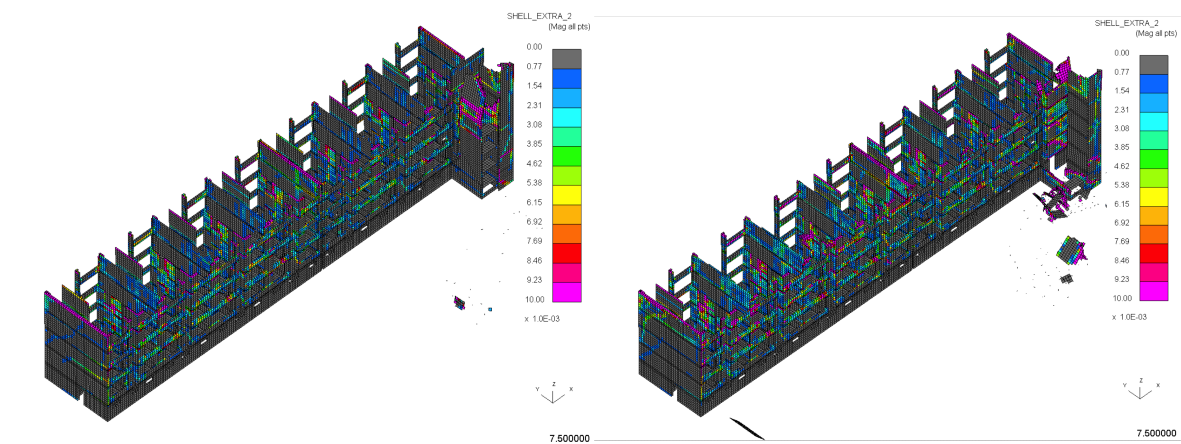


Figure D.21 Collapse states A and B of LS-DYNA Schuitenzandflat 2-56 model (Record 12 scaled to 0.35g and 0.5g, respectively)

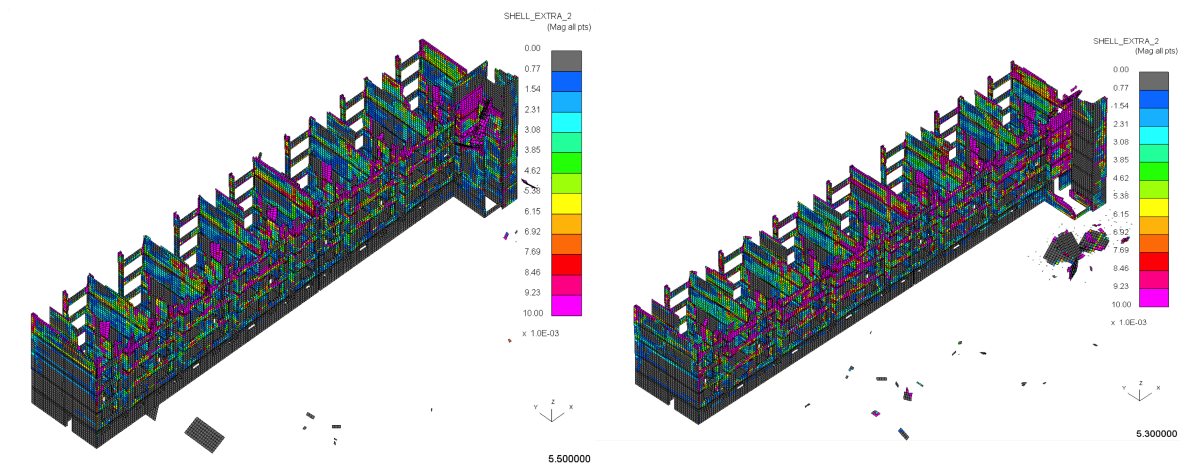


Figure D.22 Collapse states C and D of LS-DYNA Schuitenzandflat 2-56 model (Record 13 scaled to 0.8g and 1.0g, respectively)

²As discussed in Arup (2017c), this is an older model that has been run with incremental dynamic analysis (IDA, Vamvatsikos and Cornell, 2002), rather than with a suite of records with increasing levels of intensity. Unusual behaviour has been observed, with a given collapse mechanism occurring much earlier as the IDA progresses, and this is believed to be due to unrealistic ground motions being created through scaling. For this model, the displacement for a given mechanism has been taken from the results of the lowest intensity ground shaking for which it has been observed.

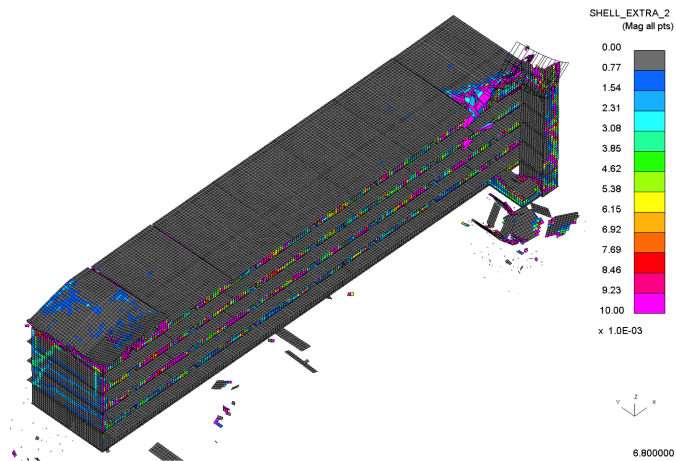


Figure D.23 Collapse state E of LS-DYNA Schuitenzandflat 2-56 model (Record 12 scaled to 0.8g)

Table D.9 SDOF drift limits for the collapse states of Schuitenzandflat 2-56

Collapse State	Description	Attic displacement (mm)	θ_{SDOF}
A	OOP collapse of elevator shaft walls	49.2	0.30
B	Collapse of elevator shaft and collapse of 20% of 4th floor	103.8	0.63
C	Collapse of elevator shaft and collapse of 50% of 4th floor	106.2	0.64
D	Collapse of elevator shaft and collapse of 75% of 4th floor	119.4	0.72
E	Collapse of elevator shaft and collapse of 100% of 4th floor	196.2	1.19

D.9 Badweg 12

The collapse states observed in the LS-DYNA model of Badweg 12 from partial gable collapse up to global collapse are shown in Figures D.24, D.25 and D.26. The lowest attic displacements and associated SDOF drift limits observed for each collapse state are reported in Table D.10. All three collapse states are used in the derivation of the fragility and consequence models.

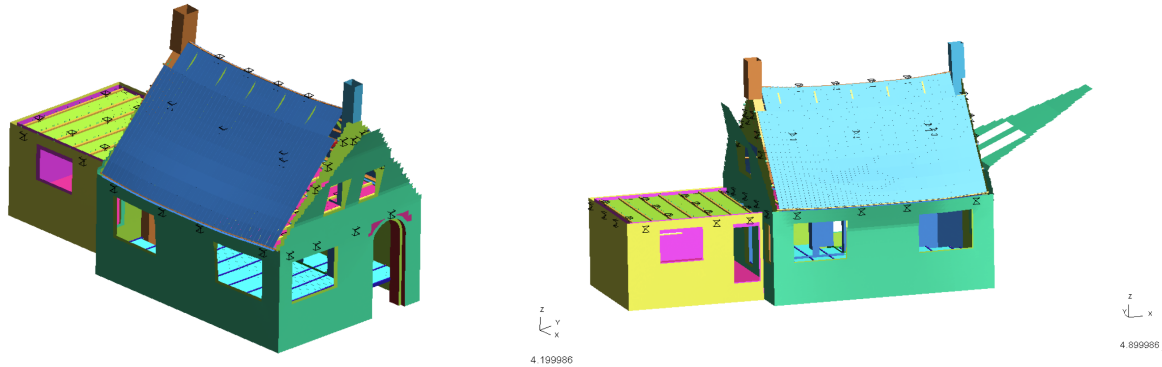


Figure D.24 Collapse state A of LS-DYNA Badweg 12 model (Record 5)

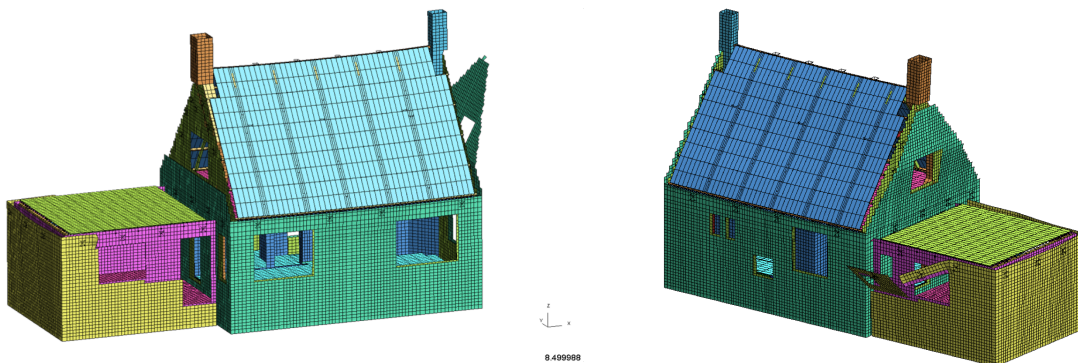


Figure D.25 Collapse state B of LS-DYNA Badweg 12 model (Record 6)

Table D.10 SDOF drift limits for the collapse states of Badweg 12

Collapse State	Description	Attic displacement (mm)	θ_{SDOF}
A	OOP failure of external gable wall leaf	2.34	0.085
B	OOP failure of external gable wall leaf and part of longitudinal walls	9.52	0.34
C	Global collapse	19.9	0.71

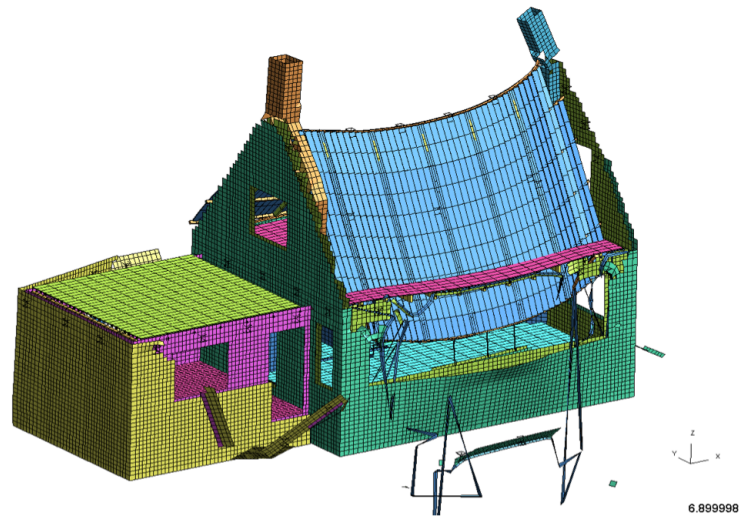


Figure D.26 Collapse state C of LS-DYNA Badweg 12 model (Record 7)

Appendix E

Structural Fragility Functions

The following plots illustrate the damage and collapse state fragility functions for all models presented in Chapter 4. It is noted that the majority of the structural systems require a vector intensity measure that is based on spectral acceleration at one or two periods of vibration and the 5-75% significant duration. However, for simplicity of presentation, the functions are illustrated only in terms of the spectral acceleration at the first period of vibration (T_1). The short codes for the structural systems, presented previously in Table C.1, have been used in the figure labels.

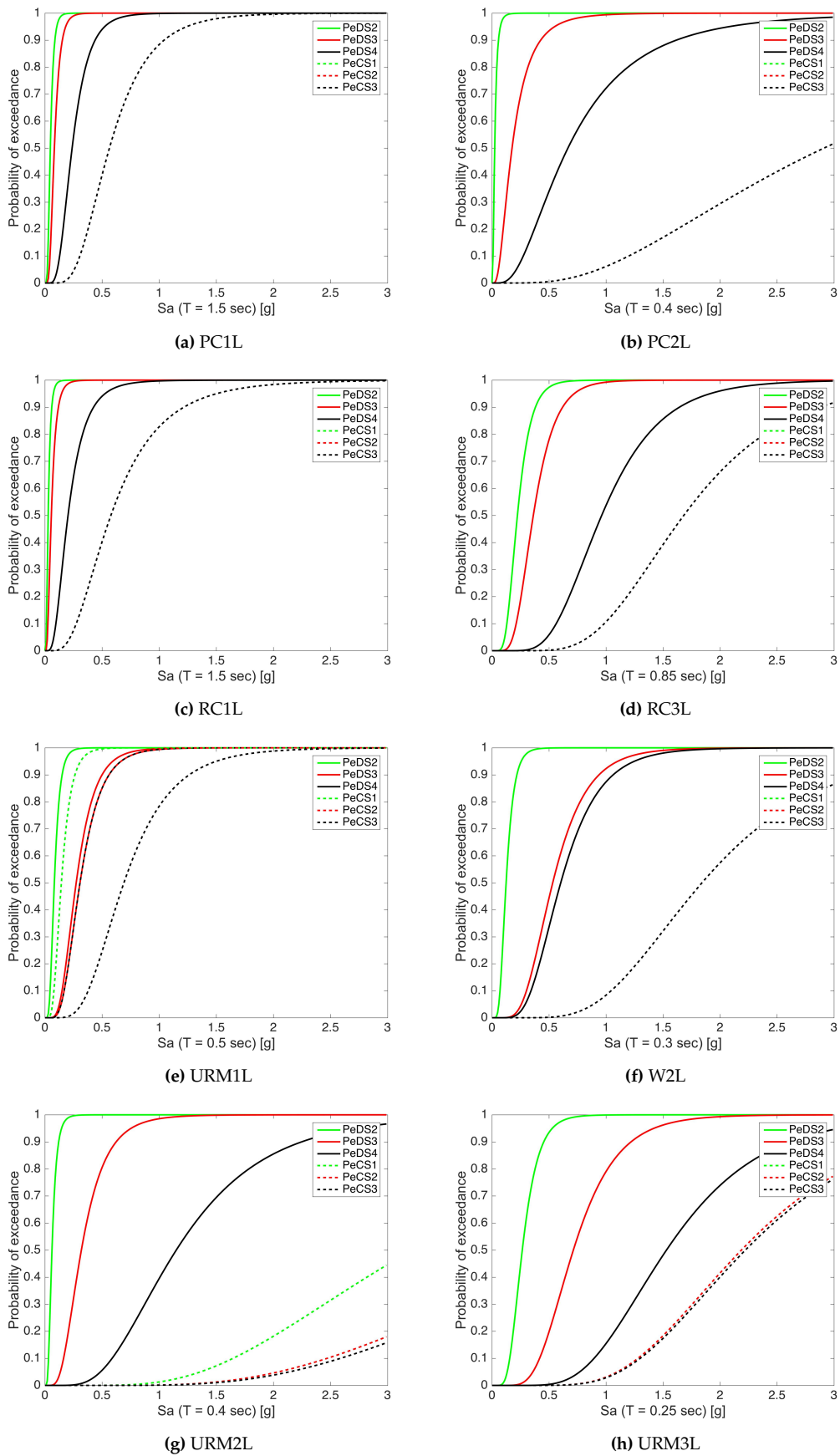


Figure E.1 Fragility functions for each structural system

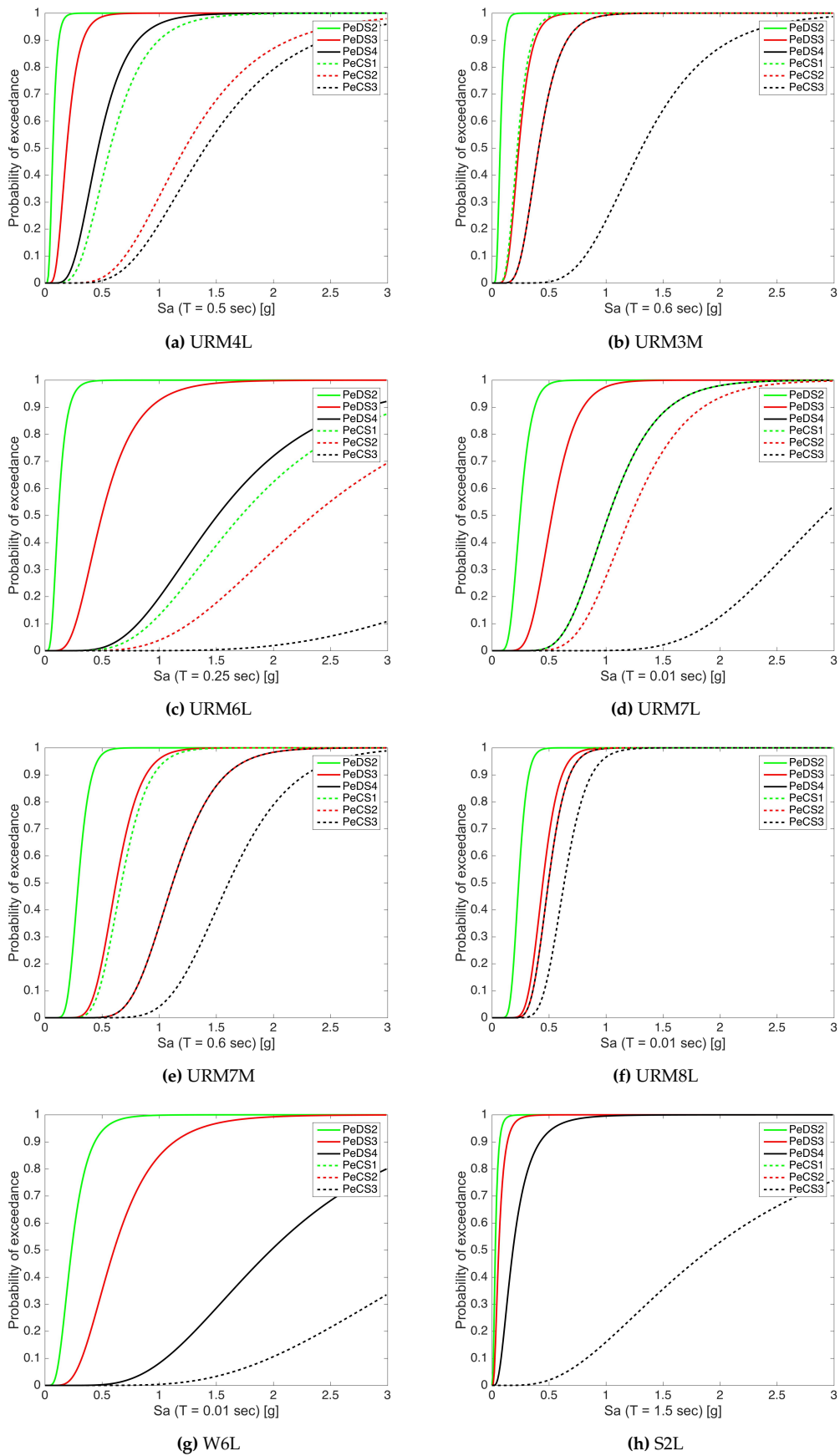


Figure E.2 Fragility functions for each structural system (cont.)

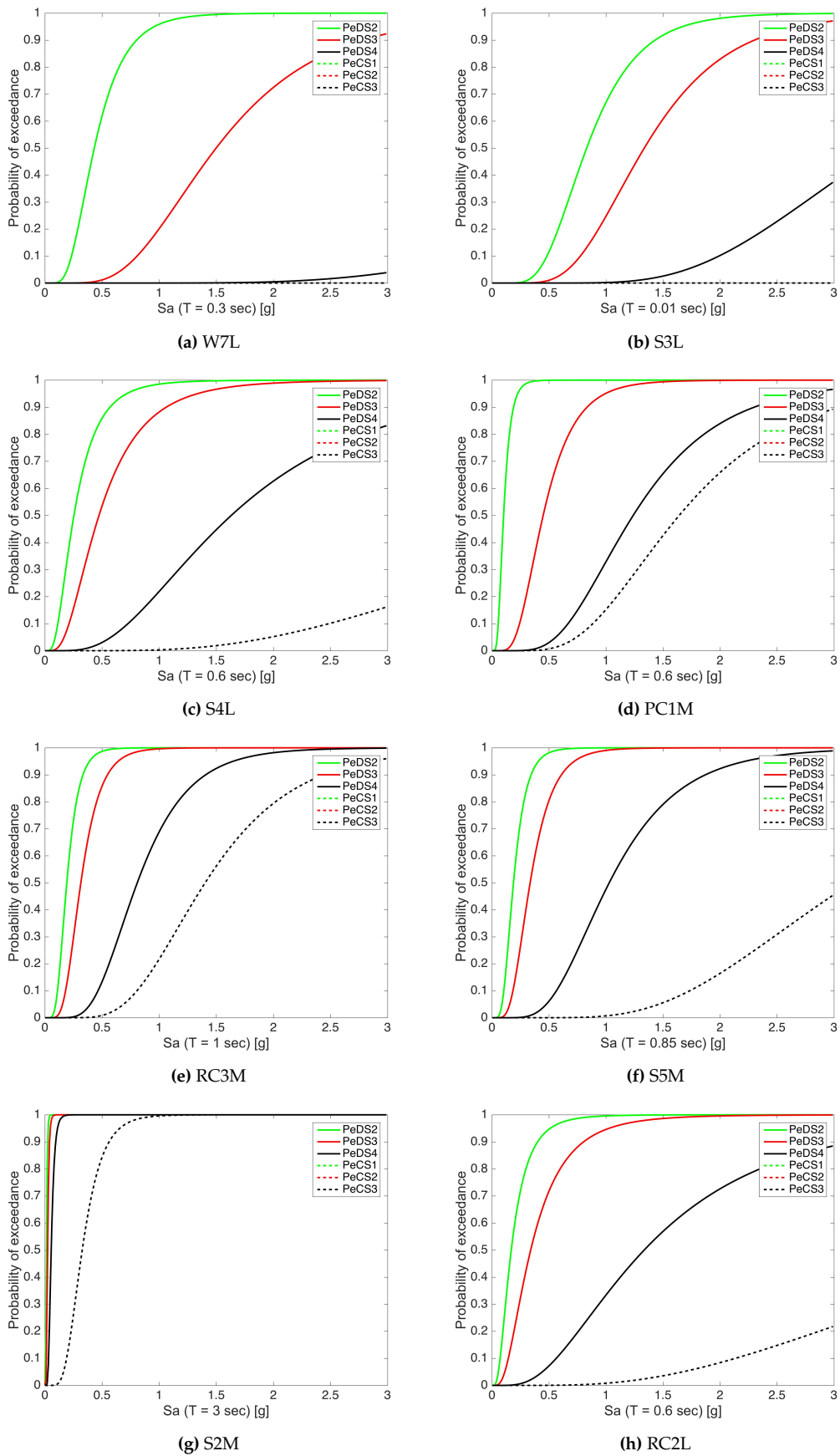


Figure E.3 Fragility functions for each structural system (cont.)

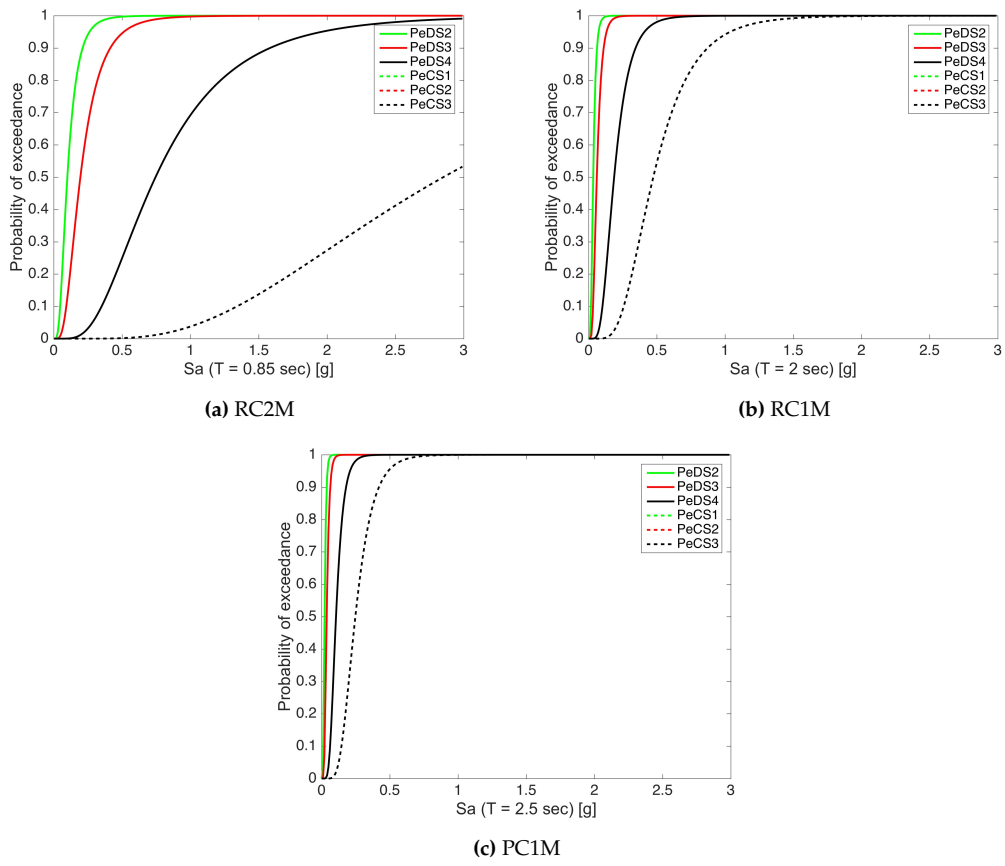


Figure E.4 Fragility functions for each structural system (cont.)